

THE ROLE OF INTERNAL ENERGY IN GAS-PHASE REACTIONS

A THESIS

Presented to

The Faculty of the Division of Graduate  
Studies and Research

By

Philip Charles Cosby


In Partial Fulfillment  
of the Requirements for the Degree  
Doctor of Philosophy  
in the  
School of Chemistry

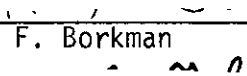
Georgia Institute of Technology

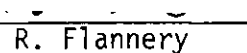
April, 1974

THE ROLE OF INTERNAL ENERGY IN GAS-PHASE REACTIONS

Approved:

  
\_\_\_\_\_  
T. F. Moran, Chairman

  
\_\_\_\_\_  
R. F. Borkman

  
\_\_\_\_\_  
M. R. Flannery

Date approved by Chairman: April 9, 1974

## ACKNOWLEDGMENTS

It is with sincere appreciation that I acknowledge the invaluable guidance, encouragement, and assistance of my advisor, Dr. Thomas F. Moran, during the course of this research. I am also indebted to Dr. M. R. Flannery for our association in the molecular charge-transfer investigations.

Much of the acquisition and interpretation of the experimental data reported in this work was accomplished through the dedicated assistance of Virgil Hornstein and Steve Geddes.

I thank Dr. R. F. Borkman for serving on my reading committee. I also thank Dr. Wm. M. Spicer and Dr. J. A. Bertrand for generously granting me a teaching assistantship.

Financial support from the Veterans Administration is gratefully acknowledged.

## TABLE OF CONTENTS

	Page
ACKNOWLEDGMENTS . . . . .	ii
LIST OF TABLES . . . . .	v
LIST OF ILLUSTRATIONS . . . . .	vi
Chapter	
I. INTRODUCTION . . . . .	1
General	
Charge-Transfer Reactions	
Metastable Reactions	
II. MOLECULAR CHARGE TRANSFER: EXPERIMENTAL AND THEORETICAL INVESTIGATION OF THE ROLE OF INCIDENT-ION VIBRATIONAL STATES IN $N_2^+ - N_2$ AND $CO^+ - CO$ COLLISIONS . . . . .	9
III. MOLECULAR CHARGE TRANSFER II: EXPERIMENTAL AND THEORETICAL INVESTIGATION OF THE ROLE OF INCIDENT-ION VIBRATIONAL STATES IN $O_2^+ - O_2$ AND $NO^+ - NO$ COLLISIONS . . . . .	10
Introduction	
Theory	
Calculations	
Experimental Analysis	
Comparison Between Theory and Experiment	
Conclusion	
IV. PARTICIPATION OF INCIDENT-ION INTERNAL ENERGY IN MOLECULAR $O_2^+ - Ar$ CHARGE-TRANSFER COLLISIONS . . . . .	45
V. COMPETITION BETWEEN DOUBLE AND SINGLE ELECTRON TRANSFER IN 2-8 KEV $Ar^{++} - Ar$ COLLISIONS . . . . .	46
VI. PRODUCT INTERNAL STATE DISTRIBUTIONS FROM INTERACTIONS OF METASTABLE $Ar$ WITH $N_2$ . . . . .	47
VII. CONCLUSIONS . . . . .	48

## TABLE OF CONTENTS (Continued)

APPENDICES	Page
I. SELECTED OVERLAPS AND ENERGETICS . . . . .	51
II. MOLECULAR CHARGE TRANSFER: EXPERIMENTAL AND THEORETICAL INVESTIGATION OF THE ROLE OF INCIDENT-ION VIBRATIONAL STATES IN $N_2^+ - N_2$ AND $CO^+ - CO$ COLLISIONS . . . . .	56
III. PARTICIPATION OF INCIDENT-ION INTERNAL ENERGY IN MOLECULAR $O_2^+ - AR$ CHARGE-TRANSFER COLLISIONS . . . .	74
IV. COMPETITION BETWEEN DOUBLE AND SINGLE ELECTRON TRANSFER IN 2-8 KEV $AR^{++} - AR$ COLLISIONS . . . . .	81
V. PRODUCT INTERNAL STATE DISTRIBUTIONS FROM INTERACTIONS OF METASTABLE $AR$ WITH $N_2$ . . . . .	84
LITERATURE CITED . . . . .	90
VITA . . . . .	94

## LIST OF TABLES

Table	Page
1. Overlap Integrals and Energy Defects for the Charge-Transfer Reactions: $O_2^+(X^2\Pi_g, v_0')$ + $O_2(X^3\Sigma_g^-, v_0''=0) \rightarrow O_2(X^3\Sigma_g^-, v'') + O_2^+(X^2\Pi_g, v')$ . . . . .	52
2. Overlap Integrals and Energy Defects for the Charge-Transfer Reactions: $NO^+(X^1\Sigma^+, v_0')$ + $NO(X^2\Pi_r, v_0''=0) \rightarrow NO(X^2\Pi_r, v'') + NO^+(X^1\Sigma^+, v')$ . . . . .	54
3. Effect of Nonresonant Product Channels on the Total Charge-Transfer Cross Section ( $\text{\AA}^2$ ) for the Reactions: $O_2^+(X^2\Pi_g, v_0'=0) + O_2(X^3\Sigma_g^-, v_0''=0) \rightarrow O_2(X^3\Sigma_g^-, v'') + O_2^+(X^2\Pi_g, v')$ . . . . .	21
4. Effect of Nonresonant Product Channels on the Total Charge-Transfer Cross Section ( $\text{\AA}^2$ ) for the Reactions: $NO^+(X^1\Sigma^+, v_0'=0) + NO(X^2\Pi_r, v_0''=0) \rightarrow NO(X^2\Pi_r, v'') + NO^+(X^1\Sigma^+, v')$ . . . . .	24
5. Total Charge-Transfer Cross Sections ( $\text{\AA}^2$ ) Calculated for the Reactions: $O_2^+(X^2\Pi_g, v_0')$ + $O_2(X^3\Sigma_g^-, v_0''=0) \rightarrow O_2(X^3\Sigma_g^-, v'') + O_2^+(X^2\Pi_g, v')$ . . . . .	26
6. Total Charge-Transfer Cross Sections ( $\text{\AA}^2$ ) Calculated For the Reactions: $NO^+(X^1\Sigma^+, v_0')$ + $NO(X^2\Pi_r, v_0''=0) \rightarrow NO(X^2\Pi_r, v'') + NO^+(X^1\Sigma^+, v')$ . . . . .	27

## LIST OF ILLUSTRATIONS

Figure	Page
1. Interaction Potential Energy for $O_2^+ - O_2$ Collisions . . . . .	16
2. Interaction Potential Energy for $NO^+ - NO$ Collisions . . . . .	17
3. Partial Multistate Cross Sections as a Function of $O_2^+$ Kinetic Energy. The Numbers ( $v'', v'$ ) Designate the Final Vibrational States of the Neutral and Ionic Products . . . . .	19
4. Partial Multistate Cross Sections as a Function of $NO^+$ Kinetic Energy. The Numbers ( $v'', v'$ ) Designate the Final Vibrational States of the Neutral and Ionic Products . . . . .	23
5. Total Charge-Transfer Cross Sections for Three Reactant $O_2^+$ Vibrational States Computed Using Multistate <sup>2</sup> Treatment (Solid Curves) and the Low Velocity Approximation (Dashed Curves) . . . . .	28
6. Total Charge-Transfer Cross Sections for Three Reactant $NO^+$ Vibrational States Computed Using Multistate Treatment (Solid Curves) and the Low Velocity Approximation (Dashed Curves) . . . . .	29
7. Total $O_2^+ - O_2$ Charge-Transfer Cross Sections for a Reactant Ion Vibrational Distribution Characteristic of 13 eV Electron Impact Ionization . . . . .	35
8. Total $NO^+ - NO$ Charge-Transfer Cross Sections for a Reactant Ion Vibrational Distribution Characteristic of 11 eV Electron Impact Ionization . . . . .	36
9. Cross Sections Measured for $O_2^+ - O_2$ Charge-Transfer Reactions as Function of Ionizing <sup>2</sup> Electron Energy. Those Calculated Using the Multistate Model are Given as Solid Curves . . . . .	39
10. Cross Sections Measured for $NO^+ - NO$ Charge-Transfer Reactions as Function of Ionizing Electron Energy. Those Calculated Using the Multistate Model are Given as Solid Curves . . . . .	41

## LIST OF ILLUSTRATIONS (Continued)

Figure		Page
11.	Comparison Between Theoretical and Experimental Charge-Transfer Cross Sections for $O_2^+ - O_2$ Reactions as a Function of Ion Kinetic Energy . . . . .	42
12.	Comparison Between Theoretical and Experimental Charge-Transfer Cross Sections for $NO^+ - NO$ Reactions as a Function of Ion Kinetic Energy . . . . .	43

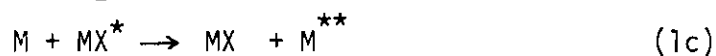


## CHAPTER I

## INTRODUCTION

General

Nearly half a century ago Michael Polanyi observed strong fluorescence from alkali metal vapor when it was mixed with halogen gas. To account for the excitation of the metal atoms, he proposed the reaction mechanism:<sup>1</sup>



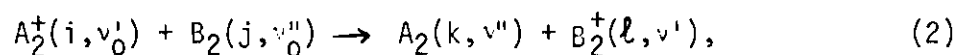
where  $M^{**}$  and  $MX^*$  represent the electronically excited metal atom and the vibrationally excited alkali halide molecule, respectively. This mechanism for reaction (1) was novel in that large fractions of the reaction heats produced in the highly exothermic steps (1a) and (1b) were required to be retained in the form of vibrational excitation of the product halide. In such form, the energy could be efficiently transferred to electronic excitation of the metal via (1c), which would otherwise be highly endothermic at room temperature.

A more recent study<sup>2</sup> of reaction (1) in a tandem molecular beam experiment has confirmed the role of vibrational excitation in a chemical reaction. Formation and reaction of excited species, however, is

not limited to only neutral-neutral interactions. The rates of endothermic ion-molecule reactions have also been shown to be strongly influenced by the internal energy state of either the ionic<sup>3</sup> or neutral<sup>4</sup> reactant. Differences in the reaction rates of excited and ground state atoms or molecules is of considerable importance in the accurate simulation of a complex reaction system, such as the upper atmosphere, in which the internal energy content of the reactants is subject to temporal variations.<sup>4,5</sup> Furthermore, the coupled nature of the reactions in such a system necessitates an explicit knowledge of the internal states in which the reaction products are formed. Quantitative information concerning the role of excited species in gas-phase reactions, however, is remarkably limited.<sup>6,7</sup> It is the purpose of this dissertation to investigate the production and reaction of excited species in two types of gas-phase reactions: charge-transfer reactions of ions with molecules and reactions of a metastable atom with a diatomic gas.

### Charge-Transfer Reactions

Perhaps the most basic process in which to investigate the role of internal energy in a reaction involves the transfer of an electron between a neutral molecule and an ion.<sup>8-10</sup> Consider the molecule charge-transfer reaction:



in which the diatomic molecular ion  $A_2^+$  having electronic and vibrational coordinates  $(i, v_0')$  and a given kinetic energy, interacts with the neutral diatomic molecule  $B_2(j, v_0'')$  which is at rest in the laboratory

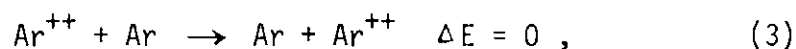
frame of reference. During the interaction, an electron is transferred from the molecule to the ion forming a product ion  $B_2^+(l, v')$  and product neutral  $A_2(k, v'')$ . The transfer of the electron characteristically takes place at separations of the reactants which are large with respect to their molecular dimensions. Consequently, little momentum is transferred during the exchange and the product  $A_2$  molecule retains essentially all the initial kinetic energy of the reactant  $A_2^+$  ion. If the reaction occurs at a sufficiently high relative velocity, it is possible to produce electronically or vibrationally excited products. The magnitude of the interconversion of translational and internal energy in the charge-transfer reaction is expressed in terms of an energy defect,  $\Delta E$ , representing the difference between the total internal energy of the products and that of the reactants. Those elastic processes, which involve no net change of internal energy ( $\Delta E = 0$ ), are referred to as resonant charge-transfer reactions, whereas nonresonant charge-transfer reactions ( $\Delta E \neq 0$ ) produce products having internal states different from those of the reactants. If the energy defect of a nonresonant process is small with respect to the relative velocity of the interaction, it is termed near-resonant.

It is advantageous to further separate charge-transfer reactions into categories on the basis of the mechanism governing transfer of the electron.<sup>11</sup> When  $A_2^+$  and  $B_2$  in reaction (2) represent a molecular ion and its parent neutral molecule ( $A = B$ ), the potential field acting on the active electron is symmetric about the midpoint of the line joining the centers of mass of  $A_2^+$  and  $B_2$ , and the electron is described by a linear

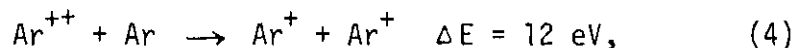
combination of gerade and ungerade eigenfunctions of  $(A_2B_2)^+$ . During the encounter, changes in the relative phase of these eigenfunctions are brought about by the time-dependent variation of the electrostatic interaction caused by the classical relative motion of the two centers of mass. This permits the electron to transfer. If the wavefunctions describing the ionic and neutral species are considered separable into electronic and nuclear parts using the Born-Oppenheimer approximation, vibrational transitions are permitted during the electron exchange without disturbing the symmetry of the electrostatic interaction. This process is termed a symmetric charge-transfer reaction.

For the case in which  $A_2$  and  $B_2$  represent two different molecular species ( $A \neq B$ ) or in which the electronic states of the separated reactants and products are not the same ( $i \neq l$  or  $j \neq k$ ), the reaction is termed asymmetric. Such an interaction requires an electronic transition between the states described by the eigenfunctions of the reactant  $A_2^+ - B_2$  and product  $B_2^+ - A_2$  systems.

Experimentally, the difference between the electron transfer mechanisms of symmetric and asymmetric charge-transfer reactions is manifested in the kinetic energy dependence of the cross section for each process.<sup>8</sup> These differences can be illustrated by the atomic  $Ar^{++} - Ar$  system in which both symmetric and asymmetric reaction channels are accessible. The cross sections for the charge-transfer reactions of this system have been measured over a range of incident  $Ar^{++}$  kinetic energies of 2.0 to 8.0 keV and are discussed in Chapter V. The cross section for the symmetric (resonant) channel,

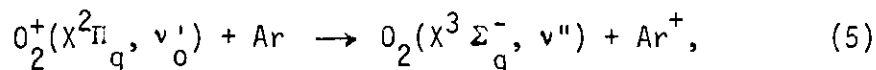


is found to increase approximately 50 per cent as the kinetic energy is reduced from 8 keV to 2 keV. In contrast, the cross section for the asymmetric (nonresonant) channel,



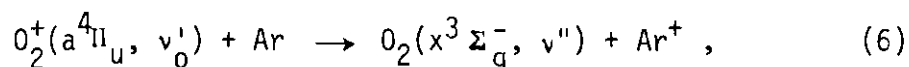
is considerably smaller than that of the symmetric channel and decreases by approximately 70 per cent over the same range of kinetic energies. This decrease in the cross section for the asymmetric channel as the relative velocity of the interaction is reduced, is a consequence of the electronic transition required for the electron transfer.

A similar behavior of the total cross section for molecular asymmetric charge-transfer reactions may not necessarily be observed at all incident ion kinetic energies. As a result of the large number of internal degrees of freedom present in a molecular reaction, numerous near-resonant product channels are accessible through the excitation or de-excitation of the electronic and vibrational states of the molecule. Consider the asymmetric charge-transfer reaction of  $\text{O}_2^+ - \text{Ar}$ , which is presented in Chapter IV. When the reactant  $\text{O}_2^+$  ion is initially in its ground electronic state, the reaction:



is nonresonant ( $\Delta E \sim 4 \text{ eV}$ ), and its cross section is observed to decrease as the kinetic energy of the incident ion is reduced from 3 keV to 0.7 keV. However, when the incident  $\text{O}_2^+$  ion is in its first

excited electronic state, the charge-transfer reaction:



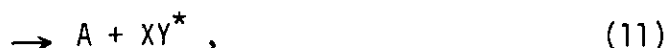
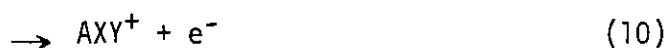
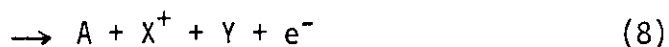
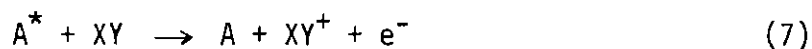
is near-resonant with one particular channel having an energy defect of only 0.00018 eV. The cross section for this process is significantly larger than that of reaction (5) and increases as the kinetic energy of the incident ion is decreased. The behavior of the asymmetric near-resonant charge-transfer channel is similar to that of a symmetric resonant reaction at these relatively high kinetic energies. In the limit of low velocity, however, the cross sections for both reactions (5) and (6) must approach zero, regardless of the magnitude of the energy defect.<sup>11</sup>

Resonant as well as near-resonant and non-resonant channels exist in symmetric molecular charge-transfer reactions. At a given kinetic energy, the relative contribution of the elastic and inelastic processes to the total charge-transfer cross section is governed by the magnitude of the energy defect and the vibrational overlap between the corresponding reactant and product states. A multistate impact parameter model can be utilized to describe the influence of reactant vibrational state on the symmetric charge-transfer reaction and to predict the final vibrational states of the products. Such a model is applied to the  $\text{N}_2^+ - \text{N}_2$ ,  $\text{CO}^+ - \text{CO}$ ,  $\text{O}_2^+ - \text{O}_2$ , and  $\text{NO}^+ - \text{NO}$  systems in Chapters II and III. The charge-transfer cross sections computed using the multistate model are compared with the total cross sections for these systems as a function of both initial reactant state and incident kinetic energy.

#### Metastable Reactions

The relaxation of an electronically excited atom by a diatomic

molecule at thermal energy can proceed through a number of product channels:<sup>7</sup>



where the asterisk denotes internal excitation of the neutral species. The dynamics of reactions (7) - (10) can be established through mass and velocity analysis of the charged products. The study of reaction (11), in which the electronic energy of the atom is converted into internal excitation of the diatomic molecule, is inherently more difficult since charged species are not produced. In principle, the partitioning of the excitation energy of the atom among the electronic, vibrational, and rotational states of the molecule can be determined from spectroscopic analysis of spontaneous radiative emission from these states. Recent use of time-resolved spectroscopy in a flowing afterglow has permitted the identification<sup>12</sup> of the rotational and vibrational distributions of molecular electronic states produced in the reaction, prior to their collisional deactivation. However, the relatively high pressures which must be maintained in the flow stream in order to achieve an adequate concentration of reactants, as well as the walls of the vacuum system itself, limit such investigations to states having short radiative lifetimes.

Because of the limitations on obtaining a complete experimental

product state identification, the possibility of using a statistical phase space description of reaction (11) to compute product state distributions was investigated. Such a model assumes that the interaction of the reactants results in the formation of an intermediate complex,



in which the internal energy of both reactants is distributed among all the internal degrees of freedom of the complex. Product state formation occurs through a decomposition of the complex governed by the constraints of conservation of energy and angular momentum. The probability that a product will be formed in a given electronic, vibrational, or rotational state is determined by that state's fraction of the total available phase space. The application of the statistical phase space model to the reaction of  $\text{Ar}(^3\text{P}_{2,0})$  atoms with ground nitrogen molecules is considered in Chapter VI. The computed vibrational and rotational distributions expected for the excitation of  $\text{N}_2$  into the  $\text{C}^3\Pi_u$  and  $\text{B}^3\Pi_g$  states by the metastable argon are compared with recent experimental observations.



## CHAPTER II

MOLECULAR CHARGE TRANSFER: EXPERIMENTAL AND THEORETICAL  
INVESTIGATION OF THE ROLE OF INCIDENT-ION VIBRATIONAL  
STATES IN  $N_2^+ - N_2$  AND  $CO^+ - CO$  COLLISIONS

Chapter II was published in the Journal of Chemical Physics,  
Volume 59, pages 5494 to 5510, 15 November, 1973. This article  
appears as Appendix II of this dissertation and also as Reference 18.

## CHAPTER III

MOLECULAR CHARGE TRANSFER II: EXPERIMENTAL AND THEORETICAL  
 INVESTIGATION OF THE ROLE OF INCIDENT-ION VIBRATIONAL  
 STATES IN  $O_2^+ - O_2$  AND  $NO^+ - NO$  COLLISIONS

Introduction

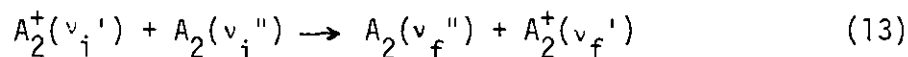
The relatively high abundance of  $O_2^+$  and  $NO^+$  ions in the equatorial ionosphere has been verified by measurements<sup>13-15</sup> using rocket-borne mass spectrometers. Investigations of the subsequent charge-transfer reactions are important not only to the detailed understanding<sup>16,17</sup> of the ionosphere but also to the development of theoretical models of molecular collisions in general. Experimental examination of the  $O_2^+ - O_2$  and  $NO^+ - NO$  collision systems provides an opportunity to critically evaluate the theoretical multistate impact parameter description of charge transfer and its corresponding low velocity limit. A previous study<sup>18</sup> of these two theoretical treatments was carried out for  $N_2^+ - N_2$  and  $CO^+ - CO$  charge-transfer reactions where: a) the similarity of fundamental vibrational frequencies in both the ionic and neutral species resulted in a grouping of nearly degenerate energy defects for the different vibrational product channels into various "bands" separated by approximately one vibrational quanta; and b) the reaction channels with largest vibrational overlaps were those associated with the near-resonant band. As a consequence of the above characteristics, convergence of the computed cross sections was attained by including only a minimal number of product channels in the wavefunction

expansion. It was also shown that because of the existence of a distinct near-resonant band with large vibrational overlaps, the low velocity approximation of Bates and Reid<sup>19</sup> could be successfully applied over a wide range of ion kinetic energies.

The present  $O_2^+ - O_2$  and  $NO^+ - NO$  systems are inherently different from those studied previously<sup>18</sup> in that: a) the dissimilar vibrational frequencies of the ion and neutral preclude the distinct grouping of different vibrational reaction channels into energy bands; and b) the magnitudes of vibrational overlaps for different channels is more evenly distributed over reaction pathways that have a wide range of energy defects. These features suggest that a larger number of nonresonant channels need be considered in order to obtain convergence of the calculated cross sections and that application of the low velocity approximation may be restricted to a more limited range of incident kinetic energies. The effectiveness of each theoretical approach is to be gauged by comparison with cross sections measured as a function of ion kinetic energy and reactant ion vibrational state.

### Theory

The multistate impact parameter treatment of the symmetric charge-transfer process



has been previously developed<sup>18,19</sup> and need only be briefly outlined. In (13), the incident molecular ion in vibrational level  $v_i'$  captures an electron from the molecular target, initially in vibrational level  $v_i''$ , to

form a neutral molecule in vibrational state  $v_f''$  with the neutral target converted to an ion in vibrational state  $v_f'$ . Only the ground electronic state of each species is considered to be involved at low impact energies and the rotational states of each diatomic are assumed unchanged. The wavefunction  $\Psi(t)$  for the internal motions, denoted by  $\underline{r}$ , is expanded as

$$\Psi(t) = \sum_{\alpha=D,X} \sum_n a_n^\alpha(t) \phi_n^\alpha(\underline{r}) \exp(-iE_n^\alpha t), \quad (14)$$

where  $\phi_n^\alpha$  are molecular eigenfunctions (with electronic, vibrational, and rotational parts) of the unperturbed Hamiltonian  $H_0^\alpha$  for the isolated molecular systems  $A_2^+$  and  $A_2$ , at infinite center-of-mass separation  $R_\infty$  with eigenenergies  $E_n^\alpha$ . The index  $\alpha$  labelling certain quantities denotes that the associated quantities refer to either direct channels D, where no charge transfer occurs, or to the exchange channels X. The outer summation is over all D and X channels. By inserting (14) into the appropriate time-dependent Schrodinger equation for the internal coordinates, and by working to lowest-order to two-center one-electron overlaps, the charge-transfer cross section is given by the following expression,

$$Q_{if}^X = 2\pi \int_0^\infty |C_f^X(r, \varphi)|^2 r dr, \quad (15)$$

in terms of the transition amplitudes  $C_f^\alpha(r, t) \equiv a_f^\alpha(t) \exp i\varphi(t)$ , where  $\varphi$  is a certain phase factor which need not be specified since the probabilities  $|C_f^\alpha|^2 = |a_f^\alpha|^2$  remain unaffected. The transition amplitudes are the solutions, for a given impact parameter  $\rho$ , of the set of first-order coupled differential equations,

$$i \frac{\partial C_\ell^\alpha}{\partial t}(r, t) = V(R) \sum_{m=1}^N P_{\ell m} C_m^{\bar{\alpha}}(r, t) \exp [i(E_\ell - E_m)t] \quad \ell=1,2,\dots,N, \quad (16)$$

subject to the boundary condition that only the direct channel  $i$  is occupied initially, i.e.  $C_m^D(r, -\infty) = \delta_{mi}$ ,  $C_m^X(r, -\infty) = 0$ . When  $\alpha$  denotes  $X$ ,  $\bar{\alpha}$  in (16) denotes  $D$  and vice-versa. The matrix elements  $P_{\ell m}$  are equal to  $F(v_\ell^+ v_m^-) F(v_m^+ v_\ell^-)$ , where  $F(v_i^+ v_n^-)$  is the vibrational overlap for the  $A_2^+(v_i^+) - A_2^-(v_n^-)$  transition. The maximum number of states included in the above set of equations is  $2N$ . The energy difference  $E_\ell^D - E_\ell^X$  between the  $\ell$ 'th direct,  $A_2^+(v_\ell^+) + A_2^-(v_\ell^-)$ , and the  $\ell$ 'th exchange,  $A_2^-(v_\ell^-) + A_2^+(v_\ell^+)$ , channels in (13) depends only on the initial rotational states of  $A_2$  and  $A_2^+$  and is negligible such that  $E_\ell^D = E_\ell^X = E_\ell$ . The excitation defect between vibrational channels  $\ell$  and  $m$  is therefore written as  $E_\ell - E_m$ .

It is important to note that not all  $O_2^+ - O_2$  electron capture collisions involving species in their ground electronic states are symmetrical resonance charge-transfer processes. For homonuclear systems, symmetrical resonance characteristics only occur in those collisions for which the axes of the ion and the neutral molecule are parallel. We assume, however, that the electronically integrated interaction  $V(R)$  responsible for charge transfer is orientation independent and is therefore related to the splitting between the gerade and ungerade eigenenergies of the molecular complex by

$$V(R) = 1/2 [\epsilon_g(R) - \epsilon_u(R)] . \quad (17)$$

From a knowledge of the Morse function

$$\epsilon_g(R) = D_e \{ \exp[-2\beta(R-R_e)] - 2 \exp[-\beta(R-R_e)] \} , \quad (18)$$

Sato<sup>20</sup> has proposed that the ungerade energy can be approximated by

$$\epsilon_u(R) = \frac{1}{2} D_e \{ \exp[-2\beta(R-R_e)] + 2[\exp -\beta(R-R_e)] \}, \quad (19)$$

where  $R_e$  is the internuclear distance corresponding to the potential minimum of depth  $D_e$  and  $\beta$  is a constant controlled by the shape of the potential. For the ion-molecule systems under consideration, the interaction energy of the symmetric (gerade) stationary state is determined by curvefitting (6) to the potential

$$V_{LJ4}(R) = 4\epsilon [(d/R)^{12} - (d/R)^6] - \alpha e^2/2R^4 \quad (20)$$

in which the Lennard-Jones parameters  $\epsilon$  and  $d$ , together with the polarizability,  $\alpha$ , are known.<sup>21</sup> Yang and Conway<sup>22</sup> have presented convincing evidence that  $V_{LJ4}(R)$  reproduces their observed data on the  $O_2^+ - O_2$  ion-molecule interaction. Values of the Morse parameters derived for the  $O_4^+$  system from (8) are  $\beta = 1.7010 \text{ \AA}^{-1}$ ,  $R_e = 3.3322 \text{ \AA}$ , and  $D_e = 0.079505 \text{ eV}$ . The  $NO^+ - NO$  interaction is also assumed to be spherically symmetric. The charge-transfer reactions for this system can therefore be considered symmetrical resonance with the total electronic angular momentum component  $\Lambda = 1$  along the  $NO(\Pi)$  internuclear axis unchanged. The values of the Morse parameters derived for the  $(NO)_2^+$  system from Equation (8) are  $\beta = 1.6605 \text{ \AA}^{-1}$ ,  $R_e = 3.3865 \text{ \AA}$ , and  $D_e = 0.078081 \text{ eV}$ . The variation of the splitting with distance  $R$  is expressed in terms of these parameters by the relation

$$\begin{aligned} \epsilon_g - \epsilon_u &= 1/2 D_e \exp[-2\beta(R-R_e)] - 3D_e \exp[-\beta(R-R_e)], \quad R > R^* \\ &= 0, \quad R < R^* \end{aligned} \quad (21)$$

where the cutoff at  $R^* \equiv R_e - \ln 6/\beta$  is imposed because of the (unphysical)

change of sign in  $\epsilon_g - \epsilon_u$ .

Knowledge of the gerade potential is mainly determined by the behavior of the ion-molecule interaction at intermediate and large  $R$ . The overall reliability of this potential can be assessed by comparing its short-range behavior with the repulsive potentials derived from scattering experiments of the neutral-neutral species. Such a comparison is made in Figures 1 and 2 for the  $O_2^+ - O_2$  and  $NO^+ - NO$  interactions, respectively. The solid curves in these figures represent  $\epsilon_g$  and  $\epsilon_u$  as a function of intermolecular separation, while the solid circles are those repulsive potentials derived from high energy neutral-neutral scattering experiments.<sup>23</sup> The dotted curves displayed in these figures represent the  $R$  dependence of the stationary state gerade-ungerade splittings ( $\epsilon_g - \epsilon_u$ ) which are to be used in the present computation of total charge-transfer cross sections.

### Calculations

#### Full Multistate Treatment

The solution of the coupled differential equations (16) describing the processes

$$O_2^+(X^2\Pi_g, v_0') + O_2(X^3\Sigma_g^-, v_0''=0) \rightarrow O_2(X^3\Sigma_g^-, v'') + O_2^+(X^2\Pi_g, v') \quad (22)$$

and

$$NO^+(X^1\Sigma^+, v_0') + NO(X^2\Pi_r, v_0''=0) \rightarrow NO(X^2\Pi_r, v'') + NO^+(X^1\Sigma^+, v') \quad (23)$$

involves knowledge of the vibrational overlaps,  $F(v_l, v_m)$ , and energy defects for transitions between initial states of the reactant and

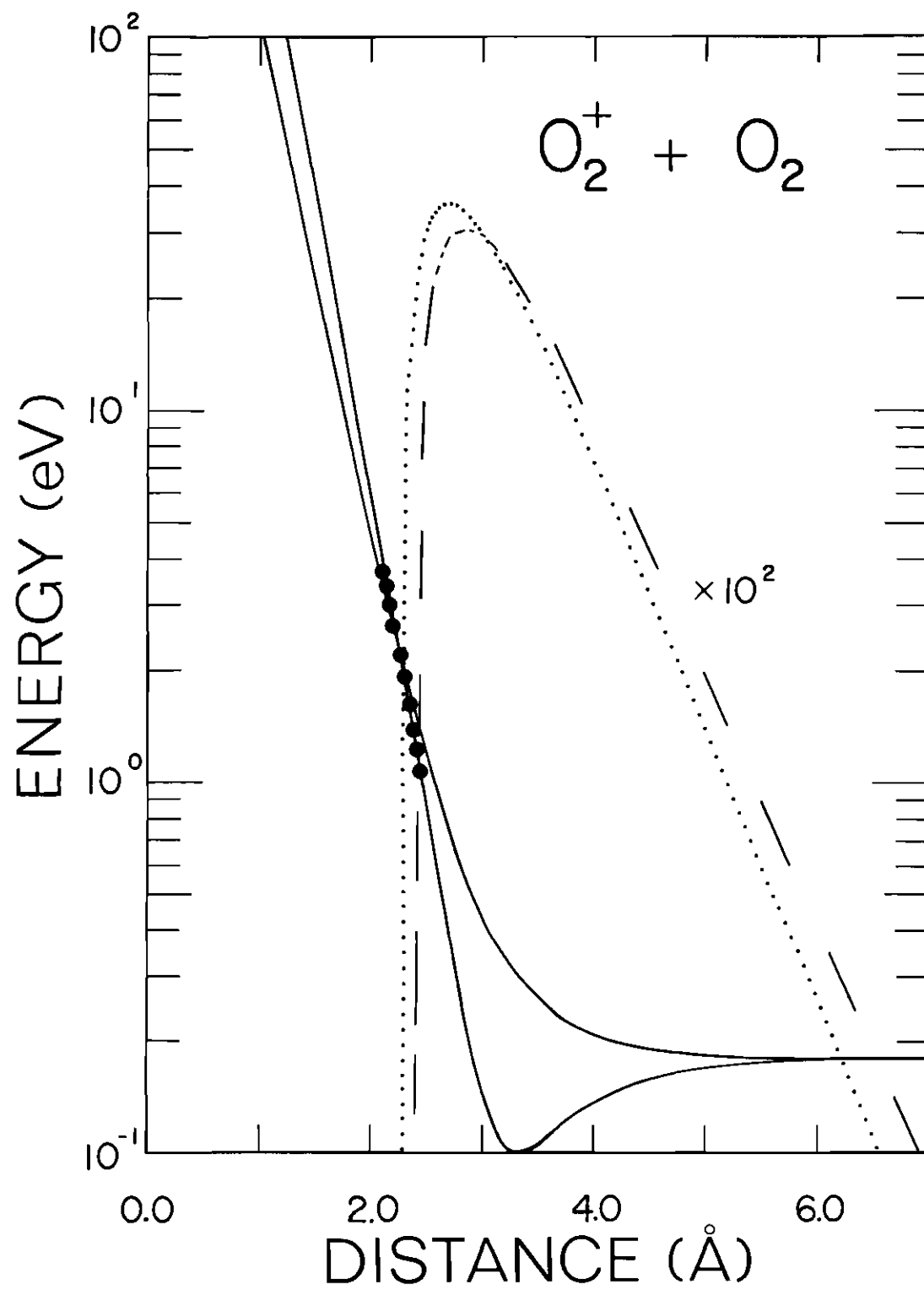


Figure 1. Interaction Potential Energy for  $O_2^+ - O_2$  Collisions.



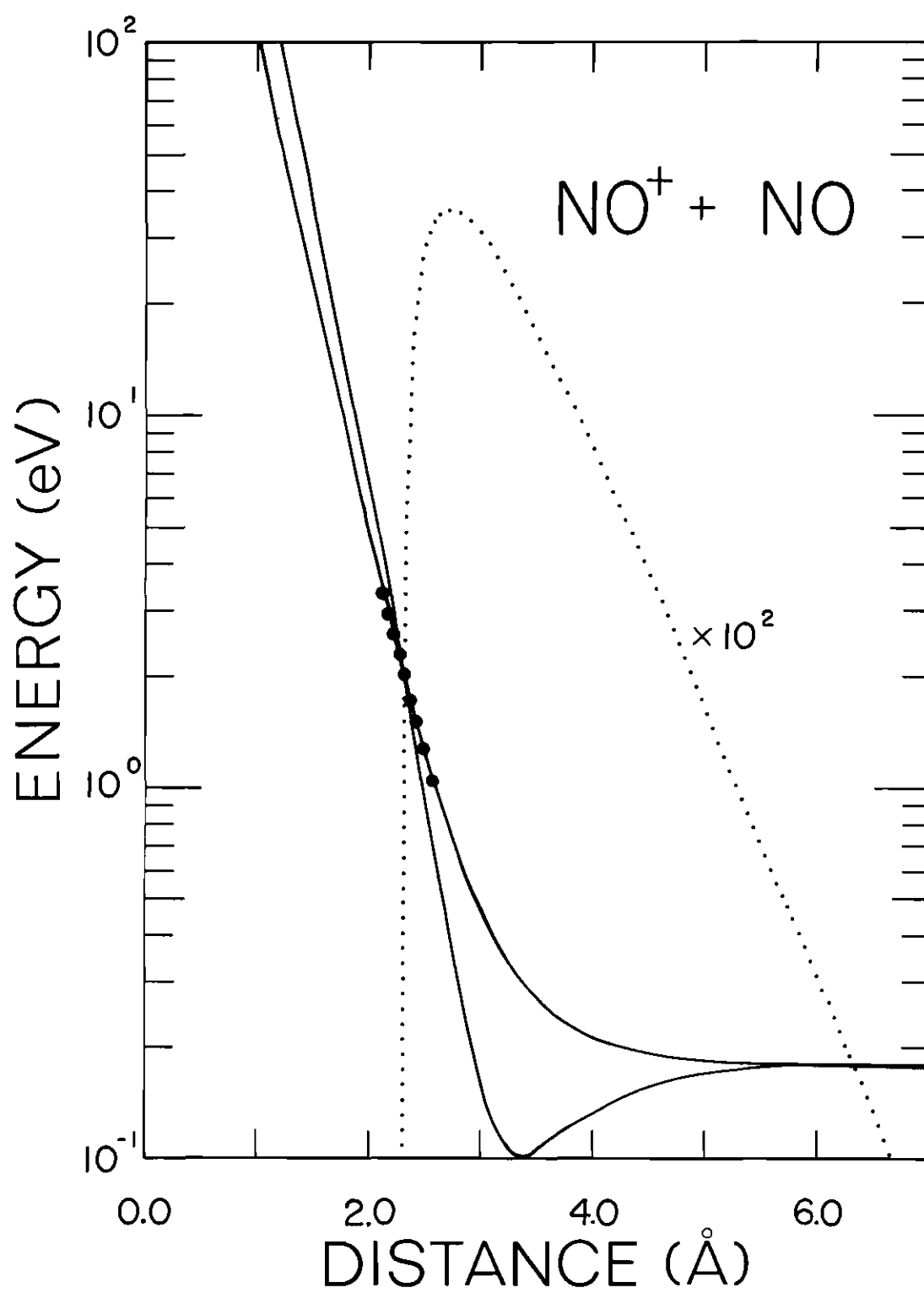


Figure 2. Interaction Potential Energy for  $\text{NO}^+ - \text{NO}$  Collisions.

final state product channels. Accurate Franck-Condon factors and sufficient spectroscopic data on the oxygen and nitric oxide systems<sup>24</sup> permit evaluation of the overlaps and energy defects, some of which are displayed in Tables 1 and 2. The magnitudes of the vibrational overlaps and energy defects are observed to be homogeneously distributed over a large number of product channels. This characteristic is in sharp contrast with that previously noted<sup>18</sup> for the  $N_2^+ - N_2$  and  $CO^+ - CO$  systems in which the largest vibrational overlaps occurred in the resonant and near-resonant product channels. This causes a significant increase in the difficulty of obtaining convergent multistate total cross sections.

The transition amplitudes,  $C_f^X(\rho, \epsilon)$ , are calculated as a function of impact parameter,  $\rho$ , by solving the coupled equations (16) numerically by the Adams-Moulton method. The transition probabilities  $|C_f^X(\rho, \epsilon)|^2$  in (15) are then integrated over impact parameter by Simpson's rule to obtain the partial charge-transfer cross sections  $Q_{if}^X$  for the production of specific final states of the ion and neutral for given initial states of the reactants. The total cross sections are then obtained by summing the partial cross sections of all possible product states.

The partial cross sections for charge transfer to a variety of final product states are displayed in Figure 3 as a function of ion kinetic energy for reactions between  $O_2^+(X^2\Pi_g, v_o'=0,2,4)$  incident ions and ground state oxygen molecules. For the  $O_2^+(X^2\Pi_g, v_o'=0)$  incident state shown in Figure 3A, the resonant channel  $(v_o', v_o'' | v'', v') = (0,0 | 0,0)$  clearly contributes most to the total charge-transfer cross section at the lower velocities. The small partial cross sections for the nonresonant channels

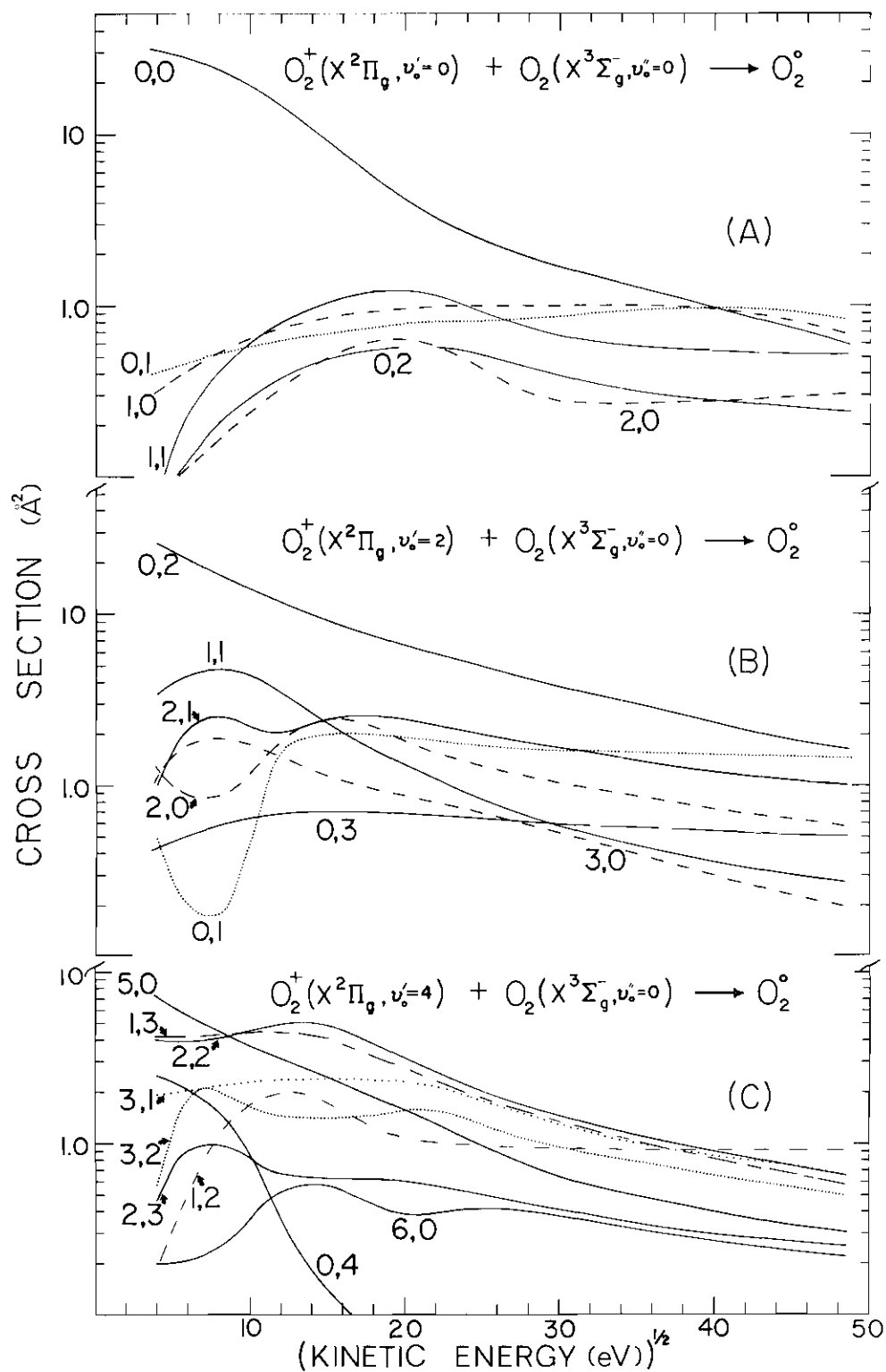


Figure 3. Partial Multistate Cross Sections as a Function of  $O_2^+$  Kinetic Energy. The Numbers (v'', v') Designate the Final Vibrational States of the Neutral and Ionic Products.

at low ion kinetic energies arise from the comparatively large energy defects that these channels have with respect to the  $(0,0|0,0)$  resonant channel (c.f. Table 1). At low energies, a large energy defect introduces oscillations in the exponential terms of (16), thereby causing a reduction in the partial cross section for the associated product channel. The two inelastic product channels closest to resonance,  $(0,0|1,0)$  and  $(0,0|0,1)$ , have relatively large energy defects  $\sim 0.2$  eV and their contribution to the total cross section is two orders of magnitude less than that of the resonant channel, in spite of their somewhat larger vibrational overlaps. Since the difference between the energy defects in these two channels is small, the relative magnitudes of their cross sections in the limit of low velocities is primarily controlled by their respective overlaps. At high velocity, the charge-transfer cross section is largely independent of the different energy defects with the result that both the  $(0,0|1,0)$  and  $(0,0|0,1)$  nonresonant cross sections exceed that for the resonant  $(0,0|0,0)$  channel, which has the smallest vibrational overlap.

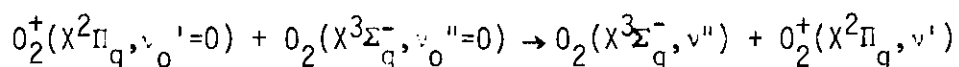
In Figure 3B, partial charge-transfer cross sections for the reactions of  $O_2^+(X^2\Pi_g, v_0'=2)$  are shown. Two reaction channels,  $(2,0|1,1)$  and  $(2,0|2,0)$  have energy defects within 0.08 eV of the resonant  $(2,0|0,2)$  channel and at the lower velocities, their relative contribution to the total cross section is larger than was observed in Figure 3A for nonresonant channels. However, these channels do not dominate the total cross section because their overlaps are small compared to that of the resonant channel. At higher kinetic energies, the relative contribution arising from each channel is mainly determined by relative vibrational

overlap.

Figure 3C illustrates the case of reactant  $O_2^+(X^2\Pi_g, v_o'=4)$  ions in which three product channels,  $(4,0|1,3)$ ,  $(4,0|5,0)$ , and  $(4,0|2,2)$ , have energy defects within only 0.06 eV of the resonant  $(4,0|0,4)$  channel. The overlaps for these three channels are an order of magnitude greater than that of the resonant channel (c.f. Table 1). As can be seen from Figure 3C, the combination of small energy defect and large overlap associated with these channels is responsible for their significant contribution to the total cross section at the higher kinetic energies.

The major contribution of nonresonant product channels in the  $O_2^+ - O_2$  system is indicative of the number of product channels that must be included in the solution of Equations (16) to obtain convergent total charge-transfer cross sections. The effect of including progressively more product states to compute total cross sections is shown in Table 3 for the reaction of ground state ions at two incident kinetic

Table 3. Effect of Nonresonant Product Channels on the Total Charge-Transfer Cross Section ( $\text{\AA}^2$ ) for the Reactions



Number of Product Channels	Ion Energy	
	733 eV	2210 eV
2	2.619	0.884
12	6.252	3.696
30	7.070	4.627
40	7.074	4.841
50		4.896

energies. As many as 50 product states must be considered before convergence of the cross section is approached, a situation which is to be compared with the corresponding calculations<sup>18</sup> for  $N_2^+ - N_2$  and  $CO^+ - CO$  where energetics and overlaps favored the resonant channel and only 12 product states were required for convergence of the multistate charge-transfer cross sections.

Charge-transfer cross sections computed for the reactions of  $NO^+(X^1\Sigma^+, v_0'=0,2,4)$  ions with ground state NO molecules to form products in specific vibrational states are displayed in Figure 4 as a function of reactant ion kinetic energy. The qualitative behavior of these partial cross sections is essentially that exhibited by the  $O_2^+ - O_2$  because the variations of vibrational overlaps and energy defects are similar for both systems. The slightly larger energy defects for nonresonant reaction channels in the  $NO^+ - NO$  system, however, is manifested by the reduced importance of these channels at low impact energies. Also, the impact energy at which the nonresonant channels begin to cause significant contribution to the total cross section becomes somewhat increased. The relative magnitudes of the partial cross sections for the resonant and nonresonant charge-transfer channels at the higher incident ion kinetic energies re-emphasizes the increase in influence of the vibrational overlap of each channel at these energies, with a corresponding reduction in the importance of energy defect. The effect of increasing the number of product states considered in solving the coupled equations (16) on the  $NO^+ - NO$  total charge-transfer cross section is illustrated in Table 4 for the case of both reactants in the ground vibrational state.

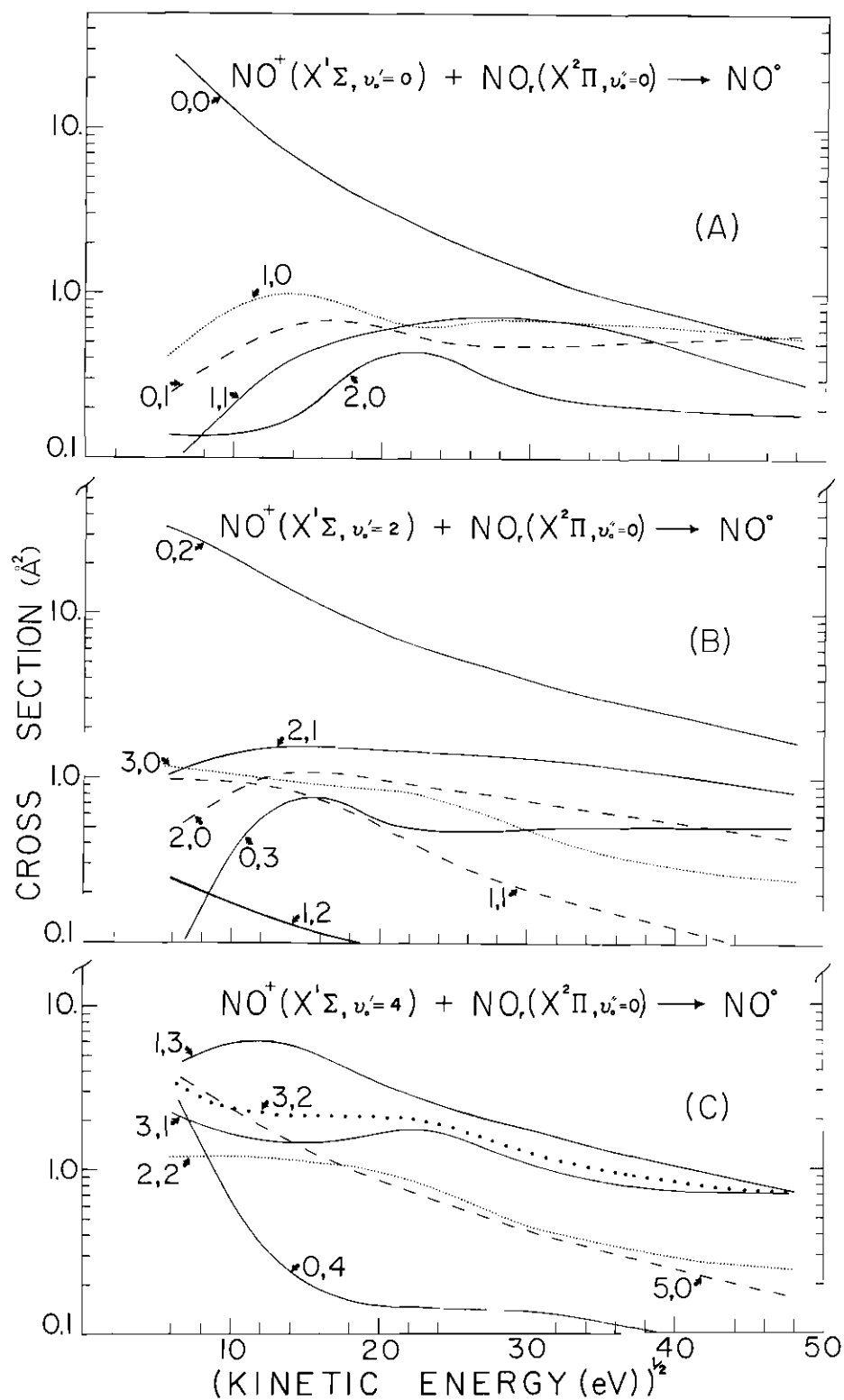


Figure 4. Partial Multistate Cross Sections as a Function of  $\text{NO}^+$  Kinetic Energy. The Numbers (v'', v') Designate the Final Vibrational States of the Neutral and Ionic Products.

Table 4. Effect of Nonresonant Product Channels on the Total Charge-Transfer Cross Section ( $\bar{A}^2$ ) for the Reactions  
 $\text{NO}^+(\text{X}^1\text{Z}^+, v_0'=0) + \text{NO}(\text{X}^2\Pi_r, v_0''=0) \rightarrow \text{NO}(\text{X}^2\Pi_r, v'') + \text{NO}^+(\text{X}^1\text{Z}^+, v')$

Number of Product Channels	Ion Energy	
	733 eV	2210 eV
2	1.900	0.638
12	4.711	2.489
20	5.093	3.016
30	5.224	3.395
40	5.220	3.497
50		3.524

#### Low Velocity Limit

In the limit of low velocities, only channels with vanishing energy defect contribute to the charge-transfer cross sections, with the result that  $E_\ell - E_m$  in (16) can be neglected to give

$$i \frac{\partial C_\ell^a}{\partial t}(r, t) = V(R) \sum_{m=1}^B P_{\ell m} C_m^a(r, t), \quad \ell = 1, 2, \dots, B, \quad (24)$$

where  $B$  is the number of resonant or near-resonant channels. It has been shown<sup>18,19</sup> that these equations can be uncoupled by diagonalizing the overlap matrix,  $\underline{P} = [P_{\ell m}]$ , and solved exactly to give

$$Q^X(i \rightarrow B) = 2\pi \sum_{n=1}^B x_{in}^2 \int_0^\infty r \sin^2\left\{\frac{\pi n}{2v} D_e \exp(\beta R_e)\right\} \times \\ \int_{\max(r, R^*)}^\infty [6\exp(-\beta R) - \exp(\beta R_e) \exp(-2\beta R)] R(R^2 - r^2)^{-\frac{1}{2}} dR \} dr,$$

the total cross section for charge transfer from initial states



$i(v_i', v_i'')$  to all near-resonant final states  $B$ . The eigenvalues,  $\tilde{\Pi} = [\tilde{\Pi}_n]$ , and associated eigenvectors,  $\tilde{\chi} = [\chi_{in}]$ , of the overlap matrix  $P$  are defined by the similarity transformation

$$\tilde{\Pi} = \tilde{\chi}^{-1} P \tilde{\chi} = \tilde{\chi} \tilde{P} \tilde{\chi} . \quad (26)$$

For the case of  $\rho > R^*$ , the integral over  $R$  is evaluated in terms of modified Bessel functions  $K_1(X)$  so that the argument of the sine in (13) becomes

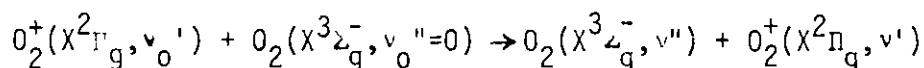
$$\frac{\Pi_n}{2v} = \rho D_e \exp(\rho R_e) [6K_1(\beta r) - \exp(\beta R_e) K_1(2\beta r)] \quad (27)$$

The above eigenvectors and eigenvalues of the overlap matrix  $P$  are obtained by the Jacobi method. The integrals in (25) over  $R$  for  $\rho < R^*$  and over  $\rho$  are evaluated numerically by Simpson's rule. These total charge-transfer cross sections were close to those calculated from the exact multistate equations (16) over a wide range of kinetic energies for the  $N_2^+ - N_2$  and  $CO^+ - CO$  systems<sup>18</sup> when the reactant ions were initially in the first several vibrational levels. The band structure of the energy defects in these systems allowed a natural separation of the resonant or near-resonant channels  $B$  from nonresonant product channels. Due to the distribution of the energy defects in the  $O_2^+ - O_2$  and  $NO^+ - NO$  systems; however, a priori selection of the near-resonant channels to be included in the summation of (24) is less definitive. For low velocity limit calculations in the oxygen and nitric oxide systems, those product channels having energy defects within 0.082 eV and 0.1 eV of resonance are chosen as degenerate. The validity of such a choice is dependent

upon the degree of coupling among the product channels which, as was shown in Figures 3 and 4, varies with both reactant ion state and kinetic energy. However, the cross sections computed via the low velocity approximation are insensitive to the inclusion of other channels having energy defects in slight excess of the 0.083 eV and 0.1 eV limits. Total charge-transfer cross sections calculated using the full multistate treatment (M) and the low velocity limit (LVL) are presented in Tables 5 and 6 for reactions (22) and (23), respectively. Figures 5

Table 5. Total Charge-Transfer Cross Sections ( $\text{\AA}^2$ )

Calculated for the Reactions

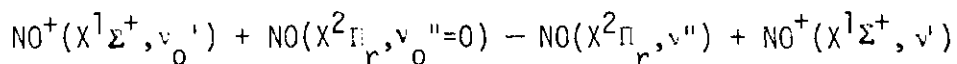


$v_0'$	METHOD*	Ion Energy				
		49 eV	156 eV	400 eV	733 eV	2210 eV
0	LVL	26.93	11.12	4.69	2.62	0.88
	M	27.36	13.97	9.34	7.07	4.90
1	LVL	30.07	27.35	15.83	9.73	3.55
	M	32.12	25.66	16.77	12.36	7.33
2	LVL	22.68	23.17	13.84	8.57	3.15
	M	27.46	21.80	15.43	13.06	7.61
3	LVL	33.41	25.50	13.35	7.95	2.83
	M	25.44	23.56	15.23	12.17	7.06
4	LVL	28.72	18.43	9.32	5.51	1.95
	M	21.10	19.64	13.36	12.03	6.79

\*Method LVL refers to the low velocity limit where only product channels within 0.082 eV of energy resonance are included and are assumed to be degenerate. Method M refers to the multistate treatment in which full account is taken of near-resonant and nonresonant product channels.

Table 6. Total Charge-Transfer Cross Sections ( $\text{\AA}^2$ )

Calculated for the Reactions



$v_0'$	METHOD*	Ion Energy				
		49 eV	156 eV	400 eV	733 eV	2210 eV
0	LVL	21.90	8.32	3.43	1.90	0.64
	M	23.37	10.51	6.57	5.22	3.52
1	LVL	29.52	24.84	13.67	8.27	2.98
	M	33.60	23.57	14.59	10.37	5.89
2	LVL	24.78	20.33	12.60	7.96	2.98
	M	33.15	21.50	14.37	11.04	6.19
3	LVL	33.43	26.32	14.01	8.38	3.00
	M	23.19	19.39	12.60	10.51	5.84
4	LVL	30.89	20.86	10.85	6.47	2.30
	M	17.20	13.38	10.42	9.70	5.78

\*Method LVL refers to the low velocity limit where only product channels within 0.1 eV of energy resonance are included and are assumed to be degenerate. Method M refers to the multistate treatment in which full account is taken of near-resonant and nonresonant product channels.

and 6 illustrate the energy variation of the total charge-transfer cross sections for reactions (22) and (23) in which the reactant  $\text{O}_2^+(\text{X}^2\Pi_g)$  and  $\text{NO}^+(\text{X}^1\Sigma^+)$  ions are initially in vibrational levels  $v_0' = 0, 2, 4$ . The solid curves represent (convergent) total cross sections obtained from solution of the multistate equations (15) and (16) in which explicit account is taken of the energy defects and all possible couplings between product channels. The dotted curves represent the total cross sections computed in the low velocity limit (25) - (27) for which only near-resonant

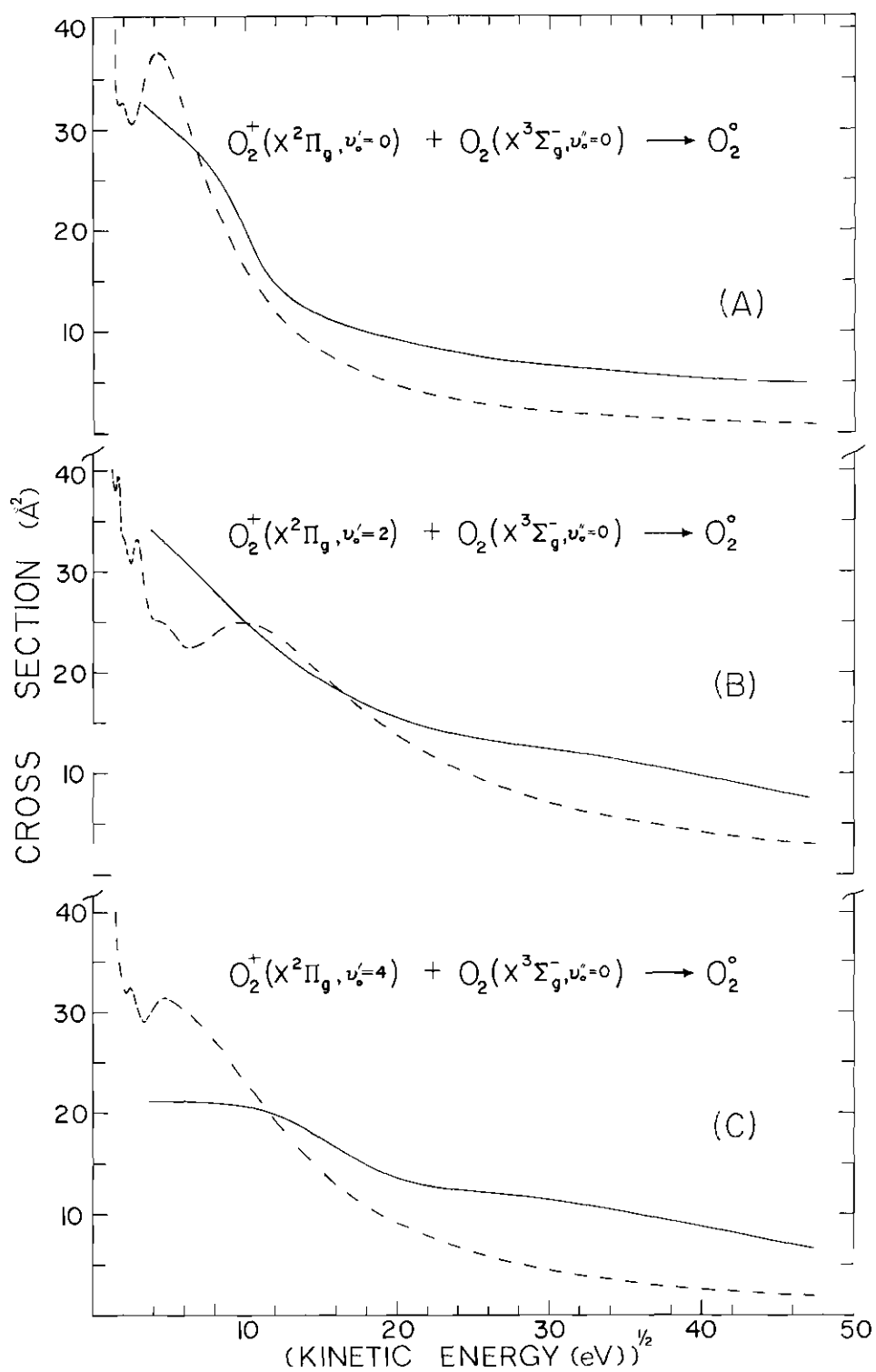


Figure 5. Total Charge-Transfer Cross Sections for Three Reactant  $O_2^+$  Vibrational States Computed using Multistate Treatment (Solid Curves) and the Low Velocity Approximation (Dashed Curves).

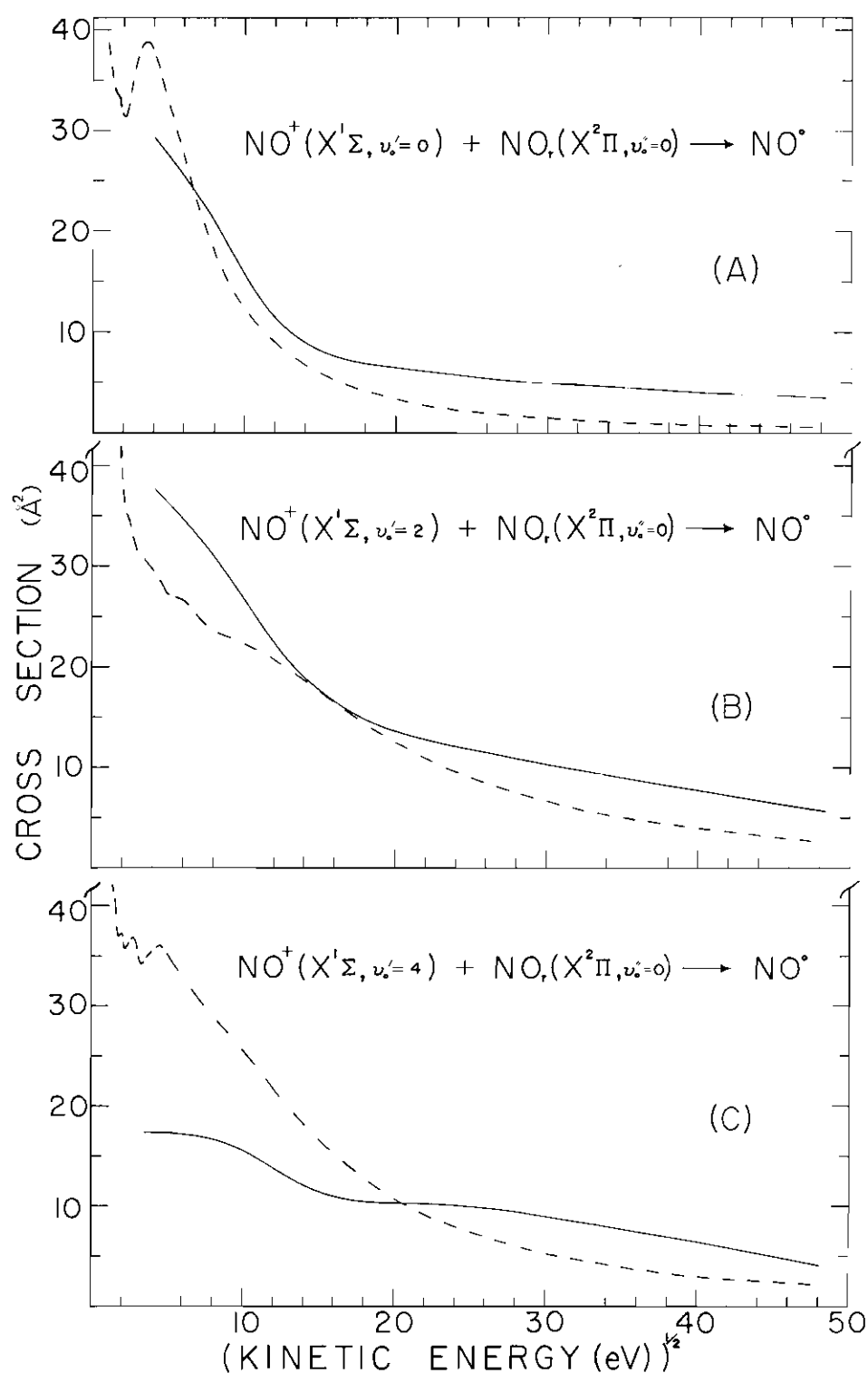


Figure 6. Total Charge-Transfer Cross Sections for Three Reactant NO<sup>+</sup> Vibrational States Computed using Multistate Treatment (Solid Curves) and the Low Velocity Approximation (Dashed Curves).

channels are considered and their energy defects neglected. As observed in  $\text{CO}^+ - \text{CO}$  and  $\text{N}_2^+ - \text{N}_2$  systems, the cross sections computed in the low velocity limit approach those for the full multistate treatment at low kinetic energies except for the case of highly excited incident ions. Similarly, at higher energies the low velocity approximation underestimates the total cross section due to the neglect of the higher inelastic channels which become increasingly important both for increased incident energy and higher vibrational state of the incident ion. Due to the stronger coupling with the nonresonant product channels this underestimate is more severe for the  $\text{O}_2^+ - \text{O}_2$  and  $\text{NO}^+ - \text{NO}$  reactions than for the systems previously<sup>18</sup> investigated.

### Experimental Analysis

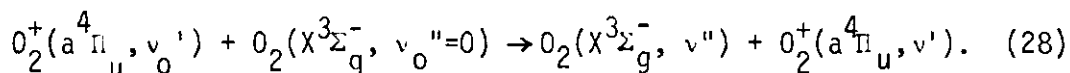
The preceeding computations carried out on the oxygen and nitric oxide systems enable us to examine the influence of energetics and overlaps in the charge-transfer process and further test the multistate model by comparing the theoretical cross sections with those measured in laboratory investigations. The effect of reactant ion vibrational energy on the charge-transfer reaction can be examined experimentally for the case of both the oxygen and nitric oxide reactions since ionization of the neutral molecules by low energy electron impact produces ions with broad vibrational distributions. The relative abundance of each vibrational level in the reactant ion beam can be changed in a controlled manner by varying the energy of the ionizing electron beam.

A previously described<sup>18</sup> time-of-flight apparatus has been used to monitor the neutral products from charge-transfer reactions.

Ionizing electrons emitted from a thorium oxide filament were accelerated to form a beam spatially confined by an external collimating magnet. The kinetic energy of the electron beam was variable from 2 to 100 eV with a full-width-half-maximum energy distribution of approximately 0.3 to 0.5 eV. The absolute energy of the beam, calibrated relative to the rare gas ionization potentials, was reproducible to within  $\pm 0.15$  eV. Reactant ions produced in the electron impact process are pulsed out of the source, accelerated to the desired kinetic energy, and focused into a field-free drift region in which charge-transfer reactions occur. Neutral gas pressures in this collision region were sufficiently low to insure that reactions take place only through bimolecular encounters. Separation of the fast neutral products of the charge-transfer reactions from the unreacted primary ion beam was accomplished by the use of a grid assembly placed directly in front of the detector. A deceleration voltage placed on this grid assembly gave the ionic species a longer arrival time than the fast neutral products of the same mass, permitting the flux of each species to be monitored by gating the output of the electron multiplier detector with respect to the ion formation pulse. The gate pulses were sufficiently narrow to insure products from the competing dissociative channels<sup>25,26</sup> were not similarly detected.

In order to compare charge-transfer cross sections computed for discrete reactant ion states with measured total cross sections, the state composition of the reactant ion beam must be established as a function of the ionizing electron energy. The formation of  $O_2^+$  in the ground  $X^2\Pi_g$ , and excited  $a^4\Pi_u$ ,  $A^2\Pi_u$ ,  $b^4\Sigma_g^-$ ,  $B^2\Sigma_g^-$  states is clearly observed in photoelectron spectroscopy<sup>27-32</sup> as well as electron impact

experiments<sup>33-36</sup> in which spectral techniques are used to monitor spontaneous radiative processes from the excited states. The radiative lifetimes of the  $A^2\Pi_u$ ,  $b^4\Sigma_g^-$ , and  $B^2\Sigma_g^-$  states are sufficiently short<sup>24,36</sup> for spontaneous decay to occur prior to the ions undergoing reaction in our experiment. Franck-Condon factors<sup>24</sup> for these transitions indicate the vibrational distribution of the long-lived  $O_2^+(a^4\Pi_u)$  state is very broad due to its mode of production in direct ionization processes as well as by radiative  $b^4\Sigma_g^- \rightarrow a^4\Pi_u$  transitions. Moreover, the percentage of the  $a^4\Pi_u$  state ions in an  $O_2^+$  ion beam formed at electron impact energies above approximately 20 eV is large.<sup>37,38</sup> Thus, an attempt to compute the total charge-transfer cross section for an ion beam formed at electron energies above the ionization threshold of the  $a^4\Pi_u$  state requires, as a minimum, explicit knowledge of cross sections for the additional processes



The smaller vibrational spacing of the  $a^4\Pi_u$  state and the broader distribution of vibrational overlaps between it and the  $X^3\Sigma_g^-$  state indicate a stronger degree of coupling is to be expected among the product channels than was observed in reaction (22). Preliminary calculations of the multistate charge-transfer cross section for reaction (28) with the reactant ion in its ground vibrational state reflect the strong coupling among the product channels and suggest considerably more than 50 states must be included in the calculation to achieve convergence; an investment of computer time not justified in the absence of a reliable interaction potential for the excited species. We therefore limit our comparison



between theory and experiment to ion beams formed at electron energies below the ionization potential of the  $O_2^+(a^4\Pi_u)$  state. The relative vibrational populations of  $O_2^+(X^2\Pi_g)$  ions formed by direct ionizing transitions from the ground state neutral molecule are estimated<sup>18</sup> as a function of ionizing electron energy from the appropriate Franck-Condon factors.<sup>24</sup> Electron<sup>39-41</sup> and photon<sup>30-32,42-44</sup> impact studies of oxygen, however, have observed significant quantities of  $O_2^+(X^2\Pi_g)$  state ions formed in autoionizing transitions from Rydberg states of the neutral molecule<sup>45</sup> at excitation energies above 12.3 eV. Retarding potential photoelectron spectra<sup>44</sup> of the major autoionizing transitions in the region of 12.3 to 13.2 eV have recently identified the vibrational levels of the  $O_2^+(X^2\Pi_g)$  state populated in these processes. The reactant  $O_2^+$  ion beam vibrational level population distribution at each ionizing electron energy thus represents contributions from both direct and autoionizing transitions.

Theoretical studies<sup>46</sup> of the  $NO^+$  ion have predicted a large number of low energy excited states, many of which have been observed in the photoelectron spectrum<sup>47,48</sup> of the molecule. Examination of radiative emission from  $NO^+$  ion beams produced by electron impact has identified formation of the  $A^1\Pi$ <sup>49,50</sup> and  $b^3\Pi$ <sup>51</sup> excited states. The lifetime of the  $A^1\Pi$  state<sup>52</sup> is sufficiently short (56 nsec) to insure complete radiative cascade to the ground  $X^1\Sigma^+$  state prior to the ions leaving the source region of our apparatus. Ions formed in the long-lived (160  $\mu$ sec)<sup>51</sup>  $b^3\Pi$  state remain as a component of the reactant beam. A comparison of the estimate for the  $b^3\Pi$  state ionization cross section<sup>49</sup> to the total ionization cross section<sup>53</sup> for  $NO^+$  indicates this state represents only

a small percentage of the total population of long-lived  $\text{NO}^+$  excited states<sup>54,55</sup> formed by high energy electron impact. The scarcity of spectroscopic data on the excited states of  $\text{NO}^+$  discourages a quantitative estimate of ion beam state composition for electron impact energies above approximately 15 eV. The vibrational levels of  $\text{NO}^+(\text{X}^1\Sigma^+)$  populated in direct ionizing transitions from the ground state molecule are calculated<sup>18</sup> from the corresponding Franck-Condon factors.<sup>24</sup> Weak autoionizing transitions from molecular Rydberg states are observed in the region of the  $\text{NO}^+(\text{X}^1\Sigma^+)$  threshold in both photon<sup>56</sup> and electron impact<sup>57</sup> ionization studies. Perturbation of the vibrational distribution produced by direct ionizing transitions by these processes, however, is insignificant. More intense autoionization is observed in the photoionization spectrum<sup>58,59</sup> of NO at excitation energies above approximately 11 eV. A number of molecular Rydberg states<sup>47,59</sup> have been assigned from these spectra, but overall identification of the autoionizing transitions is largely incomplete. Consequently, we limit our estimate of the  $\text{NO}^+(\text{X}^1\Sigma^+)$  vibrational state composition to electron impact energies between threshold at 10.6 eV.

#### Comparison Between Theory and Experiment

The kinetic energy dependence of the total charge-transfer cross sections for reaction (22), weighted to reflect the vibrational state distribution of an  $\text{O}_2^+(\text{X}^2\Pi_g)$  reactant ion beam formed by 13 eV electron impact ionization, is shown in Figure 7. Cross sections computed using the low velocity approximation (24) and the full multistate equations (16) are denoted by circles and squares, respectively. The figure

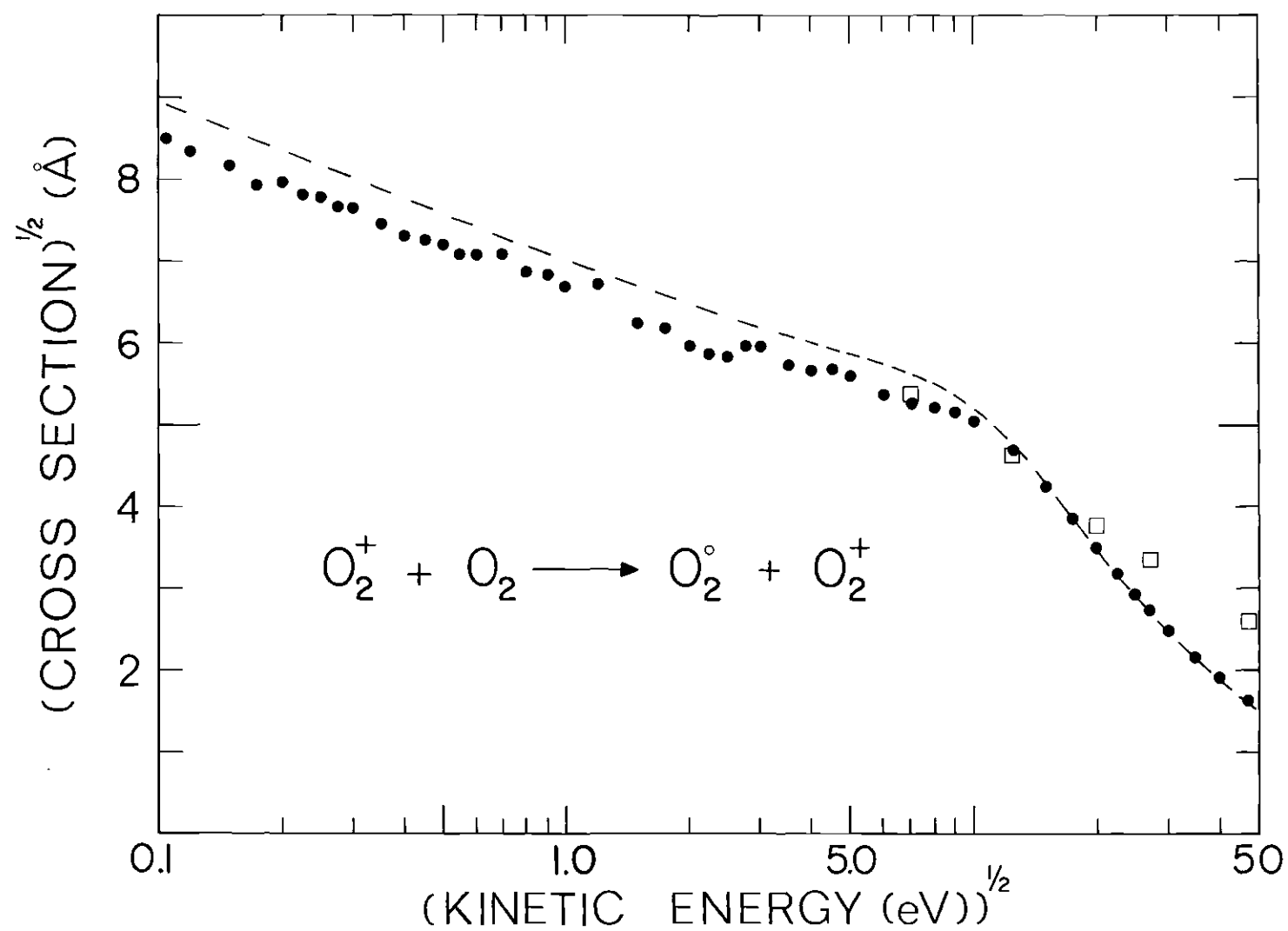


Figure 7. Total  $\text{O}_2^+ - \text{O}_2$  Charge-Transfer Cross Sections for a Reaction Ion Vibrational Distribution Characteristic of 13 eV Electron Impact Ionization.

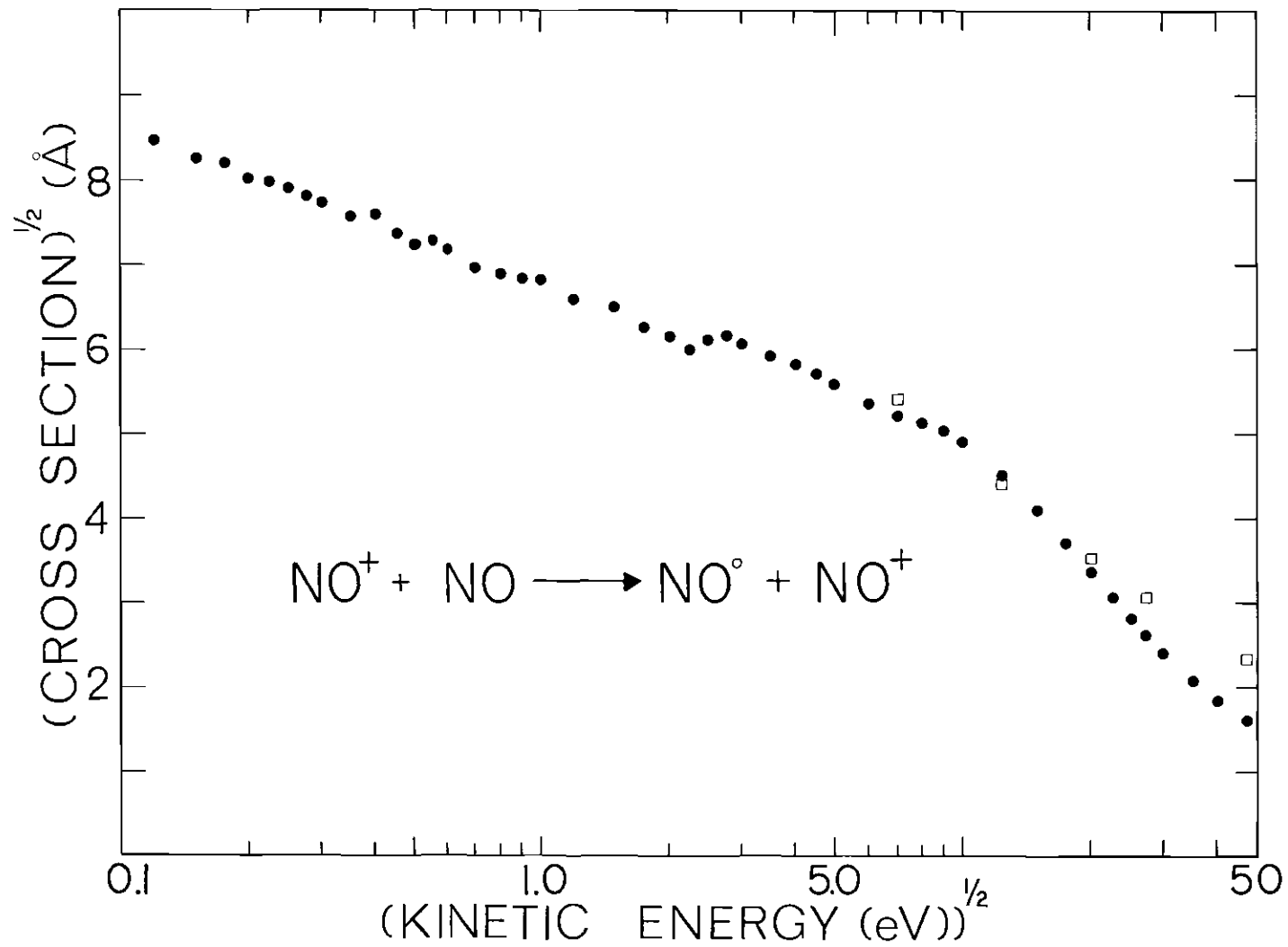


Figure 8. Total  $\text{NO}^+$  - NO Charge-Transfer Cross Sections for a Reactant Ion Vibrational Distribution Characteristic of 13 eV Electron Impact Ionization.

indicates an approximate exponential relationship between the square root of the total cross section and the velocity of impact. The major change of slope in the region of 200 eV exhibited by the cross sections in the low velocity approximation is attributed to the neglect of important inelastic contributions at the higher kinetic energies arising from the nonresonant product channels. In order to assess the role of the interaction potential in determining the kinetic energy region over which the low velocity approximation is applicable, the above calculations were repeated by using different molecular parameters for the gerade-ungerade splitting. The results computed with an interaction potential for the  $N_2^+ - N_2$  system<sup>18</sup> (represented by the dashed curve in Figure 1), but using the  $O_2^+ - O_2$  overlaps and energy defects, are given by the dashed curve in Figure 7. Comparison of these two curves in Figure 7 demonstrates quite markedly the apparent insensitivity of the cross section to changes in the interaction potential. In Figure 8, the variation of the total charge-transfer cross sections with kinetic energy is shown for the  $NO^+ - NO$  reaction (23), weighted for a reactant  $NO^+(X^1\Sigma^+)$  vibrational level distribution characteristic of 11 eV electron impact ionization. Because nonresonant channels with favorable vibrational overlaps and relatively large energy defects are neglected in the low velocity approximation, these cross sections (circles) diverge from the multistate values (squares) at incident ion kinetic energies above approximately 200 eV.

In order to examine the ability of the multistate model to describe the role that reactant ion vibrational energy plays in these processes, the vibrational state distribution of the incident ion beam

was systematically varied by changing the electron energy from threshold to 90 eV and the charge-transfer process measured. The  $O_2^+ - O_2$  cross sections at incident kinetic energies of 1175, 733, and 400 eV are shown in Figures 9A, B, and C respectively. The cross sections measured at 90 eV electron impact have been normalized to 100 in this figure. At each reactant ion kinetic energy, the experimental total charge-transfer cross sections increase sharply as the ionizing electron energy is increased above the  $v_0'=0$  threshold. As the electron energy is raised, the fraction of the reactant  $O_2^+$  beam in the higher vibrational levels is increased with a corresponding increase in the measured cross sections, as expected from the data shown in Table 5. The theoretical multistate cross sections for (22) with  $v_0' = 0-4$  are weighted according to the vibrational population of the incident ion beam at the various electron energies and are given as the solid lines in Figure 9. Lack of information about the autoionizing states of oxygen above 13.2 eV does not permit direct comparison between theory and experiment at the higher electron energies. Moreover, at electron energies above 16.1 eV, the  $O_2^+$  ions can be formed in the long-lived  $a^4\Pi_u$  state. The decrease observed in these total cross sections as the electron energy is increased above 16 eV in the 400 eV incident kinetic energy data, Figure 9C, demonstrates the increasing population<sup>37,38</sup> of  $O_2^+(a^4\Pi_u)$  ions which have relatively small charge-transfer cross sections at low kinetic energies. At higher kinetic energies, the contribution from nonresonant channels with favorable overlaps in reaction (28) approaches that for ground state ions

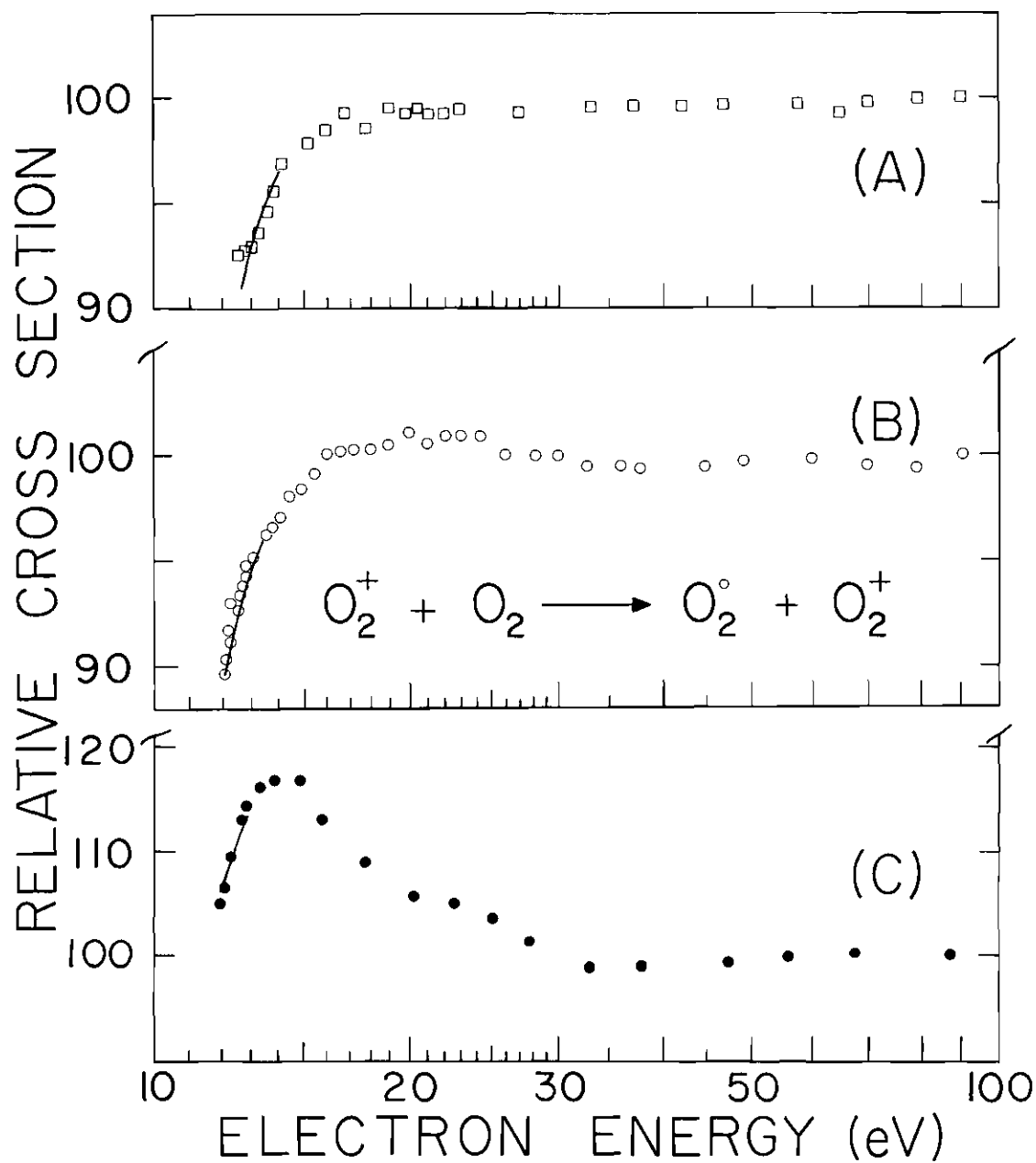


Figure 9. Cross Sections Measured for  $O_2^+ - O_2$  Charge-Transfer Reactions as Function of Ionizing Electron Energy. Those Calculated using the Multistate Model are Given as Solid Curves.

with the result that the relative cross sections are almost constant for electron energies above 16 eV. Quantitative examination of the multistate model at these higher electron energies has not been fully pursued since prohibitively long computer times would be required to obtain convergent cross sections for each vibrational level of the  $O_2^+(a^4\Pi_u)$  reactant ions. However, for electron energies between threshold and 13.2 eV, where comparisons can be made, the vibrational dependence of the total charge-transfer cross sections predicted by the multistate model is fully consistent with experimental measurements. A similar examination of the effect of vibrational energy on  $NO^+ - NO$  charge-transfer reactions is shown in Figure 10 where the relative cross sections are found to be increasing functions of ionizing electron energy throughout the 400 - 1175 eV range of ion kinetic energy. This behavior is reproduced in the theoretical electron energy dependence, given by the solid lines, which are computed using the  $NO^+(X^1\Sigma^+)$  vibrational distribution and the multistate cross sections of Table 6. The difference exhibited by the curves in Figures 9C and 10C can be attributed to the presence of long-lived electronically excited states of  $NO^+$  which are expected to have large vibrational overlap with  $NO(X^2\Pi_r)$  in resonant and near-resonant channels.

Total experimental and theoretical charge-transfer cross sections for these systems are displayed in Figures 11 and 12 as a function of incident ion kinetic energy. In these figures, the solid and dotted curves are computed from the full multistate treatment (16) and the low velocity approximation (24), respectively, and have each been weighted according to the reactant  $O_2^+(X^2\Pi_g)$  and  $NO^+(X^1\Sigma^+)$  vibrational distributions



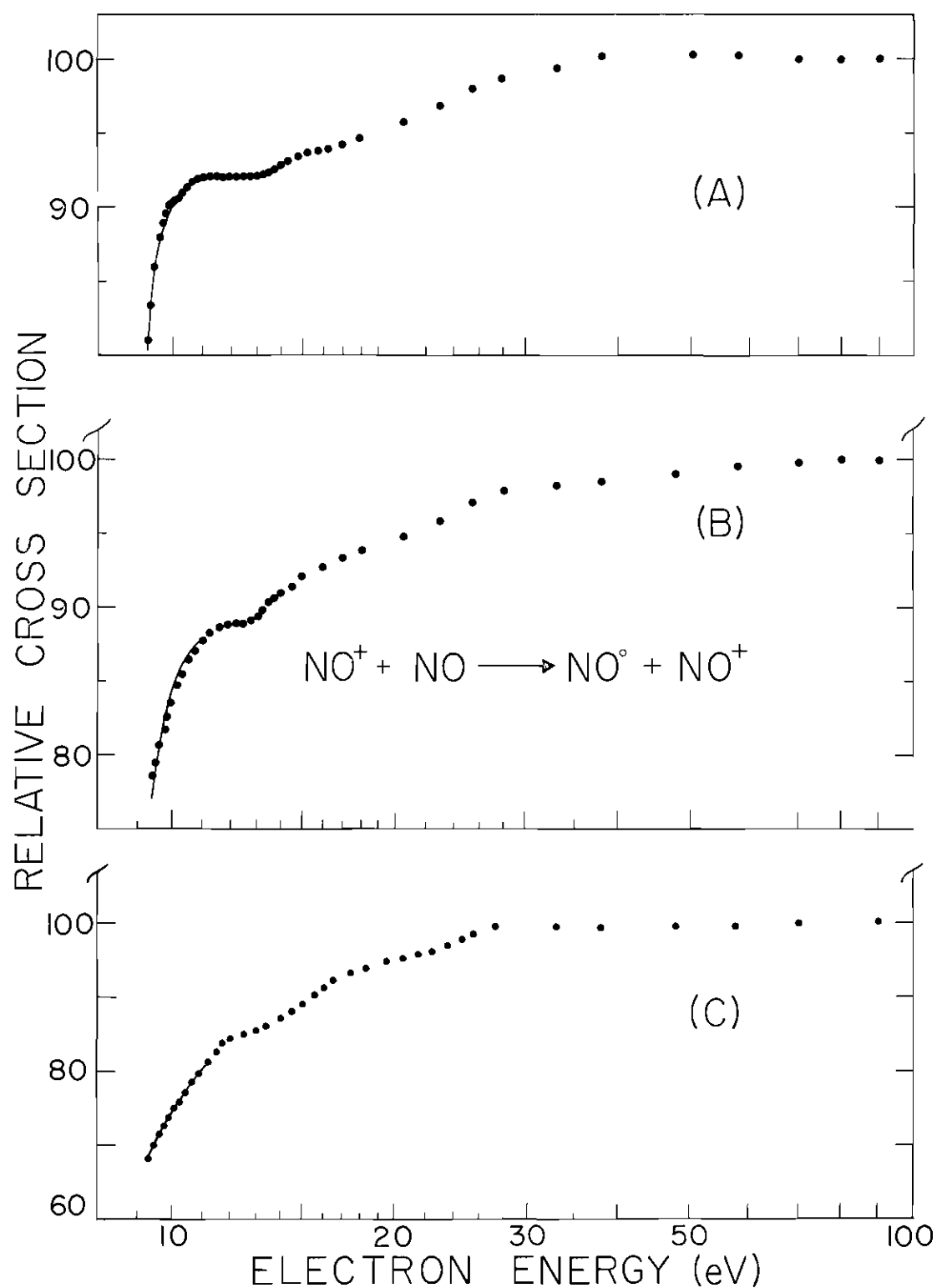


Figure 10. Cross Sections Measured for  $\text{NO}^+$  -  $\text{NO}$  Charge-Transfer Reactions as Function of Ionizing Electron Energy. Those Calculated using the Multistate Model are given as Solid Curves.

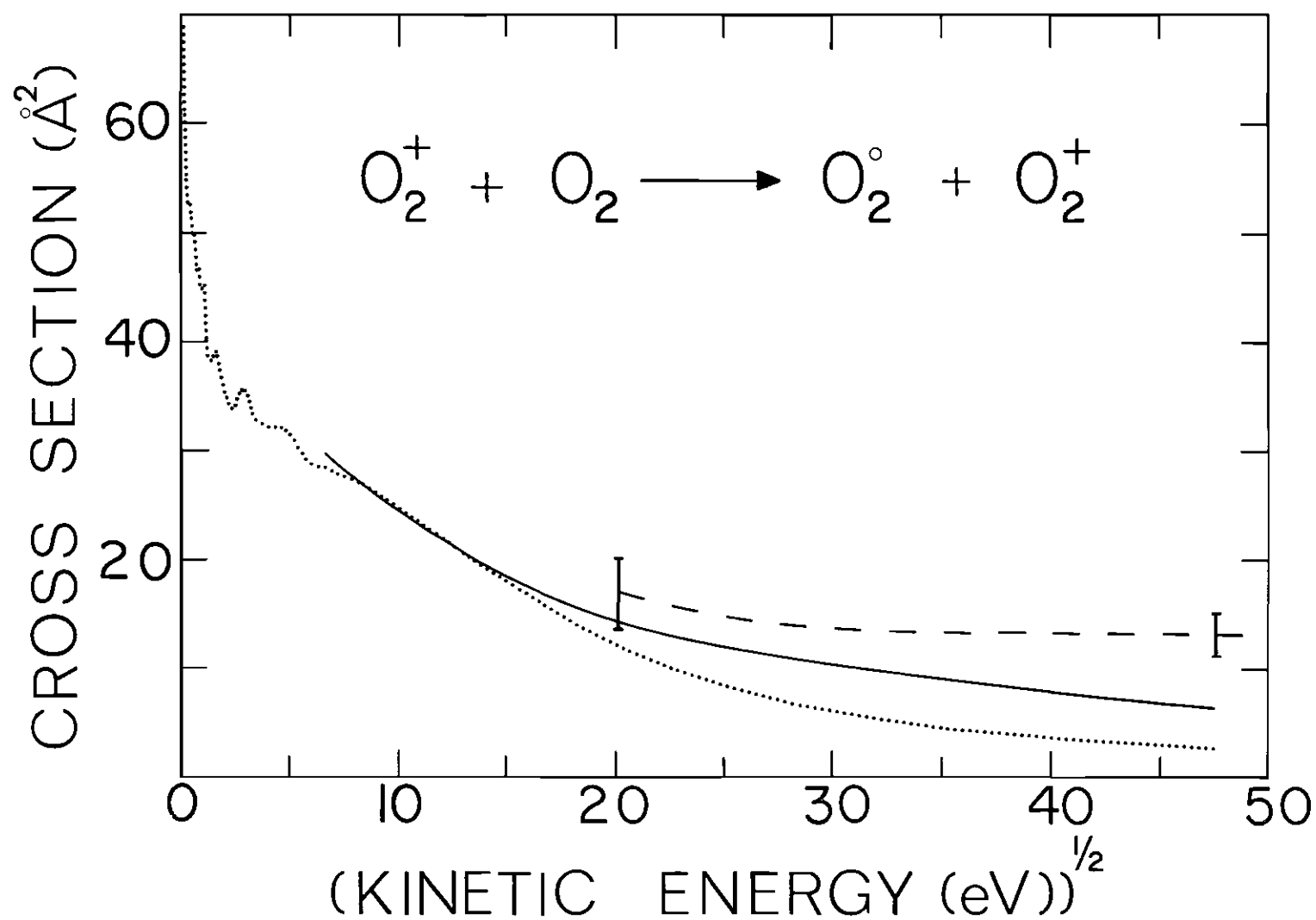


Figure 11. Comparison Between Theoretical and Experimental Charge-Transfer Cross Sections as a Function of Ion Kinetic Energy.

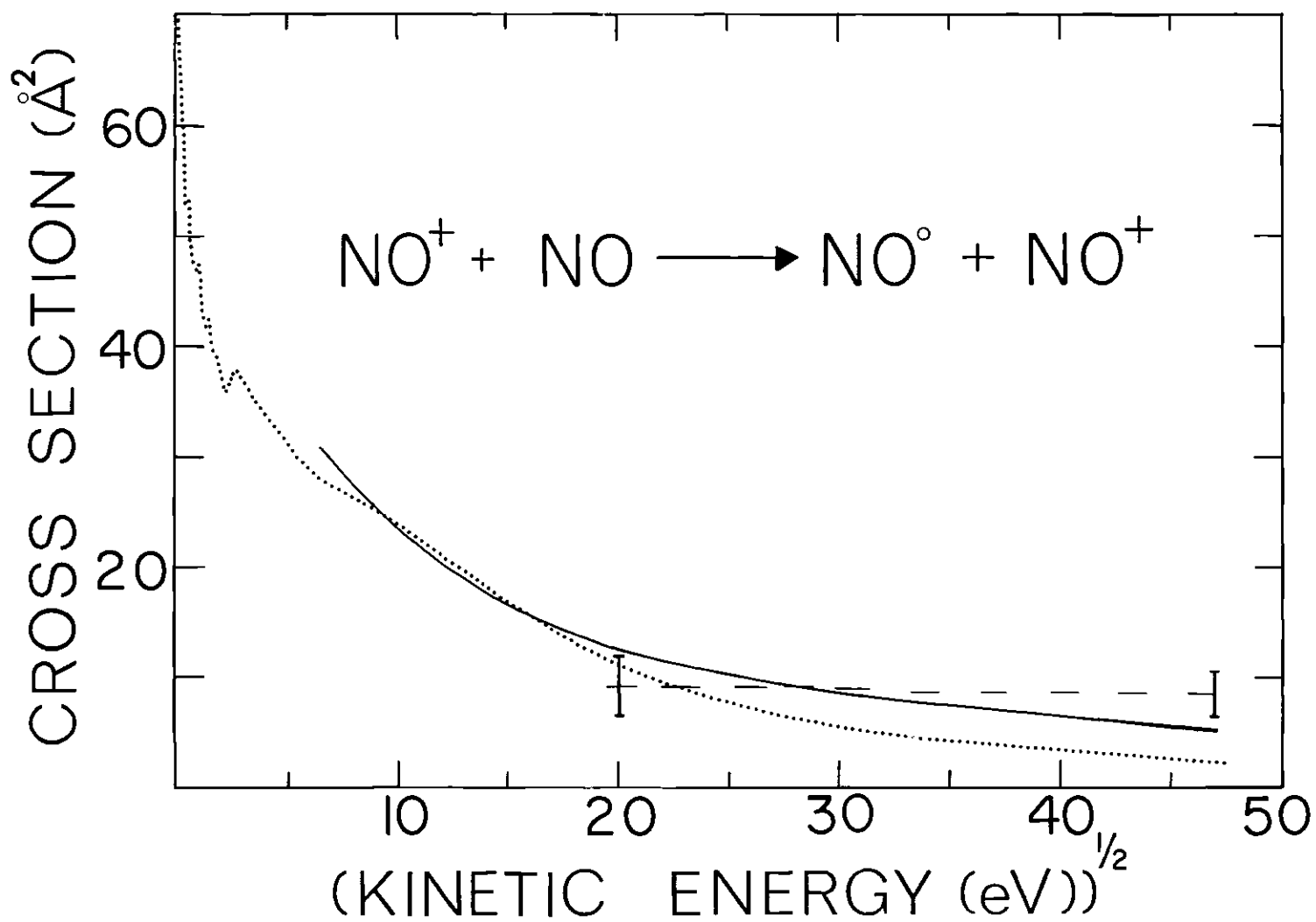


Figure 12. Comparison Between Theoretical and Experimental Charge-Transfer Cross Sections as a Function of Ion Kinetic Energy.

characteristic of 13 and 11 eV electron impact ionization. The dashed curves are the experimental cross sections measured using reactant ion beams formed by 13 eV and 11 eV electron impact ionization. An absolute basis for these cross sections was established by calibrating our measurements at 90 eV electron impact to the data of Ref. 60, who also used high energy electrons to form their reactant ion beam. The estimated uncertainty in the accuracy of these cross sections is represented by the error bars in each figure. The absolute cross sections for the  $\text{NO}^+ - \text{NO}$  system are subject to large uncertainty caused by variations in the excited state composition of the reactant ion beam with source gas pressure encountered by Ref. 60 during measurement of the absolute cross sections for this system, but not observed at the relatively low ( $4 \times 10^{-6}$  torr) source pressures used in the present experiment. At incident ion kinetic energies below approximately 1 keV, total charge-transfer cross sections computed from the multistate equations are in agreement with the experimental data. However, at higher kinetic energies the present multistate model appears to increasingly underestimate the total cross section, a behavior consistent with the neglect of electronically excited and dissociative<sup>25,26</sup> channels in the current theoretical framework.

### Conclusion

The agreement between the present theoretical and experimental cross sections, when compared as a function of either incident ion vibrational state or incident ion kinetic energy, is satisfactory. This is interpreted as a meaningful indicator of the overall reliability of the present model of the charge-transfer process.

## CHAPTER IV

PARTICIPATION OF INCIDENT ION INTERNAL ENERGY IN  
MOLECULAR  $O_2^+$  - AR CHARGE-TRANSFER COLLISIONS

Chapter IV was published in Chemical Physics Letters, Volume 24, pages 431 to 436, 1 February 1974. This article appears as Appendix III of this dissertation.

## CHAPTER V

COMPETITION BETWEEN DOUBLE AND SINGLE ELECTRON TRANSFER  
IN 2-8 KEV  $\text{AR}^{++}$  - AR COLLISIONS

Chapter V was published in the Journal of Chemical Physics, Volume 57, pages 3569 to 3570, 15 October 1972. This article appears as Appendix IV of this dissertation.

## CHAPTER VI

PRODUCT INTERNAL STATE DISTRIBUTIONS FROM  
INTERACTIONS OF METASTABLE AR WITH N<sub>2</sub>

Chapter VI was published in the Journal of Chemical Physics, Volume 57, pages 4111 to 4115, 15 November 1972. This article appears as Appendix V of this dissertation.

## CHAPTER VII

## CONCLUSIONS

A time-of-flight technique was utilized to measure relative total charge-transfer cross sections as a function of reactant ion kinetic energy and ionizing electron energy for the systems  $N_2^+ - N_2$ ,  $CO^+ - CO$ ,  $O_2^+ - O_2$ , and  $NO^+ - NO$ . Variations in the total cross section of as much as 35 per cent were observed when the energy of the electron beam used to form the reactant ions decreased from 90 eV to the ionization threshold. Such variations are partially due to the presence of ions in long-lived excited electronic states in the reactant ion beam. However, most of the variation occurred near the ionization threshold and is attributed to a dependence of the charge-transfer cross section on reactant ion vibrational state.

A multistate impact parameter treatment has been applied to the examination of charge transfer between the above ions occupying various vibrational levels and ground state neutral molecules. The resulting first-order coupled equations were solved numerically and convergence of the calculated cross sections was achieved by systematic introduction of additional states to the wavefunction expansion for the total system. Partial cross sections were computed for the formation of product ions and neutral molecules in discrete vibrational states. At high energy ( $\sim 2$  keV) the relative contribution of each product channel to the total cross section was found to be primarily determined by the relative magnitudes of the vibrational overlap between the reactant



states and the individual product states. At lower incident kinetic energies, the magnitude of the energy defect was also found to strongly influence the relative contribution of the product channels. Comparison was made between the experimental and theoretical cross sections by weighting the multistate cross sections according to the vibrational distribution present in the reactant ion beam formed at a given electron energy. The experimental and theoretical total charge-transfer cross sections was found to be in general accord with respect to variations in both ionizing electron energy and reactant ion kinetic energy.

The asymmetric  $O_2^+$  - Ar charge-transfer reactions were studied at  $O_2^+$  kinetic energies of 700 eV to 3 keV. The total cross sections were resolved into discrete contributions attributed to  $O_2^+(X^2\Pi_g)$  and  $O_2^+(a^4\Pi_u)$  ions in the reactant ion beam. The  $O_2^+(X^2\Pi_g)$  - Ar cross sections exhibited distinctly nonresonant behavior over the kinetic energy range investigated and were insensitive to the vibrational state of the reactant ions. The  $O_2^+(a^4\Pi_u)$  - Ar cross sections exhibited a resonant-like behavior over the same range of kinetic energies. The cross sections for both reactions were fully consistent with semiquantitative theoretical considerations.

A similar resonant/nonresonant dependence on incident velocity was exhibited by the double and single charge-transfer channels of the  $Ar^{++}$  - Ar reaction. The total cross sections for each of these channels was measured over a kinetic energy range of 2 - 8 keV. The present measurements were consistent, within experimental uncertainty, with those of other investigators made at lower and higher  $Ar^{++}$  kinetic energies.

Internal energy state distributions of the products from reactions

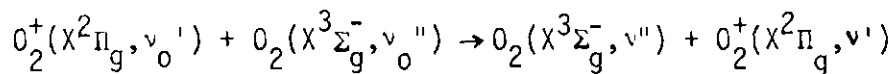
of metastable  $\text{Ar}(^3\text{P}_{2,0})$  atoms with ground state nitrogen molecules were computed from a statistical phase space treatment of the interactions. The theoretical rotational and vibrational distributions were compared with those measured in recent spectroscopic experiments involving metastable Ar atoms. Those distributions computed for the  $\text{N}_2(\text{C}^3\Pi_u)$  channels were in qualitative accord with the experimental distributions. However, the vibrational distribution calculated for the production of  $\text{N}_2(\text{B}^3\Pi_g)$  molecules was considerably broader than that measured experimentally. Such disagreement between the predictions of the phase space model and experimental measurements has been observed for highly exothermic product channels in a number of reaction systems and indicates that these channels may not be populated statistically. On the other hand, application of the statistical model to slightly exothermic reaction channels is generally reliable.

## APPENDIX I

## SELECTED OVERLAPS AND ENERGETICS

Table 1. Overlap Integrals and Energy Defects

for the Charge-Transfer Reactions



$v'', v'$	$v_0', v_0''$				
	0,0	1,0	2,0	3,0	4,0
0,0	.1884* .0000	.2621 -.2320	.2338 -.4600	.1521 -.6841	.0749 -.9040
1,0	-.2260 .1930	-.1238 -.0391	.0921 -.2670	.2214 -.4911	.2104 -.7110
0,1	.2621 .2320	.3645 .0000	.3252 -.2280	.2115 -.4521	.1041 -.6720
2,0	.2078 .3830	-.0319 .1510	-.1768 -.0770	-.0537 -.3011	.1465 -.5210
1,1	-.1343 .4250	-.1722 .1930	.1281 -.0350	.3079 -.2591	.2926 -.4790
0,2	.2338 .4600	.3252 .2280	.2901 .0000	.1887 -.2241	.0929 -.4440
3,0	-.1679 .5701	.1258 .3381	.0993 .1101	-.1183 -.1140	-.1340 -.3339
2,1	.2890 .6150	-.0443 .3830	-.2459 .1550	-.0747 -.0691	.2037 -.2890
1,2	-.2804 .6530	-.1537 .4210	.1143 .1930	.2747 -.0311	.2611 -.2510
0,3	.1521 .6841	.2115 .4521	.1887 .2241	.1227 .0000	.0604 -.2199
4,0	.1255 .7544	-.1588 .5224	.0113 .2944	.1435 .0703	-.0299 -.1496
3,1	-.2335 .8022	.1750 .5702	.1381 .3422	-.1645 .1181	-.1863 -.1018
2,2	.2578 .8430	-.0395 .6110	-.2194 .3830	-.0666 .1589	.1818 -.0610

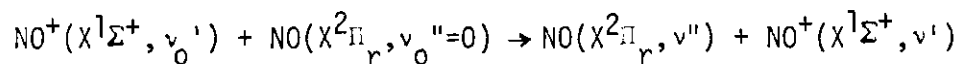
Table 1. (Continued)

$v'', v'$	$v_0', v_0''$				
	0,0	1,0	2,0	3,0	4,0
1,3	-.1824 .8770	-.0999 .6450	.0743 .4170	.1787 .1929	.1698 -.0270
0,4	.0749 .9040	.1041 .6720	.0929 .4440	.0604 .2199	.0298 .0000
5,0	-.0893 .9359	.1532 .7039	-.0918 .4759	-.0753 .2518	.1252 .0319
4,1	.1746 .9865	-.2208 .7545	.0157 .5265	.1995 .3024	-.0415 .0825
3,2	-.2083 1.0302	.1561 .7982	.1232 .5702	-.1568 .3461	-.1662 .1262
2,3	.1677 1.0670	-.0257 .8350	-.1427 .6070	-.0433 .3829	.1182 .1630
1,4	-.0898 1.0970	-.0492 .8650	.0366 .6370	.0880 .4129	.0836 .1930
6,0	.0614 1.1146	-.1299 .8826	.1301 .6546	-.0378 .4305	-.1178 .2106
0,5	.0280 1.1200	.0389 .8880	.0347 .6600	.0226 .4359	.0111 .2160

\*The upper number in each set is the overlap  $P_{if} = F(v_0', v'') \cdot F(v', v_0'')$  between the indicated reactant and product vibrational states. The lower number is the corresponding energy defect expressed in units of electron volts.

Table 2. Overlap Integrals and Energy Defects

for the Charge-Transfer Reactions



$v'', v'$	$v_0', v_0''$				
	0,0	1,0	2,0	3,0	4,0
0,0	.1618*	.2312	.2184	.1564	.0894
	.0000	-.2907	-.5773	-.8598	-1.1383
1,0	-.2048	-.1320	.0484	.1781	.1979
	.2326	-.0581	-.3447	-.6272	-.9057
0,1	.2312	-.1886	.0692	.2544	.2827
	.2907	.0000	-.2866	-.5691	-.8476
2,0	.1956	-.0079	-.1576	-.0881	.0805
	.4617	.1710	-.1156	-.3981	-.6766
1,1	-.2927	-.1886	.0692	.2544	.2827
	.5233	.2326	-.0540	-.3365	-.6150
0,2	.2184	.3121	.2948	.2112	.1206
	.5773	.2866	.0000	-.2825	-.5610
3,0	-.1619	.1044	.1115	-.0774	-.1426
	.6873	.3966	.1100	-.1725	-.4509
2,1	.2794	-.0113	-.2252	-.1259	.1150
	.7524	.4617	.1751	-.1074	-.3859
1,2	-.2765	-.1782	.0654	.2403	.2671
	.8099	.5192	.2326	-.0499	-.3284
0,3	.1564	.2235	.2112	.1512	.0864
	.8598	.5691	.2825	.0000	-.2784
4,0	.1228	-.1453	-.0125	.1345	.0187
	.9095	.6188	.3322	.0497	-.2287
3,1	-.2313	.1491	.1593	-.1106	-.2038
	.9780	.6873	.4007	.1182	-.1602

Table 2. (Continued)

$v'', v'$	$v_0', v_0''$				
	0,0	1,0	2,0	3,0	4,0
2,2	.2639 1.0390	-.0107 .7483	-.2127 .4617	-.1189 .1792	.1086 -.0993
1,3	-.1980 1.0924	-.1276 .8017	.0468 .5151	.1721 .2326	.1913 -.0459
5,0	-.0879 1.1283	.1464 .8376	-.0708 .5510	-.0918 .2684	.0939 -.0100
0,4	.0894 1.1383	.1277 .8476	.1206 .5610	.0864 .2784	.0494 .0000
4,1	.1755 1.2002	-.2076 .9095	-.0179 .6229	.1922 .3404	.0268 .0619
3,2	-.2185 1.2646	.1409 .9739	.1504 .6873	-.1045 .4048	-.1925 .1264
2,3	.1891 1.3215	-.0076 1.0308	-.1524 .7442	-.0852 .4617	.0778 .1832
6,0	.0604 1.3436	-.1269 1.0529	.1167 .7663	.0123 .4838	-.1184 .2053
1,4	-.1131 1.3709	-.0729 1.0802	.0268 .7936	.0983 .5110	.1093 .2326
0,5	.0416 1.4126	.0595 1.1219	.0562 .8353	.0403 .5528	.0230 .2744

\*The upper number in each set is the overlap  $P_{if} = F(v_0', v'') \cdot F(v', v_0'')$  between the indicated reactant and product vibrational states. The lower number is the corresponding energy defect expressed in units of electron volts.

## APPENDIX II

MOLECULAR CHARGE TRANSFER: EXPERIMENTAL AND THEORETICAL  
INVESTIGATION OF THE ROLE OF INCIDENT-ION VIBRATIONAL STATES IN  
 $N_2^+ - N_2$  AND  $CO^+ - CO$  COLLISIONS

This appendix is the reprint of an article published in the  
Journal of Chemical Physics, Volume 59, pages 5494 to 5510, 15 November,  
1973.



## Molecular charge transfer: Experimental and theoretical investigation of the role of incident-ion vibrational states in $N_2^+-N_2$ and $CO^+-CO$ collisions

M. R. Flannery, P. C. Cosby, and T. F. Moran

*Georgia Institute of Technology, Atlanta, Georgia 30332*

(Received 1 August 1973)

The effect of reactant-ion vibrational energy on total charge-transfer cross sections has been examined for 0.03–2.20 keV  $N_2^+-N_2$  and  $CO^+-CO$  collisions. A multistate impact parameter treatment was applied to the examination of charge transfer between the above ions occupying various vibrational levels and ground-state neutral molecules. The resulting first-order coupled equations were solved numerically, and convergence of the calculated cross sections was achieved by systematic introduction of additional states to the wavefunction expansion for the total system. The calculated cross sections were weighted according to the vibrational distribution present in the laboratory reactant-ion beam formed by electron impact and the results compared with experiment in which we employed time-of-flight techniques to measure the forward-scattered neutral  $N_2$  and CO products. Reactant-ion vibrational state distributions were varied by changing the ionizing electron beam energy in a controlled electron-impact mass spectrometer ion source. The vibrational state population of the reactant-ion beam was estimated from absolute excitation cross sections spectroscopically measured for electron-impact ionization of the above molecules, the squares of the overlap integrals of the respective ground and excited ionized states (where needed), and total electron-impact cross sections for molecular ion formation. The major contribution to the charge-transfer cross sections arises from those reaction channels with large vibrational overlaps and small energy defects with respect to the initial channel. Multistate cross sections for those channels involving near-resonant states with favorable vibrational overlaps are found to be closely approximated by the low-velocity limit proposed by Bates and Reid. Measured cross sections and their dependence on reactant-ion vibrational state distributions are correctly predicted by the multistate model below approximately 1.5 keV ion kinetic energy. There are, however, indications that competitive, inelastic, electron-transfer processes tend to occur at higher kinetic energies.

### I. INTRODUCTION

Experimental measurement and theoretical descriptions of charge-transfer reactions involving atomic species have generated widespread interest during the past decade, largely because detailed knowledge of such reactions is required for the interpretation of various phenomena occurring in planetary atmospheres and for the basic development of collision theory. There have been comparatively few theoretical investigations of the charge-transfer processes involving molecular species simply because of the difficulty associated with a proper theoretical account of couplings between the large number of internal degrees of freedom during the molecular interactions. Recently, however, Bates and Reid<sup>1</sup> have formulated the first detailed (and tractable) theoretical description of molecular charge transfer in which specific account is taken of the important couplings not acknowledged by the usual two-state treatment.<sup>2,3</sup> Their inclusion of vibrational overlaps and energy defects for the different reaction channels in the  $H_2^+-H_2$  collision system resulted not only in a predicted variation of total charge-transfer cross section with vibrational level of the reactant ion, but also in total cross sections consistent with available experimental measurements. A knowledge of the variation of cross section with reactant-ion in-

ternal energy content is particularly important when comparing independent measurements of total charge-transfer cross sections. Experimental cross sections have been observed to change with ion-source conditions, suggesting that reactant-ion internal energy is at least partially responsible for a lack of agreement when comparing cross sections determined in different laboratories. Reactions of noble-gas ions with  $N_2$  have been measured<sup>4</sup> for ion beams produced in both radio-frequency and electron-impact ion sources. Significant differences between cross sections obtained using the two different sources were observed as the ion beam kinetic energy was lowered from 80 to 10 keV and have been attributed to a greater number of metastable ions produced in the rf source. By varying the electron energy in a controlled electron-impact ion source, several investigations<sup>5–11</sup> have attempted to assay the ion beam composition and examine quantitatively the effect of atomic ion electronic excitation energy on the charge-transfer mechanism.

Corresponding studies involving diatomic ions present further complications since vibrational as well as electronic excitation energy may be present in the reactant-ion beam<sup>11–13</sup> and this can affect the measured cross sections.<sup>3,14,15</sup> The  $N_2$  and CO systems have been chosen for study in this

work since it is possible to control the electronic and vibrational distributions of the reactant-ion beam. Also, the vibrational overlaps and energy defects for these systems are particularly favorable for a detailed examination of the applicability and convergence of the multistate impact parameter description in molecular charge-transfer interactions.

## II. THEORY

### A. Theoretical Treatments of Charge Transfer

The impact parameter description<sup>18</sup> of charge transfer between an ion  $B^+$  and a neutral  $A$  is based on the assumption that changes in the internal degrees of freedom of each collision partner are brought about by time-dependent terms generated by the classical relative motion of the two centers of mass separated by  $\mathbf{R} = \mathbf{R}(t)$  at time  $t$ . The terms responsible for this change depend on the particular eigenfunction expansion adopted for  $\Psi(t)$ , the wavefunction describing the variation of the internal degrees of freedom with time. Three expansions described below in (a)–(c) are commonly invoked.

(a) When  $\Psi$  is expanded in terms of a complete set of eigenfunctions  $\phi_n(\mathbf{r}, t)$  describing the isolated systems  $B^+$  and  $A$  (at infinite center-of-mass separation) with composite internal coordinates denoted by  $\mathbf{r}$ , transitions are primarily achieved via the matrix element  $\langle \phi_i^D | V(\mathbf{r}, \mathbf{R}) | \phi_f^X \rangle$ , the instantaneous electrostatic interaction  $V$  between  $B^+$  and  $A$  at separation  $\mathbf{R}$ , averaged over the initial (direct) state  $\phi_i^D$  and the final (exchange) state  $\phi_f^X$  of the isolated systems at infinite  $\mathbf{R}$ . This "atomic" model  $A$  is suitable for high impact speeds  $v$ .

(b) When  $\Psi$  is expanded in terms of the complete set of eigenfunctions  $\chi_n(\mathbf{r}, \mathbf{R}, t)$  for the molecular complex  $AB^+$  formed at a fixed  $\mathbf{R}$ , transitions (between spherically symmetric atomic states) essentially occur via the matrix element  $\langle \chi_i | \nabla_{\mathbf{R}} | \chi_f \rangle$ . This "molecular" model  $M$  is used, when possible, for slow collisions, and is the basis of what is generally called the perturbed stationary state or PSS method.

Both models result in a set of first-order coupled differential equations which must be solved for the transition amplitudes at various impact parameters  $\rho$  in order to evaluate the cross sections. Equations identical to those obtained from the above impact-parameter methods can also be derived from a stationary-state description of the collision event in which the relative motion is treated by the JWKB approximation.<sup>17</sup>

(c) When the charge-transfer process is resonant and symmetric [i. e.,  $A^+(i) + A(j) \rightarrow A(j) + A^+(i)$ ], then a modification to model  $M$  is required. The

potential field in which the active electron moves is now symmetric with respect to the midpoint of  $\mathbf{R}$ , hence  $\Psi$  is expanded in terms of the gerade and ungerade eigenfunctions  $\chi_{g,u}(\mathbf{r}, \mathbf{R})$  for each electronic state of the quasimolecular complex formed. The coefficients of these linear combinations largely remain unaffected in slow collisions,<sup>18</sup> but the relative phase  $\eta$  arising from differences in the associated eigenenergies  $\epsilon_{g,u}(\mathbf{R})$  changes with  $\mathbf{R}$ , thereby allowing charge transfer to occur. The process as described by this treatment does not proceed via an electronic transition.<sup>19</sup>

The probability for symmetrical resonance charge transfer as determined from a two-state ( $g, u$ ) molecular  $M$  treatment (in which the coupled equations can be solved exactly) is

$$P_M^X(\rho) = \sin^2 \eta(\rho) \quad (1a)$$

with the relative phase  $\eta$  given by

$$\eta = v^{-1} \int_0^\infty [\epsilon_g(R) - \epsilon_u(R)] dZ, \quad (1b)$$

where  $\epsilon_g$  and  $\epsilon_u$  are the exact gerade and ungerade eigenenergies for the molecular complex. In (1b), a straight-line trajectory  $\mathbf{R} = \rho + \mathbf{v}t$  is assumed, the incident speed  $v$  is along the  $z$  axis, the  $z$  component of  $\mathbf{R}$  being  $Z = vt$ , and  $v$  remains unchanged over all  $\rho$  and  $Z$ . The charge-transfer cross section is therefore

$$Q^X = 2\pi \int_0^\infty \sin^2 \eta(\rho) \rho d\rho. \quad (1c)$$

The application of the atomic model  $A$  to such a collision does, however, involve an electronic transition. The two-state<sup>2</sup> atomic model  $A$ , at low incident speeds when the change in translational motion of the active electron can be neglected, yields

$$P_A^X(\rho) = \sin^2 v^{-1} \int_{-\infty}^\infty V(\mathbf{R}) dZ \quad (2a)$$

for the charge-transfer probability for resonance collisions where

$$(1 - |\langle \phi_i^D | \phi_f^X \rangle|^2) V(\mathbf{R}) = (\langle \phi_f^X | V^D | \phi_i^D \rangle - \langle \phi_f^X | \phi_i^D \rangle \langle \phi_i^D | V^D | \phi_i^D \rangle) \quad (2b)$$

$$= (\langle \phi_i^D | V^X | \phi_f^X \rangle - \langle \phi_i^D | \phi_f^X \rangle \langle \phi_f^X | V^X | \phi_f^X \rangle), \quad (2c)$$

with  $\phi_i^D(\mathbf{r}_1)$  and  $\phi_f^X(\mathbf{r}_2)$  denoting the initial and final wavefunctions (with  $\mathbf{r}_2 = \mathbf{R} + \mathbf{r}_1$ ) for the active electron attached to the target  $A^+$  and projectile  $B^+$  ionic cores, respectively. The electrostatic interactions in the incident direct ( $D$ ) channel ( $B^+ - A$ ) is  $V^D$  and the final exchange  $X$  channel ( $A^+ - B$ ) is  $V^X$ . The LCAO approximation to the exact molecular splitting  $\epsilon_g - \epsilon_u$  in (1b) yields  $2V(\mathbf{R})$  in (2b), identically,<sup>19</sup> thereby establishing the equivalence between the cross sections derived from both the atomic model and the LCAO approximation to  $M$  for symmetrically resonant charge transfer. The above

equations apply only to symmetrically resonant processes when the diagonal distortion terms  $\langle \phi_i^D | V^D | \phi_i^D \rangle$  and  $\langle \phi_f^X | V^X | \phi_f^X \rangle$  are equal. The application of (1) and (2) to accidental resonance processes (which involve ions of unlike gases when the energy balance is either close or accidentally exact) is an incorrect procedure,<sup>19</sup> since the above distortion terms are in general not equal, thereby preventing an exact solution to the two-coupled equations. McCarroll,<sup>20</sup> using model A for  $H^+(1s)$  symmetrically resonant collisions, obtained satisfactory agreement with Ferguson<sup>21</sup> who used accurate molecular wavefunctions, the more attractive approach at low incident speeds. For resonant charge transfer in the  $H_2^+-H_2$  and  $N_2^+-N_2$  collisions systems, Gurnee and Magee<sup>2</sup> calculated the two-state cross section.

$$Q^X = \int_0^\infty P_A^X(\rho) \rho d\rho \quad (3)$$

using certain simplifying assumptions concerning the matrix elements in (2b).

Bates and Reid<sup>1</sup> recently generalized this two-state treatment so as to include nonresonant channels, presenting a detailed theoretical account of the processes,

$$H_2^+(X^2\Sigma_g^+, \nu_i') + H_2(X^1\Sigma_g^+, \nu_i'') \rightarrow H_2(X^1\Sigma_g^+, \nu_f'') + H_2^+(X^2\Sigma_g^+, \nu_f'), \quad (4)$$

in which the incident molecular ion  $H_2^+$ , in vibrational level  $\nu_i'$ , captures an electron from the molecular  $H_2$  target, initially in vibrational level  $\nu_i''$ , to form a neutral molecule in vibrational state  $\nu_f''$ , with the neutral target converted to an ion in vibrational state  $\nu_f'$ . Only the ground electronic states of  $H_2^+$  and  $H_2$  were considered to be involved in (4) at low impact energies and the rotational states of each pair of protons were assumed unchanged. The wavefunction  $\Psi(t)$  for the internal motions, denoted by  $r$ , is expanded as

$$\Psi(t) = \sum_{\alpha=D,X} \sum_n a_n^\alpha(t) \phi_n^\alpha(r) \exp(-iE_n^\alpha t), \quad (5)$$

where  $\phi_n^\alpha$  are molecular eigenfunctions (with electronic, vibrational, and rotational parts) of the unperturbed Hamiltonian  $\mathcal{H}_0^\alpha$  for the isolated molecular systems,  $H_2^+$  and  $H_2$ , at infinite center-of-mass separation  $R$  with eigenenergies  $E_n^\alpha$ . The index  $\alpha$  labeling certain quantities denotes that the associated quantities refer to either direct channels  $D$ , where no charge-transfer occurs, or to the exchange channels  $X$ . The outer summation is over all  $D$  and  $X$  channels. By inserting (5) into the appropriate time-dependent Schrödinger equation for the internal coordinates and by working to lowest order in two-center one-electron overlaps, Bates and Reid<sup>1</sup> obtained the charge-transfer cross section

$$Q_{if}^X = 2\pi \int_0^\infty |C_f^X(\rho, \infty)|^2 \rho d\rho \quad (6)$$

in terms of the transition amplitudes  $C_f^\alpha(\rho, t) \equiv a_f^\alpha(t) \times \exp i\phi(t)$ , where  $\phi$  is a certain phase factor which need not be specified since the probabilities  $|C_f^\alpha|^2 = |a_f^\alpha|^2$  remain unaffected. The transition amplitudes are the solutions, for a given impact parameter  $\rho$ , of the set of first-order coupled differential equations,

$$i(\partial C_l^\alpha / \partial t) = V(R) \sum_{m=1}^N P_{lm} C_m^\alpha(\rho, t) \times \exp[i(E_l - E_m)t], \quad l=1, 2, \dots, N \quad (7)$$

subject to the boundary condition that only the direct channel  $i$  is occupied initially, i.e.,  $C_m^D(\rho, -\infty) = \delta_{mi}$ ,  $C_m^X(\rho, -\infty) = 0$ . When  $\alpha$  denotes  $X$ ,  $\bar{\alpha}$  in (7) denotes  $D$  and vice versa. The matrix elements  $P_{lm}$  are equal to  $F(\nu_i' \nu_m'') F(\nu_m' \nu_i'')$ , where  $F(\nu_i' \nu_n'')$  is the vibrational overlap for the  $H_2^+(\nu_i')-H_2(\nu_n'')$  transition. In this description, charge transfer occurs by coupling only with  $D$  channels which in turn are coupled only with  $X$  channels. The maximum number of states included in the above set of equations is  $2N$ . The excitation defect between vibrational channels  $l$  and  $m$  is  $E_l^\alpha - E_m^\alpha$ . The difference  $E_n^D - E_n^X$  depends only on the initial rotational states  $J_A$  and  $J_B$  of  $H_2$  and  $H_2^+$  and is negligible such that  $E_n^D = E_n^X = E_n$ . The electronically integrated interaction potential  $V(R)$ , assumed to be spherically symmetric, is given by the right-hand side of either (2b) or its equivalent (2c) for a symmetric collision. The electronic wavefunctions for the  $H_2^+-H_2$  isolated systems were taken to be the simple products  $\phi_i^D = A(12)B(3)$  and  $\phi_f^X = A(2)B(13)$  where  $A$  and  $B$  are electronic spatial functions, with the number of arguments denoting the number of electrons attached to each proton pair, and 1 denoting the active electron. For more complex systems, the direct evaluation of  $V(R)$  from (2a) is difficult and impractical. The recognition, however, that  $V(R)$  is the LCMO approximation to  $\epsilon_r - \epsilon_u$  in (1b) introduces considerable simplification only if the gerade-ungerade splitting of the molecular complex (in its ground electronic state) can be otherwise determined. Also the overlap matrix  $\mathbf{P} \equiv [P_{lm}]$  and the excitation defects  $E_l - E_m$  between all the  $N$  channels included in (7) must be known before the cross sections (6) can be evaluated.

## B. Interaction Potentials

The vibrational and rotational periods of each molecular species,  $N_2$  and  $CO$ , are  $\tau_{vib} \sim 2 \times 10^{-14}$  sec. and  $\tau_{rot} \sim 2 \times 10^{-12}$  sec, respectively. The duration of the ion-molecule is  $\tau_{coll} \sim 2.4(R/v) \times 10^{-17}$  sec., where  $v$ (atomic units) is the incident speed of the ion and  $R$ (atomic units) is the effective radius (depending on  $v$ ) of a charge-transfer collision.

sion. The range of incident speeds  $7 \times 10^{-3} < v < 6 \times 10^{-2}$  pertinent to the present measurements involves (large) radii in the range  $10 > R > 5$  resulting in corresponding collision times in the range  $4 \times 10^{-14} > \tau_{\text{coll}} > 2 \times 10^{-15}$ . Hence,  $\tau_{\text{coll}} \ll \tau_{\text{rot}}$  and  $\tau_{\text{coll}} < \tau_{\text{vib}}$  such that the collision is finished before the molecular axis of the colliding species can rotate or vibrate. In the low-velocity limit  $\tau_{\text{coll}} \geq \tau_{\text{vib}}$ , so that the individual oscillators are strongly coupled, thereby ensuring efficient energy transfer, which results in vibrational relaxation, such that  $P_{ii}$  is unity. The effective ion-molecule interaction is  $V(\mathbf{R})$  averaged over all vibrational and rotational motions to give  $\bar{V}(R)$ . Since  $V(\mathbf{R})$  is assumed spherically symmetric,  $\bar{V} = V(R)$ .

In the low-velocity limit, resonant collisions with  $E_i = E_f$  dominate, and a two-state approximation involving only  $C_i^P$  and  $C_i^X$  in (7), with  $P_{ii} = 1$ , is valid. These equations can be solved exactly to give

$$Q^X = 2\pi \int_0^\infty \rho \sin^2[(2/v) \int_0^\infty \bar{V}(R) dZ]. \quad (8)$$

In this limit, when changes in translational motion of the active electron can be neglected, the LCMO approximation to  $\epsilon_g - \epsilon_u$  in the molecular model M and the expression for  $2V(\mathbf{R})$ , obtained originally from the expansion (5), are equivalent (by analogy with Bates and Lynn<sup>19</sup> for the atomic case). Hence, cross sections given by (1) and (8) are identical, such that

$$\bar{V}(R) = \frac{1}{2}[\epsilon_g(R) - \epsilon_u(R)], \quad (9)$$

i. e., the gerade-ungerade splitting yields the molecular interaction  $\bar{V}(R) = V(R)$ .

Two methods can be adopted for this determination. The first method is an extension of Firsov's method (proposed by Bates and Reid<sup>1</sup>), and the second method is based essentially on the prescription of Sato.<sup>22</sup> Bates and Reid used the first method for  $\text{H}_2^+-\text{H}_2$ . This approach involved the exact prolate spheroidal wavefunction for  $\text{H}_2^+$  and single-center orbital expansion of  $\text{H}_2$ . The application of a similar approach to  $\text{N}_2$  and CO is prohibitively difficult, since accurate wavefunctions for these multielectron diatomic species are generally unavailable and would require much computational labor. Even with such knowledge, the reliability of the calculated  $V(R)$  would remain uncertain.

Fortunately, Sato<sup>22</sup> has provided a method for estimating the ungerade potential from a knowledge of the gerade potential. Given the Morse function,<sup>23</sup>

$$\epsilon_g(R) = D_e \{ \exp[-2\beta(R - R_e)] - 2 \exp[-\beta(R - R_e)] \}, \quad (10)$$

Sato proposed that the ungerade energy is determined by

$$\epsilon_u(R) = \frac{1}{2}D_e \{ \exp[-2\beta(R - R_e)] + 2 \exp[-\beta(R - R_e)] \}, \quad (11)$$

where  $R_e$  is the internuclear distance corresponding to the potential minimum of depth  $D_e$ , and  $\beta$  is a constant controlled by the shape of the potential. Porter and Karplus<sup>24</sup> have shown that the Sato potentials are in harmony with those computed from the highly accurate  $\text{H}_2$  wavefunctions of Kołos and Roothaan.<sup>25</sup> For the ion-molecule systems under consideration, the interaction energy (10) of the symmetric (gerade) stationary state is determined from the interaction potential,

$$V_{\text{LJ4}}(R) = 4\epsilon[(d/R)^{12} - (d/R)^6] - \alpha e^2/2R^4, \quad (12)$$

by using the Lennard-Jones parameters  $\epsilon$  and  $d$ , together with the polarizability,  $\alpha$ , whose values have been compiled by Hirschfelder *et al.*<sup>26</sup> Yang and Conway<sup>27</sup> have presented convincing evidence that this 12-6-4 potential reproduces their observed data on the  $\text{O}_2^+-\text{O}_2$  ion-molecule interaction. The function  $\epsilon_g(R)$  is curve fitted to  $V_{\text{LJ4}}(R)$  in the neighborhood of the potential minimum and for larger  $R$ , thereby permitting the explicit evaluation of  $D_e$ ,  $R_e$ , and  $\beta$  for each system. Values of the Morse parameters derived for the  $\text{N}_2^+$  system from this procedure are  $\beta = 1.5903 \text{ \AA}^{-1}$ ,  $R_e = 3.5262 \text{ \AA}$ , and  $D_e = 0.06917 \text{ eV}$ . Corresponding values for  $(\text{CO})_2^+$  are  $1.6008 \text{ \AA}^{-1}$ ,  $3.4730 \text{ \AA}$ , and  $0.08104 \text{ eV}$ , respectively. The variation of the stationary state splitting with distance  $R$  is given by the relation

$$\begin{aligned} \epsilon_g - \epsilon_u &= \frac{1}{2}D_e \exp[-2\beta(R - R_e)] \\ &\quad - 3D_e \exp[-\beta(R - R_e)], \quad R > R^* \\ &= 0, \quad R < R^*. \end{aligned} \quad (13)$$

The cutoff at  $R^* \equiv R_e - \ln 6/\beta$  is imposed because the change of sign in  $\epsilon_g - \epsilon_u$  at that point is unphysical. Since the main contributions to charge-transfer cross sections at low impact energies arise from intermediate and distant encounters (5–10 a. u.), any error resulting from the cutoff, which occurs at small  $R$ , is minimized. We have used the above approach to determine the  $\epsilon_g - \epsilon_u$  splitting for the  $\text{H}_2^+-\text{H}_2$  system from large values of  $R$  down to approximately  $3a_0$  and find accord with the computation of Bates and Reid<sup>1</sup> who adopted the more elaborate method.

The knowledge of  $\epsilon_g$  for the  $\text{N}_2^+$  and  $(\text{CO})_2^+$  systems is mainly determined by the behavior of the ion-molecule interaction at intermediate and large  $R$ . The over-all reliability can be assessed by comparing the short-range behavior with the repulsive potentials derived from scattering experiments of the neutral-neutral species. Such a comparison is made in Figs. 1 and 2 for the  $\text{N}_2^+-\text{N}_2$  and  $\text{CO}^+-\text{CO}$  interactions. The solid curves in these

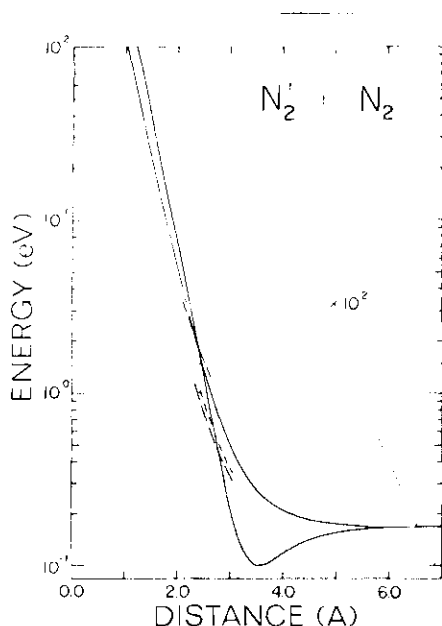


FIG. 1. Interaction potential energy  $[V(R) + D_0 + 0.1$  eV] for  $N_2^+ + N_2$  collisions as a function of distance between the centers of the collision partners. The  $\epsilon_g$  and  $\epsilon_u$  curves are given by the solid lines while the dashed curves are the  $\epsilon_g$  curves experimentally determined for the corresponding neutral systems, Ref. 28. The dotted curve represents the  $\epsilon_u - \epsilon_g$  difference as a function of distance.

figures represent  $\epsilon_g$  and  $\epsilon_u$  as a function of intermolecular separation, while the dashed lines are those repulsive potentials derived from high-energy neutral-neutral scattering experiments.<sup>28</sup> The dotted curves displayed in these figures represent the  $R$  dependences of the stationary-state gerade-ungerade splitting  $\epsilon_g - \epsilon_u$  which are to be used in our present computations of total charge-transfer cross sections.

### C. Energetics and Overlaps

Computation of cross sections from the coupled differential equations (7) requires knowledge of the overlaps and energetics of all possible initial and final states of the reaction. Vibrational overlaps  $F(\nu', \nu'')$  for the transitions between diatomic ions  $XY^+$  ( $\nu'$ ) and neutral  $XY$  ( $\nu'' = 0$ ) molecules are tabulated in the literature<sup>29,30</sup>; however, overlaps involving excited states of the neutral species are also required but not generally available. We have computed the necessary overlaps with a Morse anharmonic oscillator description<sup>13,30</sup> of the wavefunctions for the higher vibrational levels of the neutral and ionic species. Spectroscopic constants necessary for the construction of these wavefunctions were taken from existing compilations.<sup>23,31,32</sup> The Franck-Condon factors obtained using these wavefunctions are consistent with those from the RKR treatment<sup>29</sup> of ground state molecules with

excited states of the ion. The overlaps we have used as input data in the coupled equations are shown in Table I for a representative sample of the important channels in the  $N_2$  system. A similar display of overlaps for the  $CO^+$  system is shown in Table II. As indicated in each of these tables, the largest overlaps occur for ground-state ions with ground-state molecules, but for reactions of vibrationally excited ions, the overlaps with the corresponding level of the neutral are dominant, i.e., when  $\nu'_0 = \nu''$  and  $\nu'_0 = \nu'$  the overlaps are large.

The excitation defects of various reaction channels ( $E_i - E_m$ ) were computed from spectroscopic energy levels<sup>23,31,32</sup> of the ionic and neutral species. These excitation defects are shown in Tables I and II for the  $N_2$  and  $CO$  systems where it is to be noted that the defects tend to occur in groups or "bands" separated by approximately one vibrational quantum of energy. Within a given band, the energy defects are almost identical. Hence, one could consider the channels within a given energy band to be nearly degenerate. For example, the  $(1, 0 | 0, 1)$  and  $(1, 0 | 1, 0)$  channels in Table I are separated only by 0.019 eV. These channels are designated as the 0 band for the  $N_2^+(X^2\Sigma_g^+, \nu'_0 = 1) - N_2(X^1\Sigma_g^+, \nu''_0 = 0)$  reaction. The  $(1, 0 | 0, 2)$  and  $(1, 0 | 1, 1)$  channels are termed the +1 band while the  $(1, 0 | 0, 0)$  channel is denoted as the -1 band for the aforementioned system of reactants.

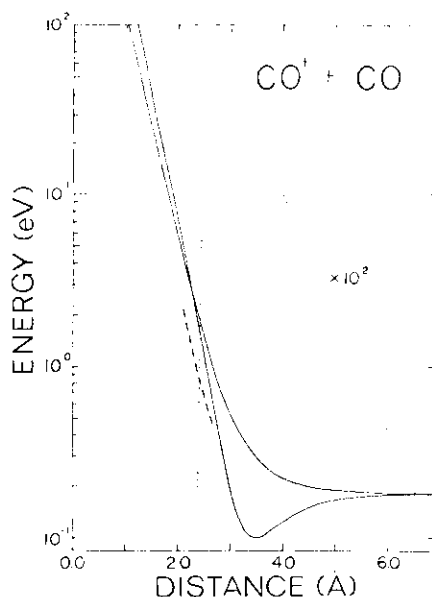


FIG. 2. Interaction potential energy  $[V(R) + D_0 + 0.1$  eV] for  $CO^+ + CO$  collisions as a function of distance between the centers of the collision partners. The  $\epsilon_g$  and  $\epsilon_u$  curves are given by the solid lines while the dashed curve is that determined experimentally for the corresponding neutral system, Ref. 28. The dotted curve represents the  $\epsilon_u - \epsilon_g$  difference as a function of distance.

TABLE I. Energetics and overlap integrals for charge-transfer reactions  $N_2^+(X^2\Sigma_g^+, \nu_0) + N_2(X^1\Sigma_g^+, \nu_0' = 0) \rightarrow N_2^0(X^1\Sigma_g^+, \nu'') + N_2^+(X^2\Sigma_g^+, \nu')$ .

$\nu_0$	$\nu_0'$	$\nu''$	$\nu'$	$P_{lm}$	Band	Energy deficit of reaction (eV)	$\nu_0$	$\nu_0'$	$\nu''$	$\nu'$	$P_{lm}$	Band	Energy deficit of reaction (eV)
0	0	0	0	9.05-1	0	0.000	1	0	2	3	-7.24-3	4	1.101
		0	1	-2.84-1	1	0.270			3	2	6.78-3		1.121
		1	0	2.92-1		0.289			4	1	-4.28-3		1.134
		0	2	7.32-2	2	0.535			5	0	1.64-3		1.139
		1	1	-9.17-2		0.558							
		2	0	4.71-2		0.574			0	2	5.92-3	0	0.000
		0	3	-1.77-2	3	0.797			1	1	-1.13-1		0.023
		1	2	2.15-2		0.824			2	0	7.48-1		0.039
		2	1	-1.48-2		0.844			0	3	-1.43-3	1	0.262
		3	0	6.42-3		0.856			1	2	-2.91-2		0.289
		0	4	4.53-3	4	1.054			2	1	-2.35-1		0.309
		1	3	-5.20-3		1.086			3	0	4.43-1		0.321
		2	2	3.81-3		1.109			0	1	-2.30-2	-1	-0.266
		3	1	-2.02-3		1.126			1	0	-3.59-1		-0.246
		4	0	6.69-4		1.134			0	0	7.32-2		-0.535
1	0	0	1	8.93-2	0	0.000			0	4	3.66-4	2	0.519
		1	0	8.32-1		0.019			1	3	7.02-3		0.550
		0	2	-2.30-2	1	0.266			2	2	6.05-2		0.574
		1	1	-2.61-1		0.289			3	1	-1.39-1		0.590
		2	0	3.70-1		0.305			4	0	1.21-1	3	0.599
		0	0	-2.83-1	-1	-0.270			0	5	-1.10-1		0.772
		0	3	5.55-3	2	0.527			1	4	-1.80-3		0.808
		1	2	6.73-2		0.554			2	3	-1.46-2		0.836
		2	1	-1.16-1		0.574			3	2	8.66-3	4	0.856
		3	0	8.37-2		0.586			4	1	-3.58-2		0.869
		0	4	-1.42-3	3	0.784			5	0	7.18-3		0.874
		1	3	-1.63-2		0.816			0	6	2.30-5		1.021
		2	2	2.99-2		0.840			1	5	5.40-4		1.061
		3	1	-2.63-2		0.856			2	4	3.75-3		1.093
		4	0	1.36-2		0.864			3	3	-8.67-3		1.117
		0	5	4.27-4	4	1.038			4	2	9.78-3		1.134
		1	4	4.17-3		1.073			5	1	-2.26-3		1.143
									6	0	3.09-3		1.145

TABLE II. Energetics and overlap integrals for charge-transfer reactions  $\text{CO}^+(\text{X}^2\Sigma^+, \nu'_0) + \text{CO}(\text{X}^1\Sigma^+, \nu'_0 = 0) \rightarrow \text{CO}^0(\text{X}^1\Sigma^+, \nu'') + \text{CO}^+(\text{X}^2\Sigma^+, \nu')$ .

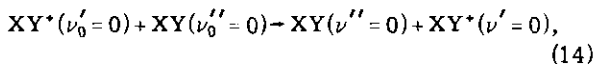
$\nu'_0$	$\nu'_0$	$\nu''$	$\nu'$	$P_{Im}$	Band	Energy deficit of reaction (eV)	$\nu'_0$	$\nu'_0$	$\nu''$	$\nu'$	$P_{Im}$	Band	Energy deficit of reaction (eV)
0	0	0	0	9.62-1	0	0.000	1	0	2	3	3.52-4	4	1.058
		0	1	1.90-1	1	0.271			3	2	6.89-4		1.054
		1	0	-1.82-1		0.266			4	1	-2.99-3		1.043
		0	2	1.05-2	2	0.538			5	0	3.36-3		1.025
		1	1	-3.61-2		0.536	2	0	0	2	1.14-4	0	0.000
		2	0	3.85-2		0.528			1	1	5.06-2		-0.001
		0	3	-1.38-3	3	0.801			2	0	8.99-1		-0.010
		1	2	-1.99-3		0.803			0	3	-1.51-5	1	0.263
		2	1	7.60-3		0.799			1	2	2.79-3		0.266
		3	0	-7.93-3		0.787			2	1	1.78-1		0.261
		0	4	-2.03-5	4	1.060			3	0	-2.84-1		0.250
		1	3	2.62-4		1.067			0	1	2.07-3	-1	-0.267
		2	2	4.18-4		1.066			1	0	2.56-1		-0.272
		3	1	-1.57-3		1.058			0	0	1.05-2	-2	-0.538
		4	0	1.57-3		1.043			0	4	-2.21-7	2	0.523
									1	3	-3.68-4		0.529
									2	2	9.80-3		0.528
									3	1	-5.63-2		0.520
									4	0	8.52-2		0.505
1	0	0	1	3.76-2	0	0.000			0	5	2.22-7	3	0.778
		1	0	9.29-1		-0.005			1	4	-5.40-6		0.788
		0	2	2.08-3	1	0.267			2	3	-1.29-3		0.791
		1	1	1.84-1		0.266			3	2	-3.10-3		0.787
		2	0	-2.45-1		0.257			4	1	1.69-2		0.776
		0	0	1.90-1	-1	-0.271			5	0	-2.29-2		0.758
		0	3	-2.73-4	2	0.530			0	6	-2.29-2	4	1.030
		1	2	1.01-2		0.533			1	5	5.41-6		1.044
		2	1	-4.85-2		0.528			2	2	1.90-5		1.051
		3	0	6.33-2		0.517			3	3	4.10-4		1.051
		0	4	-4.01-6	3	0.790			4	2	9.27-4		1.043
		1	3	-1.34-3		0.796			5	1	-4.52-3		1.029
		2	2	-2.68-3		0.795			6	0	5.60-3		1.008
		3	1	1.25-2		0.787							
		4	0	-1.51-2		0.772							
		0	5	4.02-6	4	1.045							
		1	4	-1.96-5		1.055							

#### D. Evaluation of Charge-Transfer Cross Sections

The following three procedures for calculating charge-transfer cross sections are adopted in this paper: (a) the resonant two-state treatment, (b) a low-velocity treatment proposed by Bates and Reid<sup>1</sup> which accounts for couplings to 0-band product states, and (c) the full multistate treatment<sup>1</sup> in which complete account is taken of couplings and excitation defects to all product channels. In each of these three descriptions probability is conserved for the forward and reverse transitions and detailed balance between the probabilities  $P_{if} = P_{fi}$  is satisfied at all impact parameters.

##### 1. Procedures

(a) *Two-state treatment.* For the case of resonant collisions at low incident speeds when the product band contains only one set of vibrational states ( $\nu''$ ,  $\nu'$ ), a two-state treatment can be used. Given the target molecule initially in the  $\nu_0'' = 0$  state, the two-state treatment is applicable only to the reaction,



where  $XY$  denotes either  $N_2$  or  $CO$ . Hence, with  $V(R)$  given by (9) and (13), the coupled equations (7) can be solved exactly to give the charge-transfer cross section (1c) in which  $\eta$  is expressed in terms of the potential parameters,

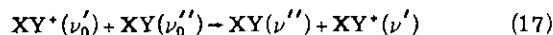
$$\eta(\rho) = (P_{00}/2\nu) D_e \exp(\beta R_e) \int_{\max(\rho, R^*)}^{\infty} [6 \exp(-\beta R) - \exp(\beta R_e) \exp(-2\beta R)] R(R^2 - \rho^2)^{-1/2} dR. \quad (15)$$

For the case of  $\rho > R^*$ , Eq. (15) permits an analytical solution in terms of modified Bessel functions,

$$\eta(\rho) = (P_{00}/2\nu) \rho D_e \exp(\beta R_e) [6K_1(\beta\rho) - \exp(\beta R_e) K_1(2\beta\rho)]. \quad (16)$$

The integrals over  $R$  in (15) when  $\rho < R^*$  and over  $\rho$  in (1c) are evaluated numerically to obtain the charge-transfer cross section.

(b) *Low-velocity approximation.* For collisions of the type



in which the reactant ion is in a vibrationally excited state and more than one set of near-resonant product states exist, the two-state description is inadequate. Bates and Reid<sup>1</sup> have explored this eventuality in the limit of velocities sufficiently low that the exponential terms in (7) may be neglected for those excitation defects corresponding to transitions into bands greater than 0. The summation in (7) is then taken over the 0-band final states,  $B$  in number, all of which are assumed to be degenerate. Thus (7) reduces to

$$i(\partial C_l^{\alpha}/\partial t) = V(R) \sum_{m=1}^B P_{lm} C_m^{\alpha}(\rho, t), \quad l = 1, 2, \dots, B, \quad (18)$$

a set of equations which can be solved exactly, to give

$$Q^X(i \rightarrow B) = 2\pi \sum_{n=1}^B X_{in}^2 \int_0^{\infty} \rho \sin^2 \left[ (\Pi_n/\nu) \int_{-\infty}^{\infty} V(R) dZ \right] d\rho, \quad (19)$$

the total cross section for charge transfer from initial channel  $i(\nu_i', \nu_i'')$  to all final states  $B$  in the resonant 0 band. The square (orthonormal) matrix  $\mathbf{X} = [X_{in}]$  diagonalizes the square matrix  $\mathbf{P} = [P_{ij}]$ , such that the product diagonal matrix  $\mathbf{\Pi} = [\Pi_n]$  is given by the similarity transformation,

$$\mathbf{\Pi} = \mathbf{X}^{-1} \mathbf{P} \mathbf{X} = \tilde{\mathbf{X}} \mathbf{P} \mathbf{X}. \quad (20)$$

The eigenvalues  $\Pi_n$  and the associated eigenvectors  $X_{in}$  are readily evaluated by the Jacobi method, for which standard matrix inversion subroutines are available. One notes that when  $V(R)$  is given by (13), Eq. (15) is identical to the argument of the sine in (19) if  $P_{00}$  is replaced by the appropriate eigenvalues  $\Pi_n$ .

(c) As the impact energy is increased, various nonresonant, vibrationally excited channels become increasingly important, i.e., states other than those belonging to the 0 band must be included in the set of coupled equations (7). These additional channels have of course increasingly large energy defects relative to the incident channel; hence it is not permissible to regard these extra states as being degenerate with the initial state. Thus, the Bates and Reid low-velocity limit is no longer appropriate and the set of coupled differential equations must therefore be solved numerically. The maximum number of states to be included in the summation in (7) obviously depends on the behavior of the energy defects and vibrational overlaps as higher states are included, and can be gauged by examining the convergence of the computed cross sections with the addition of these channels.

##### 2. $N_2^+-N_2$ Calculations

The transition probabilities,  $P_{ij} = |C_j^X|^2$ , as a function of impact parameter are calculated by solving the multistate equations (7) numerically by means of the Adams-Moulton method. Some representative probabilities,  $P_{ij}$ , are shown explicitly in Fig. 3 for the initial reactant state ( $\nu_0' = 0$ ,  $\nu_0'' = 0$ ) at the smallest and largest values of incident-ion kinetic energy studied in this paper. Examination of the curves reveals the more salient features exhibited by charge-transfer collisions in general.

For example,

(a) The number of oscillations in  $P_{ij}$  increases



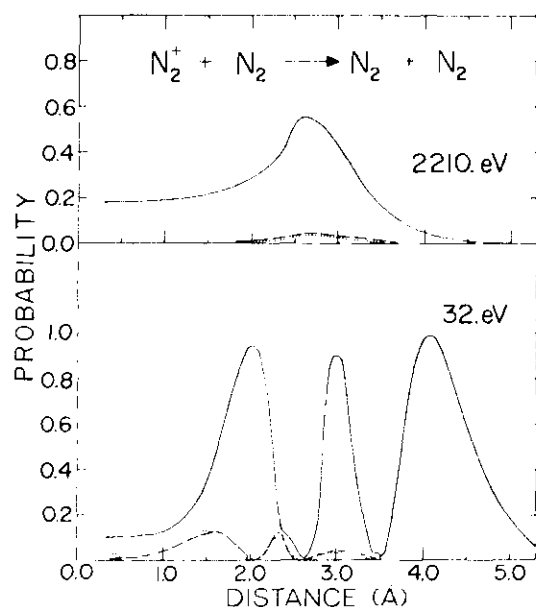


FIG. 3. Probability of charge transfer in the  $N_2^+ - N_2$  system as a function of impact parameter at 2210 and 32 eV reactant-ion kinetic energies. The solid curve represents the  $(0,0|0,0)$  transition while the dashed and dotted curves refer to  $(0,0|0,1)$  and  $(0,0|1,0)$  transitions, respectively.

with decreasing energy and at the lowest energy,  $P_{ij}$  tends to oscillate between 0 and 1. This is a direct manifestation of the  $\sin^2\eta$  behavior of  $P_{ij}$  in Eqs. (1a) and (2a) of the two-state treatment which becomes valid at low incident-ion energies for this particular case.

(b) The main contribution to the total cross section arises from more distant encounters as the impact energy is reduced.

(c) The resonant channel  $(0,0|0,0)$  is dominant at each energy. The contributions from channels  $(0,0|0,1)$  (dashed line) and  $(0,0|1,0)$  (dotted line) of band 1 are small and almost equal as shown in this figure. This is a result of overlaps which are small and almost equal. The relative contributions of these channels to the total cross section, however, increase with higher impact energies.

Charge-transfer cross sections  $Q^X$  were obtained by inserting the transition probabilities into (6), which was numerically integrated using Simpson's rule with a built-in accuracy parameter. The calculated cross sections for the processes,

$$N_2^+(X^2\Sigma_g^+, \nu_0') + N_2(X^1\Sigma_g^+, \nu_0'' = 0) \rightarrow N_2^+(X^1\Sigma_g^+, S_{\nu_0'}) + N_2(X^2\Sigma_g^+, S_{\nu_0'}), \quad (21)$$

are given in Table III for incident-ion kinetic energies of 733 and 2210 eV. The summations  $S_{\nu_0'', \nu_0'}$  are over all vibrational levels within the designated

bands of interest. For  $\nu_0' = 0$ , convergence is obtained by including all the 12 states in the 0, 1, and 2 bands. The addition of the 3 band requires the solution of 20 coupled differential equations, but results in essentially no change in the computed cross sections. For  $\nu_0' = 1$ , the 12-state calculation also yields convergence which, as expected, is reached more rapidly at the lower incident speed. In the case of  $\nu_0' = 1$ , the effect of coupling only to those states in a designated band which have relatively large vibrational overlaps is examined. Such a selection of only the larger vibrational overlaps within a band is represented by the prefix M in Table III. Cross sections so determined do not differ significantly from those obtained by coupling with all the vibrational levels in the various bands. For  $\nu_0' = 2$  and  $\nu_0' = 3$ , the calculations were performed by coupling only with those states having the largest overlaps in bands 0,  $\pm 1$  and in bands 0,  $\pm 1$ ,  $\pm 2$ . Although not much difference is observed by the inclusion of the  $\pm M2$  bands, the effect of the neighboring  $\pm M1$  bands on either side of the near-resonant 0 band is significant. For  $\nu_0' = 4-6$ , coupling to the bands  $\pm M1$ ,  $\pm M2$  is important, particularly at the highest impact velocity. The incident-ion beam in the experiment weights strongly the low vibrational levels at even the highest energies of electron-impact formation, e.g., 58%, 11%, and

TABLE III. Total cross sections (square angstroms) for charge-transfer reactions,  $N_2^+(X^2\Sigma_g^+, \nu_0') + N_2(X^1\Sigma_g^+, \nu_0'' = 0) \rightarrow N_2^+(X^1\Sigma_g^+, \nu_0') + N_2(X^2\Sigma_g^+, \nu_0')$ , from a multistate treatment.

$\nu_0'$	Number of states	Band designation	Ion energy	
			733 eV	2210 eV
0	2	0	32.442	14.702
	6	0, +1	31.471	15.801
	12	0, +1, +2	31.381	15.808
	20	0, +1, +2, +3	31.381	15.808
1	4	0	29.067	12.765
	12	0, $\pm 1$	27.850	14.897
	16	0, $\pm M1$ , + M2	28.987	15.038
	20	0, $\pm 1$ , +2	27.722	14.898
2	6	0	24.654	10.572
	14	M0, $\pm M1$	26.668	13.733
	20	M0, $\pm M1$ , $\pm M2$	26.680	13.925
3	8	0	19.850	8.450
	12	M0, $\pm M1$	23.699	12.722
	18	M0, $\pm M1$ , $\pm M2$	23.908	12.818
4	10	0	15.033	6.463
	20	M0, $\pm M1$ , $\pm M2$	21.173	11.801
5	12	0	10.612	4.691
	18	M0, $\pm M1$ , $\pm M2$	19.146	10.904
6	14	0	6.891	3.192
	20	M0, $\pm M1$ , $\pm M2$	17.941	10.156

TABLE IV. Total cross sections calculated from the Bates and Reid low-velocity limit and from the multistate impact parameter treatment of  $N_2^+(X^2\Sigma_g^+, \nu_0') \rightarrow N_2(X^1\Sigma_g^+, \nu_0'' = 0) \rightarrow N_2(X^1\Sigma_g^+, S_{\nu_0'}) + N_2(X^2\Sigma_g^+, S_{\nu_0'})$ .

$\nu_0'$	Method <sup>a</sup>	Ion energy					
		32 eV	156 eV	400 eV	733 eV	1175 eV	2210 eV
0	A	45.10	36.24	41.30	32.88	24.41	14.87
	B	45.56	36.62	41.08	32.44	24.21	14.70
	C	45.40	36.73	38.70	31.38		15.81
1	A	41.43	38.30	39.10	29.70	21.59	12.94
	B	38.54	35.72	37.91	29.07	21.23	12.77
	C	39.63	35.79	36.73	27.72		14.90
2	A	38.92	39.93	35.80	25.83	18.38	10.80
	B	30.30	32.28	33.02	24.65	17.78	10.57
	C		33.54	35.03	26.68		13.92
3	A	37.23	39.99	31.49	21.72	15.11	8.76
	B	23.95	25.49	26.75	19.85	14.26	8.45
	C		30.07	31.67	23.91		12.82
4	A	36.76	37.86	26.45	17.52	11.97	6.84
	B	21.76	17.62	19.93	15.03	10.86	6.46
	C		25.28	27.37	21.17		11.80
5	A	37.28	33.37	21.01	13.44	9.04	5.10
	B	18.92	10.72	13.56	10.61	7.80	4.69
	C		20.72	24.23	19.15		10.90
6	A	36.34	26.99	15.60	9.70	6.43	3.59
	B	11.90	6.05	8.29	6.89	5.19	3.19
	C		17.76	22.29	17.94		10.16

<sup>a</sup>Method A refers to the low-velocity limit where only states within 0.123 eV of energy resonance are included and are assumed to be degenerate. Method B is the multistate treatment where only states within 0.123 eV of energy resonance are included with explicit account being taken of the energy deficits. Method C is multistate treatment where full account is taken of all states in the 0,  $\pm 1$ , and  $\pm 2$  bands. The symbols  $S_{\nu_0', \nu_0''}$  denote that we have taken the sum of the individual contributions within the designated bands.

4% of the beam initially occupies the  $\nu_0' = 0, 1$ , and 2 states when formed at 90 eV. Convergence in the calculated cross sections was verified for these vibrational levels. Any error resulting from a possible lack of convergence for states  $\nu_0' \geq 4$  is therefore minimized by the appropriate weighting of these higher vibrational levels in the beam when comparing theory with experiment.

In Table IV are displayed charge-transfer cross sections calculated at five ion-impact energies. Method C refers to the multistate treatment (7) in which full account is taken of all states (typically 20 states) with large overlap in the 0,  $\pm 1$ ,  $\pm 2$  bands. Cross sections computed from (19), the low-velocity limit of Bates and Reid, are presented as method A. The two-state treatment (1c), is of course identical with method A only when  $\nu_0' = 0$ , since for this initial state the 0 band includes only one final state. In order to examine the assumption of method A that all states in the 0 band are degenerate, we have performed the full multistate calculation (7) for this band in which the nonzero

excitation defects of the near-resonant channels are explicitly acknowledged (Method B). A comparison between rows A and B reveals that this assumption is indeed valid for the low  $\nu_0'$  states at all energies, but that for  $\nu_0' > 3$  significant errors are introduced, particularly at the lower impact energies and for the higher  $\nu_0'$ . The comparison between rows B and C is a manifestation of the importance of coupling to the neighboring four bands, especially at the higher impact energies.

Theoretical data available for comparison with the present calculations are those due to Gurnee and Magee<sup>2</sup> who carried out a two-state treatment (2a) for the resonant process,

$$N_2^+(\nu_0' = 0) + N_2(\nu_0'' = 0) \rightarrow N_2^0(\nu'' = 0) + N_2^+(\nu' = 0), \quad (22)$$

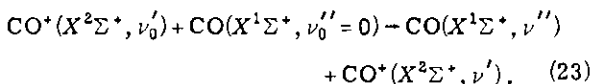
in which they directly evaluated only the first term on the right-hand side of (2b) by using Slater-type nodeless wavefunctions to obtain a cross section of 48 Å<sup>2</sup> for the charge-transfer process at 400 eV incident-ion energy. The present two-state calculations (1c) using the full potential (13) yield 41.1

$\text{\AA}^2$ . This relatively close agreement suggests that the charge-transfer cross sections are not especially sensitive to the particular form of the interaction adopted.

In an effort to examine the change in  $Q^x$  when it is assumed that both collision partners do not vibrate appreciably during a long-lived encounter (see Sec. II, B), we have carried out the two-state calculation in the opposite situation in which the vibrational modes have sufficient time to relax, thereby ensuring  $P_{00} = 1$ . This procedure yields  $Q^x$  of  $49.7 \text{ \AA}^2$  at 32 eV ion energy, to be compared with the value of  $45.1 \text{ \AA}^2$  calculated when vibrational relaxation is not permitted and  $P_{00}$  is computed from isolated molecular vibrational wavefunctions.

### 3. $\text{CO}^+ - \text{CO}$ Calculations

Similar calculations were carried out for the process,



The multistate cross sections obtained by coupling all states with large overlap in the  $0, \pm 1, \pm 2$  bands are presented in Table V, together with those cross sections calculated from the low-velocity

TABLE V. Total cross sections calculated from the Bates and Reid low-velocity limit and from the multistate impact parameter treatment of  $\text{CO}^+(X^2\Sigma^+, \nu_0') + \text{CO}(X^1\Sigma^+, \nu_0'' = 0) \rightarrow \text{CO}(X^1\Sigma^+, S_{\nu''}) + \text{CO}^+(X^2\Sigma^+, S_{\nu'})$ .

$\nu_0'$	Method <sup>a</sup>	Ion energy			
		156 eV	400 eV	733 eV	1910 eV
0	A	33.38	40.55	38.36	22.69
	C	32.96	38.81	36.78	22.86
1	A	33.34	40.80	37.39	21.52
	C	33.49	39.40	36.19	22.20
2	A	33.50	40.87	36.42	20.47
	C	33.43	41.37	36.44	22.05
3	A	33.79	40.79	35.47	19.54
	C	33.52	41.68	35.90	21.65
4	A	34.15	40.62	34.58	18.72
	C	33.85	41.60	35.28	21.31
5	A	34.50	40.42	33.78	18.00
	C	34.17	41.40	34.69	21.01
6	A	34.89	40.15	33.04	17.40
	C	34.48	41.15	34.18	20.76
7	A	35.24	39.88	32.40	16.89
	C	34.79	40.88	33.74	20.56
8	A	35.54	39.62	31.86	16.48
	C	35.14	40.60	33.40	20.38
9	A	35.77	39.40	31.43	16.15
	C	35.37	40.40	33.13	20.26
10	A	35.93	39.26	31.13	15.91
	C	35.72	40.24	32.90	20.19

<sup>a</sup>Method A refers to the low-velocity limit where all product states  $S_{\nu''}$  within 0.102 eV of energy resonance are included and are assumed to be degenerate. Method C is the multistate treatment where full account is taken of all states in the  $0, \pm 1$ , and  $\pm 2$  bands.

limit (19). In general, the multistate treatment entailed the solution of 20 coupled differential equations. A comparison of rows A and C in Table V indicates that the cross sections given by the low velocity limit are in close accord with those obtained from the full multistate treatment except at the highest incident energies and at high  $\nu_0'$ . Such agreement, particularly at the low energies of impact and high  $\nu_0'$ , is in marked contrast to that exhibited in the  $\text{N}_2^+ - \text{N}_2$  system. This difference in behavior is a direct manifestation of the individual characteristics of the vibrational overlaps in the two systems. For a given magnitude of energy deficit, those channels having the largest overlap make the greatest contributions to the charge-transfer cross section. In the low-velocity approximation, only those channels in the 0 band can contribute to the cross section, hence the larger the overlaps occurring in the 0 band relative to all other bands, the better the expected agreement between the low-velocity approximation and the complete multistate treatment. In the  $\text{CO}^+ - \text{CO}$  system, vibrational overlaps for product channels in the 0 band are very much larger than those for product channels in bands  $\pm 1$  and  $\pm 2$ , even for large values of  $\nu_0'$ . On the other hand, product channels overlaps in the  $\text{N}_2^+ - \text{N}_2$  system are more evenly distributed over channels in bands  $0, \pm 1, \pm 2$  for the higher values of  $\nu_0'$ .

### III. EXPERIMENTAL ANALYSIS

The apparatus used in this work was a time-of-flight (TOF) mass spectrometer with a gated electron multiplier which was used to monitor neutral products from the charge-transfer reactions. A more complete description of the experimental arrangement has been given<sup>33</sup>; however an outline of the experiment is appropriate. Reactant ions were produced in a controlled electron-impact ion source and newly formed ions drawn into the acceleration region where they are all given the same kinetic energy. Ionizing electrons were emitted from a directly heated thorium oxide filament. The electron energy was variable from 2 to 100 eV with the electron beam spatially confined by an external collimating magnet. The absolute energy of the electron beam was calibrated from observed rare gas ionization potentials. High-purity gases were admitted through fine-needle control valves into the source and drift tube (collision) sections of the apparatus. Neutral gas pressures in the collision region were measured using a calibrated ionization gauge attached to the drift tube with sufficient mechanical baffles to prevent stray ions produced in the gauge from diffusing into the collision region.

A fully accelerated, focused primary-ion beam enters the main drift region of the TOF spectrom-

eter where time resolution of different velocity ion groups takes place. As ions proceed through this region, it is possible for charge-transfer reactions to occur. The separation of fast neutral products resulting from reactions of primary ions with molecules and atoms in the flight tube was accomplished using a grid assembly placed immediately in front of the electron multiplier. A deceleration voltage applied to this assembly gives ionic species longer arrival time than neutral reaction products having the same mass. Charge-transfer reactions (17) occurring at large impact parameters give rise to fast neutral  $XY^0(\nu'')$  species that can be separated from the unscattered reactant ions by decelerating the ions after passage through the collision region. Neutral gas pressures in the collision region used in this investigation were in the  $10^{-6}$  torr range, similar to those used previously,<sup>33</sup> and were sufficiently low to ensure that the neutral reaction products were formed in single bimolecular collisions. Peak shapes of the neutral  $XY^0$  products were approximately symmetrical indicating that the majority of the charge-transfer products possessed a velocity approximating that of the incident ions. Small energy loss processes corresponding to vibrational excitation accompanying the electron transfer mechanism could not be clearly distinguished from the resonant processes via time-of-flight analysis due to loss of the inherent instrument resolution<sup>34</sup> associated with allowing reactions to occur throughout the spectrometer drift tube. For reactions occurring over the distance ( $l$ ), the ratio of neutral product to incident ion beam flux,  $i_s/i_p$ , is equal to  $C\sigma$ , where  $C$  is the target gas concentration and  $\sigma$  is the reaction cross section. This equality holds provided the collection efficiencies of ionic and neutral particles are identical. We have determined the variation of secondary electron emission of the electron multiplier cathode with  $XY^+$  kinetic energy and find it to be approximately equal for velocity  $XY^0$  and  $XY^+$  species, a result in agreement with previous investigations.<sup>35</sup> The effect of ion internal energy content on the multiplier sensitivity was determined by comparing molecular ionization efficiency curves measured with the multiplier to those using a Faraday cup detector. As the energy of the ionizing electrons is increased from threshold to 100 eV, the internal energy content of many  $XY^+$  molecules is increased, however multiplier sensitivity is not visibly changed by ion internal energy throughout the ion velocity range employed in these measurements. At constant  $C$ , the ratio  $i_s/i_p$  provides a measurement of reaction cross section as the reactant-ion internal state distribution is changed by varying the energy of the electron beam. At the ionization threshold only the lowest vibrational level of the reactant-ion beam is populated.

By increasing the ionizing electron energy we selectively populate higher levels of the ion beam in order to observe their effect on the total charge-transfer cross section.

The molecular ion internal energy state distribution produced by electron-impact ionization of neutral diatomics can be estimated from data existing in the literature. Total cross sections for molecular ion formation as a function of electron energy are obtained by subtracting the cross sections for dissociative ionization<sup>36</sup> from the electron-impact cross sections for total ion production<sup>37</sup> at each electron energy. The initial vibrational state composition of excited molecular ion states formed has been estimated from spectroscopic measurements of optical emissions from these states. Relative cross sections for electron-impact excitation of the  $N_2^+(B^2\Sigma_u^+, \nu') - N_2^+(X^2\Sigma_g^+, \nu'')$  bands are normalized to the absolute cross section for the (0,0) first negative transitions measured by Borst and Zipf.<sup>38</sup> Cross sections for electron impact formation of  $N_2^+(A^2\Pi_u, \nu')$  have been taken from the work of Holland and Maier.<sup>39</sup> Although there is evidence for the existence of other excited  $N_2^+$  states, their population in the beam due to the electron-impact process is small,<sup>40,41</sup> hence we have neglected them in this calculation. The initial vibrational population of the ground-state ions formed as a result of direct ionization processes can be estimated within the framework of the Born-Oppenheimer approximation. The transition probability from vibrational level  $\nu''$  of electronic state  $i$  of a diatomic molecule to a vibrational level  $\nu'$  of electronic state  $j$  of the ion is given by<sup>42</sup>

$$F_{i\nu'', j\nu'} = K(eE - I, P.) |R_{ij}^e(\bar{R}_{\nu'', \nu'})|^2 \left| \int \psi_{\nu'', i} \psi_{\nu', j} dR \right|^2, \quad (24)$$

where  $\psi_{\nu'', i}$  and  $\psi_{\nu', j}$  are the vibrational wavefunctions corresponding to states  $i\nu''$  and  $j\nu'$ , respectively, and  $(eE - I, P.)$  is the electron energy in excess of the excitation threshold. The term  $R_{ij}^e(\bar{R}_{\nu'', \nu'})$ , the  $R$  centroid for the transition, has a much slower variation with internuclear distance than the vibrational overlap integral. Hence, relative vibrational populations are primarily determined by the square of the overlap integral. Sufficient spectroscopic information exists<sup>23,31,43</sup> on the  $N_2(X^1\Sigma_g^+)$  molecule and the  $X$ ,  $A$ , and  $B$  states of the  $N_2^+$  ion to permit accurate vibrational wavefunctions to be constructed<sup>29</sup> and the respective vibrational overlap integrals evaluated<sup>29</sup> for  $N_2 - N_2^+$  ionizing transitions.

The initial vibrational distribution of the  $N_2^+(X^2\Sigma_g^+)$  state is perturbed by radiative transitions from excited ionic states occurring within the 9.6–14.2  $\mu$ sec flight times of the ions in our apparatus. The lifetimes<sup>44,45</sup> of  $N_2^+(B^2\Sigma_u^+, \nu')$  state ions with

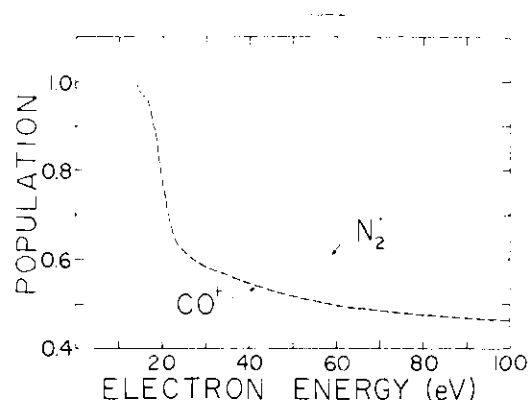


FIG. 4. Population of reactant  $N_2^+(X^2\Sigma^+, \nu'_0=0)$  ions as a function of ionizing electron energy is given by the dotted curve. The population of  $CO^+(X^2\Sigma^+, \nu'_0=0)$  ions as a function of ionizing electron energy is given by the dashed curve.

respect to  $B \rightarrow X$  radiative transitions are on the order of 60 nsec, consequently all  $N_2^+(B^2\Sigma_u^+)$  ions formed in the electron impact ionization of nitrogen undergo radiative transitions<sup>38,46-48</sup> to the  $N_2^+(X^2\Sigma_g^+)$  state within the source region of our apparatus. The lifetime,  $\tau$ , of the  $N_2^+(A^2\Pi_u)$  state formed by electron bombardment of nitrogen has been found<sup>39,49</sup> to approximate 10  $\mu$ sec with respect to spontaneous  $A \rightarrow X$  transitions. As these ions drift down the flight tube,  $A \rightarrow X$  transitions occur exponentially with distance,  $\exp(-t/\tau)$ , where  $\tau$  has been taken<sup>39</sup> to be 15.5, 13.7, 12.2, 11.0, 9.9, 9.1, 8.4  $\mu$ sec for  $\nu' = 0-6$ , respectively. We note that these lower levels are the ones most strongly populated in the electron-impact ionization process; hence a fraction of the  $A^2\Pi_u$  state ions entering the drift tube will emerge from the collision region in the same state. The presence of this small fraction of undecayed  $A^2\Pi_u$  state ions in the reactant-ion beam formed in high-energy electron impact should be considered when computing total charge-transfer cross sections in the simulation of laboratory measurements. Two possible reaction paths are available to these ions in the transfer of charge: (a) the reaction channels where secondary ions are formed in the  $X^2\Sigma_g^+$  state and (b) the channels where secondary ions are formed in the  $A^2\Pi_u$  state. Analysis of the vibrational overlaps for both reaction paths indicates reaction via path (b) is an order of magnitude more favorable than via path (a), yet even the overlaps for product channels formed via (b) are significantly smaller than those encountered for the reaction of ground-state ions. As a result, the contribution to the total charge-transfer cross section due to  $A^2\Pi_u$  ions is much smaller than the population of this state in the reactant-ion beam, however for completeness, we have considered contributions of these reactions in subsequent comparisons between theory and experiment.

Perturbation of the  $N_2^+(X^2\Sigma_g^+)$  state vibrational distribution from  $A \rightarrow X$  radiative transitions prior to reaction was computed using tabulated spectroscopic data.<sup>39</sup> The net vibrational distribution of  $N_2^+(X^2\Sigma_g^+)$  ions is obtained from direct ionizing. Franck-Condon transitions to this level and spontaneous radiative transitions from the  $A^2\Pi_u$  and  $B^2\Sigma_u^+$  states.<sup>30,39,44-50</sup> The fraction of our reactant-ion beam occupying the  $N_2^+(X^2\Sigma_g^+, \nu'_0=0)$  level is shown as the dotted line in Fig. 4 as a function of ionizing electron energy.

The  $CO^+$  reactant-ion state distribution is estimated in the same manner as that outlined for nitrogen. Spectroscopic constants<sup>32</sup> and vibrational overlaps<sup>29</sup> from  $CO(X^1\Sigma^+, \nu''=0)$  to the  $X$ ,  $A$ , and  $B$  states of the ion have been taken from the literature.<sup>29,32</sup> Vibrational overlaps from higher vibrational levels of the neutral not available in the literature have been computed using a Morse anharmonic oscillator routine.<sup>13</sup> The fraction of molecular ions produced in the electron impact ionization of  $CO(X^1\Sigma^+, \nu''=0)$  molecules was estimated from total electron-impact ionization cross section<sup>37</sup> corrected for the fraction of ionization processes that lead to dissociation.<sup>36</sup> Absolute cross sections for production of  $A^2\Pi_u$  and  $B^2\Sigma_u^+$  states of  $CO^+$  by 100 eV electron-impact ionization were taken from the compilation of Aarts and De Heer<sup>51</sup> and the variation of these cross sections with electron energy from 100 eV to threshold were taken from recent spectroscopic investigations.<sup>39,52</sup> The lifetimes of  $CO^+(A^2\Pi_u)$  vibrational levels have been measured by a number of workers (see the tabula-

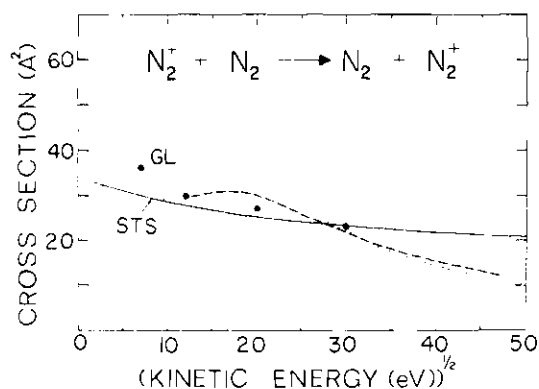


FIG. 5. Comparison between theoretical and experimental total charge-transfer cross sections for  $N_2^+ + N_2$  reactions as a function of the square root of ion kinetic energy. The closed circles are the experimental data of Gustafsson and Lindholm, Ref. 55, while the solid line represents the data of Stebbings, Turner, and Smith, Ref. 54. The dashed curve is the computed cross section using the multistate treatment while the cross sections computed from the low-velocity approximation are given by the dotted curve.

tion of Holland and Maier<sup>39</sup>) to be approximately 2  $\mu$ sec. The lifetimes of the  $\text{CO}^+(B^2\Sigma^+)$  levels approximate 45 nsec.<sup>53,44</sup> These lifetimes are sufficiently short to ensure that most of the excited ion states formed in the electron-impact process undergo radiative transitions to the  $\text{CO}^+(X^2\Sigma^+, \nu'_0)$  states prior to reaction in the collision region of our experimental apparatus. The small fraction of  $A^2\Pi_i$  ions that remains as reactant in our ion beam has been used to weight the charge-transfer cross sections we have computed for this state. The percentage of  $\text{CO}^+(X^2\Sigma^+, \nu'_0=0)$  ions in the reactant-ion beam as the ionizing electron energy is varied from threshold to 90 eV and is shown as the dashed line in Fig. 4.

#### IV. COMPARISON BETWEEN THEORY AND EXPERIMENT

The kinetic energy dependences of computed and experimental total charge-transfer cross sections are compared in Fig. 5 for the  $\text{N}_2$  system. The solid line in this figure is the data of Stebbings *et al.*,<sup>54</sup> while the filled circles are the experimental data of Gustafsson and Lindholm.<sup>55</sup> Cross sections computed using the multistate treatment (7) are shown by the dashed line and cross sections from the low velocity approximation (19) are given by the dotted line. The computed cross sections in this figure have been weighted for a reactant-ion vibrational distribution that is characteristic of 70 eV electron-impact ionization in order to match experimental conditions. There is good agreement between theory and experiment at the lower ion kinetic energies. The divergence observed to occur at the higher ion kinetic energies will be discussed later. It is to be noted that throughout the 0.15–2.2 keV kinetic energy range, the multistate treat-

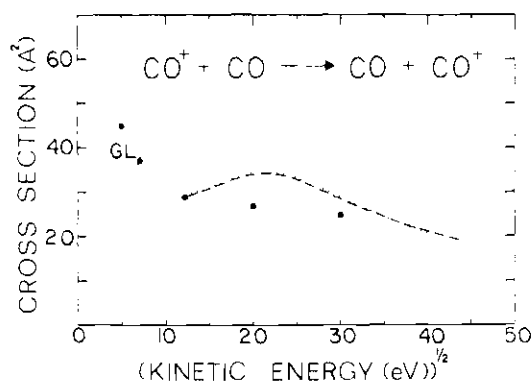


FIG. 6. Comparison between theoretical and experimental total charge-transfer cross sections for  $\text{CO}^+ + \text{CO}$  reactions as a function of the square root of ion kinetic energy. The filled circles are the experimental data of Ref. 55. The dashed curve is the computed cross section using the multistate treatment while the cross section computed from the low-velocity approximation is given by the dotted curve.

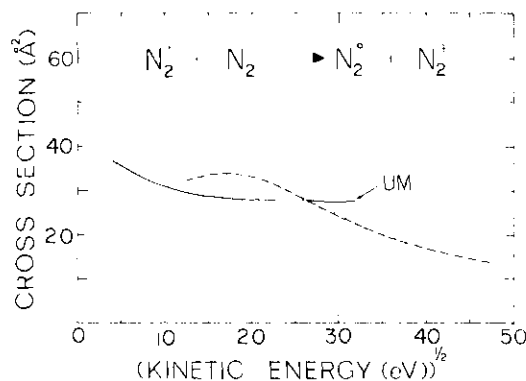


FIG. 7. Comparison between theoretical and experimental total charge-transfer cross sections for  $\text{N}_2^+ + \text{N}_2$  reactions as a function of the square root of ion kinetic energy. The solid line is the cross-section data of Utterback and Miller, Ref. 35, measured for a reactant  $\text{N}_2^+$  beam produced by 22 eV ionizing electron energy. The dashed curve is the cross section computed using the multistate treatment with a reactant-ion vibrational distribution characteristic of 22 eV electron impact. The dotted curve is the corresponding cross section computed with the low-velocity approximation.

ment is in slightly better agreement with experiment than is the low-velocity approximation.

A similar comparison for the CO system between the experimental measurements of Gustafsson and Lindholm<sup>55</sup> (filled circles) and total charge-transfer cross sections computed with the multistate treatment (dashed line) and the low-velocity approximation (dotted line) is displayed in Fig. 6. Here also, the computed cross sections have been weighted for a reactant-ion vibrational distribution characteristic of 70 eV electron-impact ionization. Undulations which occur in the computed cross sections below approximately 80 eV ion kinetic energy have been suppressed for the sake of clarity in this figure. The agreement between the theoretical predictions and measured cross sections is good, especially at the lower incident-ion energies. Almost exact agreement is obtained between the cross sections calculated in the multistate treatment and in the low-velocity approximation. As explained in Sec. II D, such coincidence is a direct result of the large overlaps in the 0-band reaction channels.

Agreement between the computed and experimental cross sections in Figs. 5 and 6 is encouraging. Such agreement could be fortuitous, however, since errors arising from the theoretical model may conveniently compensate any possible errors in the computed ion beam vibrational state distribution when comparing theory with experiment. This point is tested by examining the  $\text{N}_2^+ - \text{N}_2$  charge-transfer cross sections measured by Utterback and Miller<sup>35</sup> with a reactant  $\text{N}_2^+$  ion beam produced by

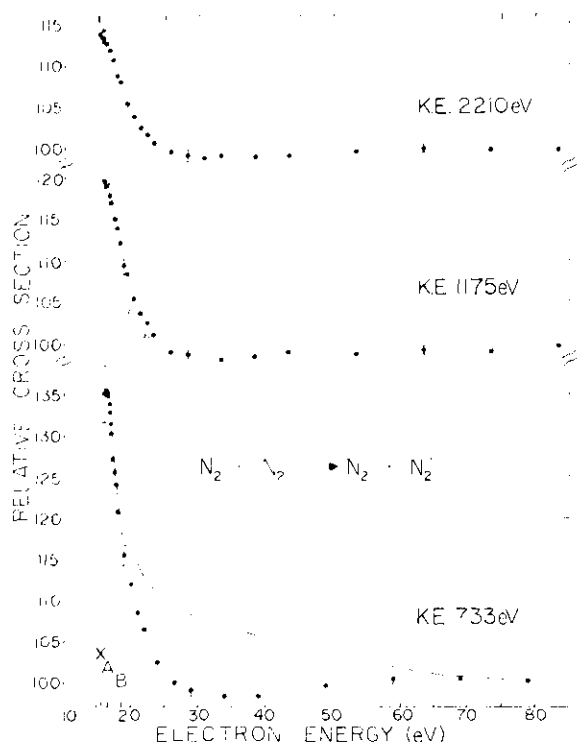


FIG. 8. Relative cross sections for  $N_2^+ + N_2$  charge-transfer reactions as a function of ionizing electron energy for different  $N_2$  initial kinetic energies. Filled circles are our experimental points while unfilled circles are the data of Ref. 56. The dashed curve represents the relative total cross sections calculated using the multistate model. Arrows indicate thresholds for various  $N_2^+$  electronic states.

22 eV electron-impact ionization. The comparison in Fig. 7 between these experimental cross sections and those computed for a reactant-ion beam vibrational distribution characteristic of the 22 eV electron-impact provides a check on the goodness of the internal state distributions used in the comparisons of theory with experiment. We note in this figure that both the experimental and theoretical cross sections are larger than those for the 70 eV data presented in Fig. 5.

A more detailed probe into the effect of reactant-ion vibrational state on the charge-transfer process has been carried out by systematically changing the state distribution of our reactant-ion beam while observing the charge-transfer reaction. This is done conveniently by changing the ionizing electron energy between 90 eV and the ionization thresholds of the respective molecules in a controlled electron-impact ion source and measuring the charge-transfer cross sections at each electron energy. Experimental data thus obtained are presented as the closed circles in Fig. 8 for three representative values of reactant-ion kinetic ener-

gy. The unfilled circles in this figure are the data obtained by McGowan and Kerwin<sup>56</sup> at approximately the same reactant-ion kinetic energy as our measurement. There is good agreement between our results using time-of-flight analysis and those of Ref. 56 who employed a magnetic mass spectrometer. The cross sections measured for 90 eV electron-impact have been normalized to a value of 100 at each ion kinetic energy. The cross sections obtained by lowering the electron energy are presented relative to the 90 eV values in order to directly reflect their percentage increase as the lower vibrational state components in the ion beam are enriched. We have computed the vibrational state distribution of the reactant-ion beam at each electron energy and have used these distributions to weight the multistate reaction cross sections for each vibrational state in order to reproduce the variation in experimental conditions. These total cross sections, the dashed line in Fig. 8, are normalized to 100 for a 90 eV distribution in order to facilitate comparison with our data. The model predicts correctly the general shape and magnitude of the cross sections, although the quantitative fit is poor in the neighborhood of 35 eV. In this intermediate electron energy region it is possible that

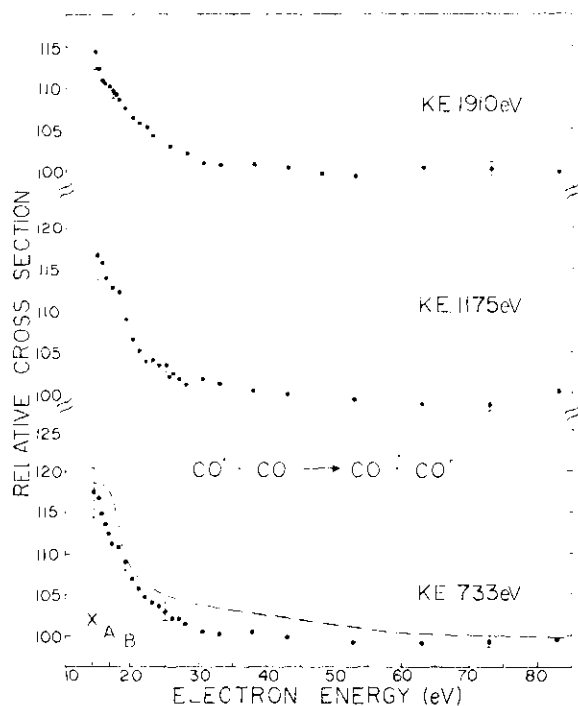


FIG. 9. Relative cross sections for  $CO^+ + CO$  charge-transfer reactions as a function of ionizing electron energy for different  $CO^+$  initial kinetic energies. Filled circles are our experimental points while the dashed curve represents the total cross sections calculated using the multistate model. Arrows indicate thresholds for various  $CO^+$  electronic states.

effects arising from higher  $N_2^+$  electronic states could perturb our computed reactant-ion distributions and thus lead to the 8% disparity between the computed and experimental cross sections. The progressively smaller variation in the relative cross section as the kinetic energy of the ions is increased is not manifested by the theoretical model since the computed relative cross sections remain invariant over this kinetic energy range. This is not surprising since we have not considered other reaction channels in the theoretical model which may strongly compete with charge transfer and which are known to be important at the higher kinetic energies.<sup>56,57</sup> Good agreement between the model and experimental observation is achieved below approximately 1.2 keV. For example, one can combine the data in Fig. 5 and relative cross sections in Fig. 8 to obtain experimental (0,0|0,0) total charge-transfer cross sections of 31.4 and 21.6 Å<sup>2</sup> at 733 and 1175 eV kinetic energies which are comparable to the computed multistate values of 31.4 and 24.2 Å<sup>2</sup>.

The corresponding variation of the relative charge-transfer cross section with ionizing electron energy for the  $CO^+-CO$  system is shown in Fig. 9. The experimental measurements are represented by the filled circles in this figure while the relative cross sections computed from the multistate model are given by the dashed line. As was observed in the  $N_2^+-N_2$  reaction, the computed cross-section variation with electron energy is approximately constant for each of the three ion kinetic energies and reflects the experimental data in Fig. 9. In general, the theoretical description of the  $CO^+-CO$  charge-transfer reactions is in accord with laboratory measurements.

- <sup>1</sup>D. R. Bates and R. H. G. Reid, *Proc. R. Soc. A* **310**, 1 (1969).
- <sup>2</sup>E. F. Gurnee and J. L. Magee, *J. Chem. Phys.* **26**, 1237 (1957).
- <sup>3</sup>J. J. Leventhal, T. F. Moran, and L. Friedman, *J. Chem. Phys.* **46**, 4666 (1967).
- <sup>4</sup>G. J. Lockwood, *Phys. Rev. A* **2**, 1406 (1970).
- <sup>5</sup>R. C. Amme and J. F. McIlwain, *J. Chem. Phys.* **45**, 1224 (1966).
- <sup>6</sup>R. C. Amme and P. O. Haugsjaa, *Phys. Rev.* **165**, 63 (1968).
- <sup>7</sup>P. O. Haugsjaa, R. C. Amme, and N. G. Utterback, *J. Chem. Phys.* **49**, 4641 (1968).
- <sup>8</sup>J. W. McGowan, P. Marmet, and L. Kerwin, *Proc. Intern. Conf. Phys. Electron. At. Collisions*, 3rd, Univ. London, 1963 (1964), p. 854.
- <sup>9</sup>R. C. C. Lao, R. W. Rozett, and W. S. Koski, *J. Chem. Phys.* **49**, 4202 (1968).
- <sup>10</sup>J. A. Rutherford and D. A. Vroom, *J. Chem. Phys.* **55**, 5622 (1971).
- <sup>11</sup>B. R. Turner, J. A. Rutherford, and D. M. J. Compton, *J. Chem. Phys.* **48**, 1602 (1968).
- <sup>12</sup>R. F. Mathis, B. R. Turner, and J. A. Rutherford, *J. Chem. Phys.* **49**, 2051 (1968).
- <sup>13</sup>T. F. Moran and L. Friedman, *J. Chem. Phys.* **42**, 2391 (1965).
- <sup>14</sup>H. C. Hayden and R. C. Amme, *Phys. Rev.* **172**, 104 (1968).
- <sup>15</sup>R. C. Amme and H. C. Hayden, *J. Chem. Phys.* **42**, 2011 (1965).
- <sup>16</sup>D. R. Bates and R. McCarroll, *Philos. Mag. Suppl.* **11**, 39 (1962).
- <sup>17</sup>D. R. Bates and A. R. Holt, *Proc. R. Soc. A* **292**, 168 (1967).
- <sup>18</sup>D. R. Bates and R. McCarroll, *Proc. R. Soc. A* **245**, 175 (1958).
- <sup>19</sup>D. R. Bates and N. Lynn, *Proc. R. Soc. A* **253**, 141 (1959).
- <sup>20</sup>R. McCarroll, *Proc. R. Soc. A* **264**, 547 (1961).
- <sup>21</sup>A. F. Ferguson, *Proc. R. Soc. A* **264**, 540 (1961).
- <sup>22</sup>S. Sato, *J. Chem. Phys.* **23**, 592 (1955).
- <sup>23</sup>G. Herzberg, *Molecular Spectra and Molecular Structure I. Spectra of Diatomic Molecules* (Van Nostrand, Princeton, NJ, 1950).
- <sup>24</sup>R. N. Porter and M. Karplus, *J. Chem. Phys.* **40**, 1105 (1964).
- <sup>25</sup>W. Kolbs and C. C. J. Roothaan, *Rev. Mod. Phys.* **32**, 219 (1960).
- <sup>26</sup>J. O. Hirschfelder, C. F. Curtiss, and R. B. Bird, *Molecular Theory of Gases and Liquids* (Wiley, New York, 1954), pp. 950 and 1110.
- <sup>27</sup>Y. Yang and D. C. Conway, *J. Chem. Phys.* **40**, 1729 (1964).
- <sup>28</sup>J. E. Jordan, S. O. Colgate, I. Amdur, and E. A. Mason, *J. Chem. Phys.* **52**, 1143 (1970).
- <sup>29</sup>D. C. Jain and R. C. Sahni, *Int. J. Quantum Chem.* **2**, 325 (1968).
- <sup>30</sup>R. W. Nicholls, *J. Res. Natl. Bur. Stand. (U.S.) A* **65**, 451 (1961).
- <sup>31</sup>A. Lofthus, "The Molecular Spectrum of Nitrogen," *Spectry. Rept. No. 2*, Department of Physics, University of Oslo, Blindern, Norway, 1960.
- <sup>32</sup>P. H. Krupenie and S. Weissman, *J. Chem. Phys.* **43**, 1529 (1965).
- <sup>33</sup>T. F. Moran and R. J. Conrads, *J. Chem. Phys.* **58**, 3793 (1973).
- <sup>34</sup>R. J. Conrads, W. Pomerance, and T. F. Moran, *J. Chem. Phys.* **57**, 2468 (1972).
- <sup>35</sup>N. G. Utterback and G. H. Miller, *Rev. Sci. Instrum.* **32**, 1101 (1961).
- <sup>36</sup>D. Rapp, P. Englander-Golden, and D. D. Briglia, *J. Chem. Phys.* **42**, 4081 (1965).
- <sup>37</sup>D. Rapp and P. Englander-Golden, *J. Chem. Phys.* **43**, 1464 (1965).
- <sup>38</sup>W. L. Borst and E. C. Zipf, *Phys. Rev. A* **1**, 834 (1970), see also B. N. Srivastava and I. M. Mirza, *Phys. Rev.* **176**, 137 (1968).
- <sup>39</sup>R. F. Holland and W. B. Maier II, *J. Chem. Phys.* **56**, 5229 (1972).
- <sup>40</sup>W. B. Maier II, *J. Chem. Phys.* **55**, 2699 (1971).
- <sup>41</sup>R. F. Holland and W. B. Maier II, *J. Chem. Phys.* **57**, 4497 (1972).
- <sup>42</sup>R. W. Nicholls and A. L. Stewart, in *Atomic and Molecular Processes*, edited by D. R. Bates (Academic, New York, 1972).
- <sup>43</sup>L. Wallace, *Astrophys. J. Suppl. Ser.* **6**, 445 (1962).
- <sup>44</sup>J. Desesquelles, M. Dufay, and D. C. Pouizac, *Phys. Lett. A* **27**, 96 (1968).
- <sup>45</sup>J. E. Hesser, *J. Chem. Phys.* **48**, 2518 (1968).
- <sup>46</sup>J. W. McConkey, J. M. Woolsey, and D. J. Burns, *Planet. Space Sci.* **19**, 1192 (1971).
- <sup>47</sup>W. R. Pendleton, Jr. and R. R. O'Neil, *J. Chem. Phys.* **56**, 6260 (1972).
- <sup>48</sup>H. Nishimura, *J. Phys. Soc. Jap.* **24**, 130 (1968).
- <sup>49</sup>D. D. Gray, T. D. Roberts, and J. L. Morack, *J. Chem. Phys.* **57**, 4190 (1972) and also J. R. Peterson and J. T. Moseley, *J. Chem. Phys.* **58**, 172 (1973).



- <sup>50</sup>D. C. Cartwright, *J. Chem. Phys.* **58**, 178 (1973).  
<sup>51</sup>J. F. M. Aarts and F. J. De Heer, *Physica (The Hague)* **49**, 425 (1970).  
<sup>52</sup>J. M. Ajello, *J. Chem. Phys.* **55**, 3158 (1971).  
<sup>53</sup>R. G. Bennett and F. W. Dalby, *J. Chem. Phys.* **31**, 434 (1959).

- <sup>54</sup>R. F. Stebbings, B. R. Turner, and A. C. Smith, *J. Chem. Phys.* **38**, 2277 (1963).  
<sup>55</sup>E. Gustafsson and E. Lindholm, *Ark. Fys.* **18**, 219 (1960).  
<sup>56</sup>W. McGowan and L. Kerwin, *Can. J. Phys.* **42**, 2086 (1964).  
<sup>57</sup>T. F. Moran, F. C. Petty, and A. F. Hedrick, *J. Chem. Phys.* **51**, 2112 (1969).

## APPENDIX III

PARTICIPATION OF INCIDENT ION INTERNAL ENERGY IN  
MOLECULAR  $O_2^+$  - AR CHARGE-TRANSFER COLLISIONS

This appendix is the reprint of an article published in Chemical  
Physics Letters, Volume 24, pages 431 to 436, 1 February 1974.

# PARTICIPATION OF INCIDENT ION INTERNAL ENERGY IN MOLECULAR $O_2^+$ -Ar CHARGE-TRANSFER COLLISIONS

P.C. COSBY, T.F. MORAN, J.V. HORNSTEIN and M.R. FLANNERY

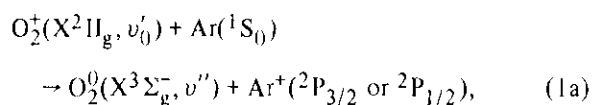
*Georgia Institute of Technology, Atlanta, Georgia 30332, USA*

Received 25 October 1973

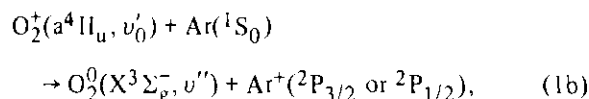
The  $O_2^+$ -Ar charge-transfer reactions have been investigated for both the  $X^2\Pi_g$  and  $a^4\Pi_u$  states of  $O_2^+$  in the kinetic energy range of 0.7 to 3.0 keV. Exhibited resonant and non-resonant behavior of the cross sections is consistent with theoretical predictions.

Charge-transfer processes involving excited ions with neutral species have received scant attention largely because of the difficulties associated with the production of well-defined, excited-state ion beams and the quantitative assessment of their state distribution. The lack of an accurate determination of the excited-state component in individual reactant-ion beams renders it difficult to make meaningful comparisons of theoretical charge-transfer cross sections with much of the existing observational data in the literature. Measured charge-transfer cross sections involving collisions of atomic ions with  $N_2$  molecules have been shown to vary with the excited-state component of the reactant-ion beam. This excited-state distribution depends on the experimental operating parameters in either radio-frequency [1] or electron-impact [2-5] sources.

The  $O_2^+$  ion has been chosen for study in this work because a large fraction of the  $O_2^+$  ions formed in electron-impact ionization populate the long-lived  $a^4\Pi_u$  excited state and sufficient spectroscopic information is available [6] so as to permit quantitative assessment of the internal state distribution of this reactant-ion beam. In order to examine competition between ground- and excited-state reaction channels, argon was chosen as the neutral target since charge transfer is endothermic in the process



only from  $v'_0 \geq 15$  of the  $X^2\Pi_g$  state where vibrational overlaps are small, while near energy balance with favorable overlap exists in the process



for all vibrational states of the ion. The excitation defects for a representative sample of the channels involving different reactant vibrational levels are given in table 1 together with vibrational overlaps between initial and final states of the diatomic.

The  $O_2^+$  internal state distribution produced by direct 90 eV electron-impact ionization initially [6-14] consists of ions in the  $X^2\Pi_g$ ,  $a^4\Pi_u$ ,  $A^2\Pi_u$ ,  $b^4\Sigma_g^-$  and dissociative [15]  $B^2\Sigma_g^-$  states. The lifetimes [6, 14] of the  $A^2\Pi_u$  and  $b^4\Sigma_g^-$  states are sufficiently short with respect to the residence time of ions in our source region so as to ensure decay into the  $X^2\Pi_g$  and  $a^4\Pi_u$  states prior to collision. The  $a^4\Pi_u$  state is spin forbidden to undergo a radiative transition to the ground state [16, 17], thus the beam is composed of  $O_2^+(X^2\Pi_g)$  and  $O_2^+(a^4\Pi_u)$  ions. Measured charge-transfer cross sections for reaction (1) must be resolved into two components [4]:

$$\sigma_{90} = f\sigma_a + (1-f)\sigma_X, \quad (2)$$

where  $f$  is the fraction of the reactant-ion beam in the  $a^4\Pi_u$  state while  $\sigma_X$  and  $\sigma_a$  are the charge-transfer cross

Table I  
 Energetics and overlaps for charge-transfer reactions  $O_2(X^2\Pi_g, v'_0) + Ar(^1S_0) \rightarrow O_2(X^3\Sigma_g^-, v'') + Ar(^1P_{1/2,3/2})$

Ion	Neutral $X^3\Sigma_g^-$ vibrational level	$\langle\psi_{v'_0} \psi_{v''}\rangle$	Energy defects $\epsilon_{nm}$ (eV)	
			$^2P_{3/2}$	$^2P_{1/2}$
$X^2\Pi_g, v'_0=0$	0	0.434	-3.688	-3.865
	1	-0.521	-3.887	-4.064
	2	0.479	-4.089	-4.266
	3	-0.387	-4.293	-4.471
$X^2\Pi_g, v'_0=1$	0	0.604	-3.447	-3.625
	1	-0.285	-3.646	-3.824
	2	-0.073	-3.848	-4.026
	3	0.290	-4.053	-4.231
$a^4\Pi_u, v'_0=0$	0	0.098	0.3445	0.1669
	1	0.232	0.1456	-0.0320
	2	0.371	-0.0564	-0.2339
	3	0.464	-0.2613	-0.4389
	4	0.480	-0.4694	-0.6469
	5	0.423	-0.6805	-0.8581
	6	0.324	-0.8948	-1.0723
	7	0.218	-1.1121	-1.2897
	8	0.130	-1.3326	-1.5102
	9	0.069	-1.5563	-1.7338
	10	0.032	-1.7830	-1.9606
$a^4\Pi_u, v'_0=1$	0	-0.188	0.4754	0.2979
	1	-0.351	0.2765	0.0989
	2	-0.398	0.0746	-0.1030
	3	-0.272	-0.1304	-0.3070
	4	-0.025	-0.3384	-0.5160
	5	0.229	-0.5496	-0.7271
	6	0.389	-0.7638	-0.9414
	7	0.423	-0.9812	-1.1587
	8	0.359	-1.2017	-1.1379
	9	0.255	-1.4253	-1.6029
	10	0.155	-1.6521	-1.8297

sections for reactions (1a) and (1b), respectively.

The apparatus [18, 19] used to measure the cross sections consisted of a time-of-flight mass spectrometer coupled with a controlled electron-impact ionization source and gated electron multiplier detector. Gas pressures in the collision region were monitored by a calibrated ionization gauge and were sufficiently low to ensure the reaction proceeded through single binary encounters. The cross sections measured for reaction (1) where the  $O_2^+$  ions are formed by 90eV electron-impact were calibrated by measurement of the resonant reaction



which has been previously investigated [20] using compatible source conditions. The relationship between these cross sections at a given reactant-ion kinetic energy is:

$$\sigma_{Ar} = \sigma_{O_2} \frac{(I_s/I_p)_{Ar}}{(I_s/I_p)_{O_2}} \frac{P_{O_2}}{P_{Ar}}, \quad (4)$$

where  $I_s$  is the intensity of the product  $O_2^0$  formed in the charge-transfer reaction,  $I_p$  is the intensity of the

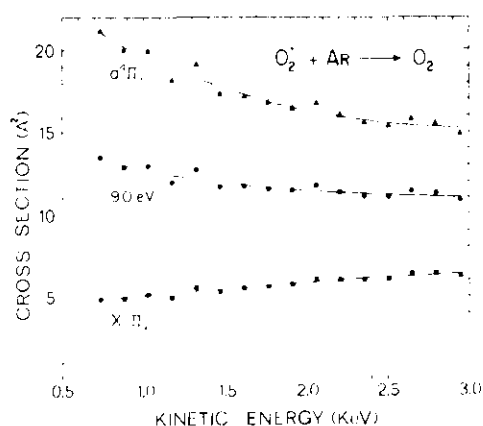


Fig. 1. Charge-transfer cross sections for  $O_2^+(X^2\Pi_g) + Ar$  reactions as a function of laboratory ion kinetic energy are shown as the squares. The triangles are the corresponding  $O_2^+(a^4\Pi_u)$  reactions, while the circles are the total charge-transfer cross sections measured at 90 eV ionizing electron energy.

incident  $O_2^+$  beam, and  $P_{O_2}/P_{Ar}$  is the ratio of the target gas pressures.

The circles in fig. 1 represent the kinetic-energy dependence measured for the  $O_2^+ - Ar$  cross section when the  $O_2^+$  is formed at 90 eV electron-impact. The variation of charge-transfer cross sections with ionizing electron energy is shown in fig. 2. The squares correspond to the cross section at 1910 eV ion kinetic energy while the dotted and dashed curves represent the corresponding electron energy dependence for incident-ion kinetic energies of 733 and 2944 eV, respectively. Each of these curves approaches a minimum at approximately 16 eV, the threshold for formation of the  $O_2^+(a^4\Pi_u)$  state. Below 15 eV, electron-impact ionization produces  $O_2^+(X^2\Pi_g, v_0')$  ions in significant concentrations only for  $v_0' \leq 6$ . The universally large energy defects for these states in reaction (1a) are consistent with the measurement of ground-state cross section which, within experimental error, is independent of  $v_0'$ . Autoionizing processes [21, 22] occurring at electron energies below 20 eV give rise to the production of  $O_2^+(X^2\Pi_g)$  ions in highly vibrationally excited states [23–29] for which near-resonant charge-transfer channels exist. The presence of these states in the beam above 15 eV electron energy may be indicated by the increasingly diffuse nature of the  $\sigma_a$  threshold at the higher incident-ion kinetic energies. The kinetic-energy dependence of the cross section for reaction (1a), shown as the squares

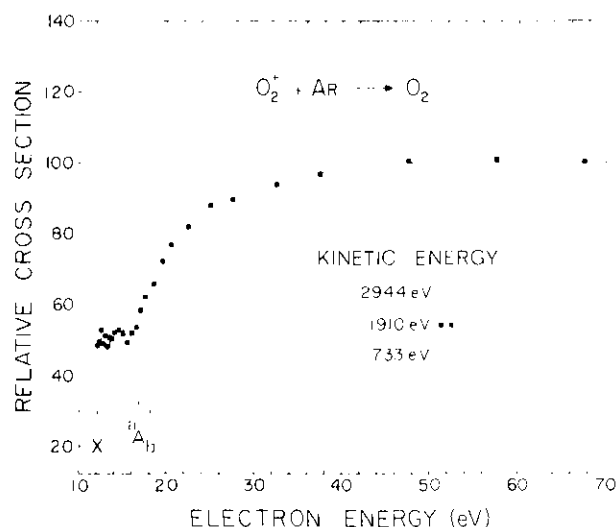


Fig. 2. Relative  $O_2^+ + Ar$  charge-transfer cross sections measured as a function of ionizing electron energy. The dashed line, squares and dotted line represent data obtained at 2944, 1910, and 733 eV laboratory ion kinetic energy, respectively.

in fig. 1, is characteristic of a non-resonant process.

The fraction of  $O_2^+(a^4\Pi_u)$  in the ion beam produced by electron-impact ionization can be estimated from existing spectroscopic data [7–17, 30, 31] using a method previously outlined [19]. We find that for 90 eV electrons, 51 percent of the ion beam consists of  $O_2^+(a^4\Pi_u)$  ions at the time of reaction, a value somewhat higher than that measured in ref. [4] using an attenuation technique. The cross section for reaction (1b) can therefore be determined using eq. (2) and is presented as a function of incident-ion kinetic energy by the triangles in fig. 1.

The general behavior displayed in fig. 1 for the cross sections for (1a) and (1b) is in keeping with the following theoretical arguments. In the low impact-velocity region, a two-state impact-parameter description of the collision is adequate [19], i.e., the wavefunction for the total system during the collision can be expanded (with all quantities in atomic units) as

$$\Psi(r_i, R_A; R(t)) = a_1(t)\phi_n^D \exp(-iE_n^D t) + a_2(t)\phi_m^X \exp(-iE_m^X t), \quad (5)$$

where

$$\phi_n^D(R_A, r_i) = P^+(v_0' | R_A) Y_{JM}(\hat{R}_A) M_i^+(r_a) X_j(r_b), \quad (6)$$

being a product of undistorted  $O_2^+$  and Ar internal functions, represents the eigenfunction for the isolated ( $O_2^+ - Ar$ ) system at infinite separation  $R$  and where

$$\phi_m^X(R_A, r_i) = P(v'' | R_A) Y_{JM}(\hat{R}_A) M_k(r_{a+1}) X_l^+(r_{b-1}) \quad (7)$$

is the corresponding eigenfunction for ( $O_2 - Ar^+$ ) well after the electron-capture collision. The internuclear distance of the diatomic species is  $R_A$ , and  $P^+$  and  $P$  denote the vibrational wavefunctions for  $O_2^+$  in state  $v_0'$  and  $O_2$  in state  $v''$ , respectively. The electronic transition causes no change in the rotation of the oxygen nuclei, leaving the rotational wavefunction  $Y_{JM}(\hat{R}_A)$  for the diatomic ion in state  $(J, M)$  unaffected. The electronic motions are described by  $M_i^+$  and  $M_k$  for the molecular ion in electronic state  $i$  and neutral in state  $k$  with composite electronic coordinates denoted by  $r_a$  and  $r_{a+1}$ , respectively, while  $X_l^+$  and  $X_j$  are the corresponding electronic wavefunctions for the atomic ion in state  $l$  and neutral in state  $j$ . In the initial (or direct D) channel, the internal energy is

$$E_n^D = \epsilon_{\text{rot}}(J_A) + \epsilon_{\text{vib}}(v_0') + \epsilon_i(O_2^+) + \epsilon_j(Ar) \quad (8)$$

and the internal energy in the final (or exchange X) channel is

$$E_m^X = \epsilon_{\text{rot}}(J_A) + \epsilon_{\text{vib}}(v'') + \epsilon_k(O_2) + \epsilon_l(Ar^+), \quad (9)$$

where  $\epsilon_i(X)$  denotes the energy of  $X$  in electronic state  $i$  and the rotational and vibrational energies are  $\epsilon_{\text{rot}}$  and  $\epsilon_{\text{vib}}$ , respectively. The energy defects  $\epsilon_{mn} = E_m^X - E_n^D$  are shown in table 1 for the various initial and final channels. The time-dependent Schrödinger equation is

$$\mathcal{H}\Psi = [H^D + V^D]\Psi = [H^X + V^X]\Psi = i\partial\Psi/\partial t, \quad (10)$$

where  $\mathcal{H}$  is the total hamiltonian for the systems at time  $t$ ,  $H^{D,X}$  are the hamiltonians for the isolated systems at  $t \rightarrow \mp \infty$ , and  $V^{D,X}$  are the (time-dependent) prior and post electrostatic interactions. By substituting (5)–(7) into (10) the following equation

$$\begin{aligned} i[\dot{a}_2 + \dot{a}_1 \langle \phi_m^X | \phi_n^D \rangle \exp(i\epsilon_{mn}t)] \\ = a_1 \langle \phi_m^X | V^D | \phi_n^D \rangle \exp(i\epsilon_{mn}t) + a_2 \langle \phi_m^X | V^X | \phi_m^X \rangle \end{aligned} \quad (11)$$

is obtained for the transition amplitude  $a_2(t) \equiv a_2(\rho, Z)$ . The impact parameter is  $\rho$  and a rectilinear trajectory is assumed such that  $Z = vt$  where  $v$  is the incident speed. The companion equation for  $a_1$  can also be written down.

Neglecting the electronic overlap  $\langle \phi_n^D | \phi_m^X \rangle$ , assuming that  $a_1(t) = \delta_{i1}$  in the right-hand side of eq. (11) and substituting (6) and (7) in (11), the transition probability for electron capture reduces to

$$|a_2(\rho, \infty)|^2 = (|\langle P | P^+ \rangle|^2 / v^2) \times \left| \int_{-\infty}^{\infty} V_{mn}(R) \exp[i(E_m^X - E_n^D)Z/v] dZ \right|^2, \quad (12)$$

where the matrix element  $V_{mn}(R) = \langle MX^+ | V^D | M^+X \rangle$ , the prior electrostatic interaction averaged over the initial and final electronic wavefunctions, is assumed to be independent of  $R_A$ , and hence  $V_{mn}$  is dependent only on  $R$ , the position of Ar relative to the diatomic center of mass. The total cross section for charge transfer is

$$Q_n^X(v) = 2\pi \int_0^\infty |a_2(\rho, \infty)|^2 \rho d\rho. \quad (13)$$

Eqs. (12) and (13) demonstrate that  $Q_n^X$  is a function of both the energy defect and the vibrational overlaps, as expected. Fig. 3 illustrates the magnitude of the vibrational overlap between each initial and final state of the diatomic together with the energy defects for reaction channels accessible via reaction path (1b) in which  $v_0', v'' \leq 10$ . Fig. 3 demonstrates that essentially every initial vibrational level of the  $a^4\Pi_u$  state has at least one channel where energy defects are minimal and overlaps are significant. The resonant character displayed for the  $a^4\Pi_u$  state cross section suggests the strong role these near-resonant channels play in charge-transfer reactions. The following general characteristics can be deduced from (12).

(i) For (1b) the oxygen ion is initially in the  $a^4\Pi_u$  state and the energy defects,  $E_m^X - E_n^D$ , are very small compared with those in (1a) when the initial state is  $X^2\Pi_g$ . The larger defects cause rapid oscillation in the integrand of (12), such that cancellation occurs, thereby reducing  $Q_n^X$ . For reaction (1b),  $E_a^D$  and  $E_X^X$  are comparatively close and no severe cancellation is evident. Moreover, the vibrational overlaps  $|\langle P^+ | P \rangle|$  in (12) are larger for the near-resonant channels of (1b), and so

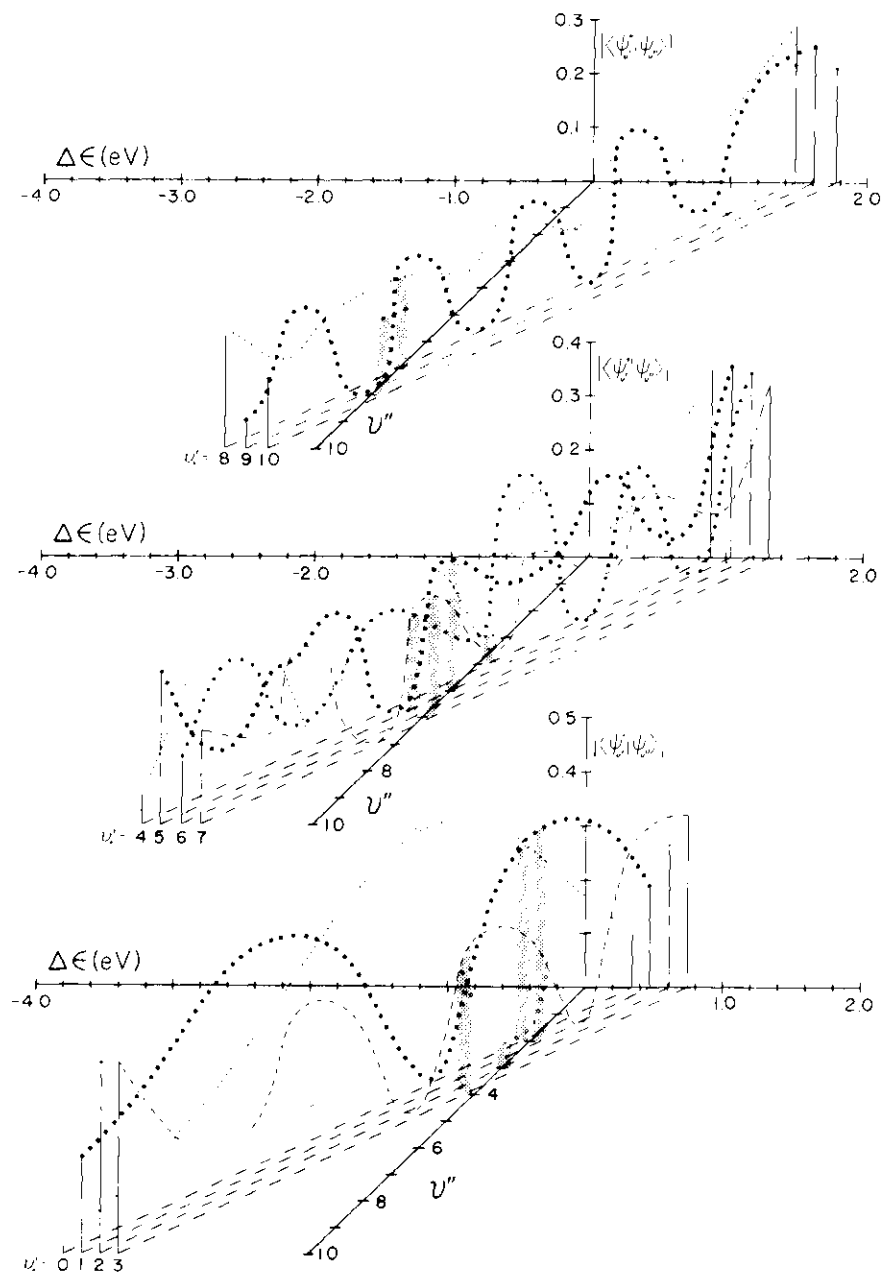
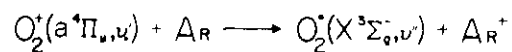


Fig.3. The variation of energy defect and magnitude of the vibrational overlap integral with  $\text{O}_2^+(\text{X}^3\Sigma_g^-, v'')$  product vibrational level for different  $\text{O}_2^+(a^4\Pi_u, v')$  reactant vibrational levels when the argon ion is formed in the  $^2\text{P}_{3/2}$  state. The shaded areas accent product channels within 0.1 eV of thermoneutrality. Corresponding values for formation of  $\text{Ar}^+(^2\text{P}_{1/2})$  requires translation of the curves by  $-0.178$  eV along the energy axis.

$Q_a^X > Q_X^X$ . The interaction matrix elements  $V_{mn}$  for the  $a$  and  $X$  molecular states, which dissociate to the same products  $O(^3P) + O(^4S)$ , are expected to be similar.

(ii) As the impact speed ( $v \ll 1$  au) decreases, the more rapid oscillations cause the integral in (12) for reaction (1a) to decrease more rapidly than  $v^2$  such that  $Q_X^X$  decreases.

(iii) For the  $a$  state,  $E_a^D = E_X^X + \Delta$  with  $\Delta$  small. The  $v^2$  variation, therefore, controls  $Q_a^X$ , which increases, until at sufficiently low velocities the  $\exp(i\Delta Z/v)$  term takes effect, thereby causing the cross section to reach a maximum and then to fall off rapidly to zero as  $v \rightarrow 0$ . The experiment was not performed at the low incident speeds where the maximum would be expected.

(iv) In the above first-order treatment, contributions arising from transitions to all higher vibrational levels are ignored. However, with increasing speed many levels which are close (cf. fig.3) become populated and hence a multistate impact-parameter description is essential. It has already been shown [19] that such a procedure preserves the basic characteristics of  $Q_n$  as noted above, but does increase the total cross section at the higher incident speeds and causes a fall-off much slower than the  $v^{-2}$  dependence predicted by (12).

In conclusion, experimental observations and the above theoretical model display that favorable vibrational overlaps and small energy defects must occur simultaneously in order that the charge-transfer cross section exhibit resonant behavior.

## References

- [1] G.J. Lockwood, Phys. Rev. A2 (1970) 1406.
- [2] J.A. Rutherford and D.A. Vroom, J. Chem. Phys. 55 (1971) 5622.
- [3] R.C.C. Lao, R.W. Rozett and W.S. Koski, J. Chem. Phys. 49 (1968) 4202.
- [4] B.R. Turner, J.A. Rutherford and D.M.J. Compton, J. Chem. Phys. 48 (1968) 1602.
- [5] R.F. Mathis, B.R. Turner and J.A. Rutherford, J. Chem. Phys. 49 (1968) 2051.
- [6] P.H. Krupenie, J. Phys. Chem. Ref. Data 1 (1972) 423.
- [7] R.K. Asundi and C.V.S. Ramachandrarao, Chem. Phys. Letters 4 (1969) 89.
- [8] D.L. Albritton, A.L. Schmeltekopf and R.N. Zare, Diatomic intensity factors (Wiley, New York), in preparation.
- [9] D.W. Turner, C. Baker, A.D. Baker and C.R. Brundle, Molecular photoelectron spectroscopy (Wiley-Interscience, New York, 1970) ch. 3.
- [10] A.J. Blake and J.H. Carver, J. Chem. Phys. 47 (1967) 1038.
- [11] R.W. Carlson and D.L. Judge, J. Chem. Phys. 54 (1971) 1832.
- [12] J.W. McConkey and J.M. Woolsey, J. Phys. B2 (1969) 529.
- [13] H. Nishimura, J. Phys. Soc. Japan 24 (1968) 130.
- [14] W.L. Borst and E.C. Zipf, Phys. Rev. A1 (1970) 1410.
- [15] P.H. Doolittle, R.I. Schoen and K.E. Schubert, J. Chem. Phys. 49 (1968) 5108.
- [16] D.W. Vance, Phys. Rev. 169 (1968) 263.
- [17] R.C. Amme and N.G. Utterback, Proceedings of 3rd international conference on the physics of electronic and atomic collisions, London, 1963 (North-Holland, Amsterdam, 1964) p. 847.
- [18] T.F. Moran and R.J. Conrads, J. Chem. Phys. 58 (1973) 3793.
- [19] M.R. Flannery, P.C. Cosby and T.F. Moran, J. Chem. Phys. 59 (1973), to be published.
- [20] R.F. Stebbings, B.R. Turner and A.C.H. Smith, J. Chem. Phys. 38 (1963) 2277.
- [21] C.E. Brion and G.E. Thomas, Intern. J. Mass Spectrom. Ion Phys. 1 (1968) 25.
- [22] J.W. McGowan, E.M. Clarke, H.P. Hanson and R.F. Stebbings, Phys. Rev. Letters 13 (1964) 620.
- [23] J.D. Morrison, J. Chem. Phys. 39 (1963) 200.
- [24] F.H. Dorman, J.D. Morrison and A.J.C. Nicholson, J. Chem. Phys. 32 (1960) 378.
- [25] E. Lindholm, Arkiv. Fysik 40 (1969) 117.
- [26] A.L. Smith, J. Quant. Spectry. Radiative Transfer 10 (1969) 1129.
- [27] J.E. Collin and P. Natalis, Intern. J. Mass Spectrom. Ion Phys. 2 (1969) 231.
- [28] G.R. Branton, D.C. Frost, T. Makita, C.A. McDowell and I.A. Stenhouse, in: Recent developments in mass spectrometry, eds. K. Ogata and T. Hayakawa (Univ. Tokyo Press, Tokyo, 1970) p. 756.
- [29] J. Geiger and B. Schroder, J. Chem. Phys. 49 (1968) 740.
- [30] D. Rapp, P. Englander-Golden and D.D. Briglia, J. Chem. Phys. 42 (1956) 4081.
- [31] D. Rapp and P. Englander-Golden, J. Chem. Phys. 43 (1965) 1464.



## APPENDIX IV

COMPETITION BETWEEN DOUBLE AND SINGLE ELECTRON TRANSFER  
IN 2-8 KEV  $\text{AR}^{++}$  - AR COLLISIONS

This appendix is the reprint of an article published in the Journal of Chemical Physics, Volume 57, pages 3569 to 3570, 15 October, 1972.

*Reprinted from:*

THE JOURNAL OF CHEMICAL PHYSICS

VOLUME 57, NUMBER 8

15 OCTOBER 1972

## Competition between Double and Single Electron Transfer in 2–8 keV $\text{Ar}^{++}$ –Ar Collisions

P. C. COSBY AND T. F. MORAN

*School of Chemistry, Georgia Institute of Technology, Atlanta, Georgia 30332*

(Received 30 June 1972)

Studies of bimolecular reactions between doubly charged atomic ions and neutral atoms have shown that it is possible for either one or two electrons to be transferred to the incident ion.<sup>1–3</sup> Cross sections for the transfer of two electrons in symmetric rare gas

ion–atom systems are comparatively large ( $\sim 5 \text{ \AA}^2$ ) at low kinetic energies and decrease with reactant ion velocity,<sup>4</sup> whereas single electron capture cross sections generally increase as a function of velocity.<sup>5</sup> Measurements of single electron transfer probabilities have

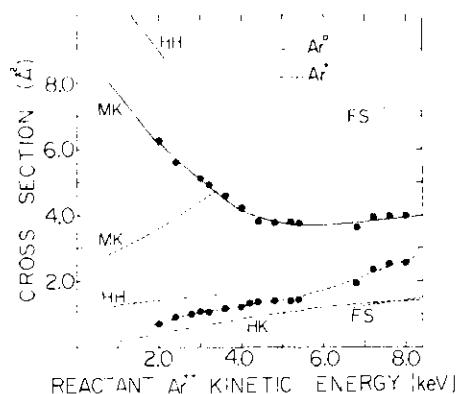
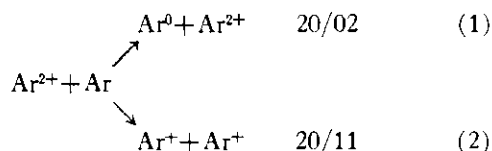


FIG. 1. Cross section as a function of  $\text{Ar}^{2+}$  kinetic energy. The solid points in the upper portion of this figure refer to those measured for Reaction (1) while those on the lower portion refer to those for Reaction (2). The labeled solid and dashed lines are previous measurements of Reactions (1) and (2), respectively, (FS are those of Ref. 1, HH those of Ref. 2, MK those of Ref. 3, and HK are those of Ref. 5).

been used<sup>6</sup> to gain information on the pseudocrossing of adiabatic potential energy curves<sup>7-10</sup> and the role of energy balance<sup>11</sup> and symmetry<sup>12</sup> in determining product exit channels. In order to examine the competition between the single and double electron transfer processes, we have used a time-of-flight (TOF) technique to measure cross sections for the two reaction channels



over a range of kinetic energies where there is a lack of experimental data. Measurements were made using a TOF spectrometer with a separate grid assembly placed at the end of the flight tube directly in front of the multiplier region.<sup>13</sup> In the absence of accelerating or retarding voltages placed on this grid assembly, the primary  $\text{Ar}^{2+}$  formed via electron impact ionization in the source region is observed as a discrete peak with a  $m/q$  of 20. Ions emerging from the source quickly achieve full acceleration and proceed down the drift tube where ion-molecule interactions can occur. The fast products of charge exchange Reactions (1) and (2) occurring in this drift region of the spectrometer also appear at mass 20 since the ion-atom interactions leading to fast  $\text{Ar}^0$  and  $\text{Ar}^+$  products have approximately the same flight times as the primary  $\text{Ar}^{2+}$  ions. Application of a retarding voltage on the aforementioned grid assembly resolves the single peak into three components. The main  $\text{Ar}^{2+}$  primary ion peak shifts to a higher apparent mass than that of the  $\text{Ar}^+$  reaction product, while the flight time of fast  $\text{Ar}^0$  produced by charge transfer reaction in the drift tube is unaffected by the retarding field. Measured arrival times of the primary and the two smaller secondary peaks are in agreement with those computed<sup>13</sup> from the ap-

plied voltages and drift distances in the spectrometer and lead to identification of the secondary peaks as products of Reactions (1) and (2). A check of the  $\text{Ar}^0$  assignment was obtained by placing a strong external magnetic field across the collector end of the flight tube region, preventing both the primary  $\text{Ar}^{2+}$  and product  $\text{Ar}^+$  from reaching the detector but allowing  $\text{Ar}^0$  produced in Reaction (1) to be collected. A pressure study of the separated mass 20 region peaks show the  $\text{Ar}^0$  and  $\text{Ar}^+$  product peaks result from single bimolecular collisions over the  $10^{-6}$ – $10^{-5}$  torr pressure range. Ionization efficiency curves and ionization potentials measured for  $\text{Ar}^+$  and  $\text{Ar}^0$  products are identical to those of  $\text{Ar}^{2+}$ , identifying this doubly charged ion as the primary ion precursor in (1) and (2). Argon gas pressure in the collision region was monitored with a calibrated ionization gauge. Variation of the secondary electron emission coefficient<sup>14-16</sup> of the electron multiplier cathode with product kinetic energy was determined with the aid of the well-documented<sup>17,18</sup> resonant  $\text{Ar}^+-\text{Ar}$  single electron transfer reaction.

Cross sections measured for Reactions (1) and (2) as a function of kinetic energy are displayed in Fig. 1 along with those obtained by other investigators. Our experiments indicate the predominance of double electron transfer processes below 8 keV with the cross section for  $\text{Ar}^0$  extrapolating to the data of Ref. 3. The cross section for single electron transfer measured between 6 and 8 keV is somewhat higher than previously reported. This may be expected since the present technique has the advantage of including contributions from fast  $\text{Ar}^+$  products inelastically scattered in the ion-atom interactions.

<sup>1</sup> I. P. Flaks and E. S. Solov'ev, *Sov. Phys. Tech. Phys.* **3**, 564 (1958) [*Zh. Tekh. Fiz.* **28**, 599 (1958)].

<sup>2</sup> J. B. Hasted and M. Hussain, *Proc. Phys. Soc.* **83**, 911 (1964).

<sup>3</sup> J. W. McGowan and L. Kerwin, *Can. J. Phys.* **45**, 1451 (1967).

<sup>4</sup> J. B. Hasted, *Physics of Atomic Collisions* (American Elsevier, New York, 1972), p. 620.

<sup>5</sup> G. R. Hertel and W. S. Koski, *J. Chem. Phys.* **40**, 3452 (1964).

<sup>6</sup> J. B. Hasted, S. M. Iqbal, and M. M. Yousaf, *J. Phys. B* **4**, 343 (1971).

<sup>7</sup> K. G. Spears, F. C. Fehsenfeld, M. McFarland, and E. E. Ferguson, *J. Chem. Phys.* **56**, 2562 (1972).

<sup>8</sup> G. V. Dubrovskii, *Zh. Eksp. Teor. Fiz.* **47**, 644 (1964) [*Soviet Phys. JETP* **20**, 429 (1965)].

<sup>9</sup> V. K. Bykhovskii and E. E. Nikitin, *Zh. Eksp. Teor. Phys.* **48**, 1499 (1965) [*Sov. Phys. JETP* **21**, 1003 (1965)].

<sup>10</sup> T. J. M. Boyd and B. L. Moiseiwitsch, *Proc. Phys. Soc. A* **70**, 809 (1957).

<sup>11</sup> K. E. Maher and J. J. Leventhal, *Phys. Rev. Lett.* **27**, 1253 (1971).

<sup>12</sup> M. W. Siegel, Y. H. Chen and J. W. Boring, *Phys. Rev. Lett.* **28**, 465 (1972).

<sup>13</sup> R. J. Conrads, W. Pomerance, and T. F. Moran, *J. Chem. Phys.* **57**, 2468 (1972).

<sup>14</sup> H. W. Berry, *Phys. Rev.* **121**, 1714 (1961).

<sup>15</sup> N. G. Utterback and G. H. Miller, *Phys. Rev.* **124**, 1477 (1961).

<sup>16</sup> H. C. Hayden and R. C. Amme, *Phys. Rev.* **141**, 30 (1966).

<sup>17</sup> D. Rapp and W. E. Francis, *J. Chem. Phys.* **37**, 2631 (1962).

<sup>18</sup> J. P. Abbe and J. P. Adloff, *Bull. Chem. Soc. (France)* **6**, 1212 (1964).

## APPENDIX V

PRODUCT INTERNAL STATE DISTRIBUTIONS FROM  
INTERACTIONS OF METASTABLE AR WITH N<sub>2</sub>

This appendix is the reprint of an article published in the Journal of Chemical Physics, Volume 57, pages 4111 to 4115, 15 November, 1972.

Product Internal State Distributions from Interactions of Metastable Ar with N<sub>2</sub>\*

P. C. COSBY AND T. F. MORAN

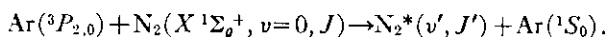
*School of Chemistry, Georgia Institute of Technology, Atlanta, Georgia 30332*

(Received 30 May 1972)

Internal energy state distributions of the products from reactions of metastable Ar(<sup>3</sup>P<sub>2,0</sub>) atoms with N<sub>2</sub>(X<sup>1</sup>Σ<sub>g</sub><sup>+</sup>) molecules have been computed from a statistical phase space treatment of the interactions. Calculated rotational and vibrational distributions have been compared with those measured in recent spectroscopic experiments involving metastable Ar atoms. For strongly exothermic reactions producing N<sub>2</sub>(B<sup>3</sup>Π<sub>g</sub>, *v*', *J*') molecules, the computed vibrational distribution is significantly broader than that measured experimentally. The corresponding vibrational and rotational distributions calculated for slightly exothermic N<sub>2</sub>(C<sup>3</sup>Π<sub>u</sub>, *v*', *J*') channels are in qualitative accord with experimental distributions; however, some features present in the experimental product distributions are not reproduced by the statistical model.

## INTRODUCTION

Interactions between a metastable atom and a diatomic molecule leading to ionization of the target molecule (Penning ionization) have been extensively studied.<sup>1</sup> The emphasis on this reaction channel has been in part due to the comparative ease with which the charged products of this reaction channel can be quantitatively identified. Complimentary to the experimental advances in this area, theoretical treatments<sup>2</sup> have been developed to describe Penning ionization process. Product ion vibrational state distributions measured<sup>3</sup> for several reactions are found to agree with those predicted from application of the Franck-Condon principle; however, exceptions<sup>4</sup> have been noted. Alternate reaction channels, in which the excitation energy of the metastable atom is partitioned among the energy states of stable diatomic product molecules, are not as well characterized due to associated experimental difficulties. Recent experimental advances<sup>5-7</sup> have been made in this area with the aid of flow systems coupled to spectroscopic instrumentation capable of analyzing radiation from spontaneous decay of excited neutrals produced via chemical interactions involving metastable atoms. Setser and Stedman<sup>6,7</sup> have determined product internal state distributions from the radiative transitions of N<sub>2</sub> excited by metastable argon atoms (<sup>3</sup>P<sub>2,0</sub>) in a discharge-flow system. The reactions investigated were



(1)

Analyses<sup>6-8</sup> of the N<sub>2</sub>\* first and second positive emissions indicate that the population distributions of the lower vibrational levels in both the N<sub>2</sub>(C<sup>3</sup>Π<sub>u</sub>) and N<sub>2</sub>(B<sup>3</sup>Π<sub>g</sub>) states differ from those expected for Franck-Condon type excitation processes. In addition, a nonequilibrium rotational population in the N<sub>2</sub>(C<sup>3</sup>Π<sub>u</sub>, *v*'=0) state was observed.<sup>7,8</sup> The possibility of a mechanism

involving ArN<sub>2</sub>\* complex formation has been proposed,<sup>7</sup> suggesting the applicability of the statistical phase space model<sup>9</sup> to the computation of product internal energy distributions. This model has been applied to a number of ion-molecule reactions<sup>10</sup> and the product state distributions estimated from the statistical treatment compare favorably with those measured for thermoneutral or slightly exothermic reactions.<sup>10a</sup> The present study applies the statistical model to the description of energy transfer processes that occur when electronically excited atoms react with neutral molecules.

## CALCULATIONS

The cross section for the formation of product state *i* in vibrational level *v*' and rotational level *J*' from reactants having a relative translational energy *E*<sub>trans</sub> is given by the equation<sup>10c</sup>

$$\sigma_i(E_{\text{trans}}, v', J') = 2\pi \int_0^{b_{\text{max}}} P_i(v', J' | E_i, K) b db, \quad (2)$$

where *P<sub>i</sub>*(*v*', *J*' | *E<sub>i</sub>*, *K*) is that fraction of the total phase space for a system with total energy *E<sub>i</sub>* and total angular momentum *K* which is accessible to product state *i* in levels *v*' and *J*'. A description of the methods we have used in computing these reaction cross sections has been previously presented.<sup>9b,9c,10g</sup> Interaction of reactant partners and separation of reaction products was assumed to occur under the influence of the effective potential<sup>11,12</sup>

$$V_{\text{eff}}(r) = \frac{L^2}{2\mu r^2} - \frac{3e\hbar}{2(m_e)^{1/2}r^6} \left( \frac{\alpha_1\alpha_2}{(\alpha_1/N_1)^{1/2} + (\alpha_2/N_2)^{1/2}} \right), \quad (3)$$

where *L* is the orbital angular momentum of the collision, *μ* is its reduced mass, *α<sub>1</sub>*, *N<sub>1</sub>*, and *α<sub>2</sub>*, *N<sub>2</sub>* represent the polarizability and number of outer-shell electrons of the atom and diatomic molecule respec-

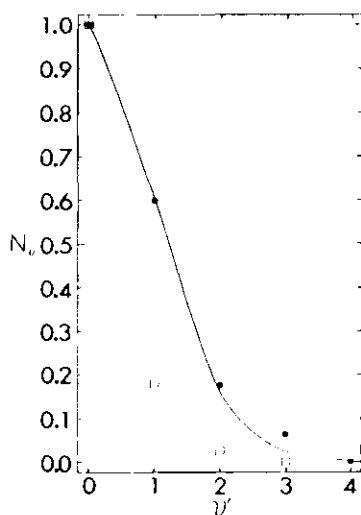


FIG. 1. Comparison of the relative vibrational level populations of the  $N_2(C^3\Pi_u)$  state formed in the reaction  $Ar^*(^3P_{2,0}) + N_2(X^1\Sigma_g^+, v=0, J) \rightarrow Ar(^1S_0) + N_2(C^3\Pi_u, v')$ . The open squares represent the experimental data of Ref. 6 while the closed circles are the vibrational populations, summed over  $J'$ , which are calculated using the statistical model. The solid curve represents the Franck-Condon factors of Ref. 20 for the transition  $N_2(X \rightarrow C)$ .

tively,  $m_e$  is the electron rest mass, and  $e$  is the elementary charge. The polarizabilities of the excited and ground state Ar atoms were taken as  $48.4 \text{ \AA}^3$  and  $1.64 \text{ \AA}^3$  from the work of Pollack *et al.*<sup>13</sup> and the tabulation of Dalgarno.<sup>14</sup> A polarizability of  $1.76 \text{ \AA}^3$  was used in the case of  $N_2$ .<sup>15</sup> The values of other potential parameters used in the phase space computations are listed in Table I for the various electronic states of nitrogen.

In order to compare the results of the statistical phase space model with experimental measurements obtained from reactions carried out at moderately high pressures, we have assumed the energy of reactant species to be equilibrated at the temperature of the surroundings. Accordingly, cross sections obtained from Eq. (2) have been averaged over the reactant's kinetic and rotational energy distributions to obtain the specific rate constant<sup>16</sup> in each of the channels

$$k_{i,v',J'} = Q_J^{-1} \left[ \sum_J f_J (2J+1) \exp(-E_J/kT) (\pi\mu)^{-1/2} \right. \\ \times (2/kT)^{3/2} \int_0^\infty \sigma_i(E_{\text{trans}}, v', J') \\ \left. \times E_{\text{trans}} \exp(-E_{\text{trans}}/kT) dE_{\text{trans}} \right], \quad (4)$$

where  $f_J$  is the degeneracy of the reactant energy level and  $Q_J$  is the partition function. Values of initial  $N_2(X^1\Sigma_g^+, v=0, J)$  rotational levels from  $J=0$  to

20 were considered in the evaluation of (4) and integration of the cross sections over the Maxwellian distribution from 0.0 to  $20.0kT$  was performed using a 74 point numerical technique.<sup>17</sup> The relative population,  $N_{i,v',J'}$ , of products formed in level  $v', J'$  of channel  $i$  is taken to be proportional to the specific rate constant for the formation of that quantum state. Consideration of the influence of possible spin states of metastable  $Ar^*$  reactants must also be incorporated into the computational framework when comparing the predictions of the statistical model with experimental results obtained using discharge<sup>6</sup> techniques. Metastable argon atoms may be formed in either the  $^3P_2$  or  $^3P_0$  spin states by a low-power, hollow discharge.<sup>6,7</sup> The energy difference between these states<sup>18</sup> is sufficient to alter the calculated internal energy distributions of the products. Consequently,  $N_{i,v',J'}$  have been computed for reactions involving both the  $^3P_2$  and  $^3P_0$  spin states of Ar and combined according to the statistical weight<sup>19</sup> of each reactant state:

$$N_{i,v',J'} = \frac{1}{6} [5N_{i,v',J'}(^3P_2) + N_{i,v',J'}(^3P_0)], \quad (5)$$

to give an averaged probability for the formation of state  $v', J'$  in channel  $i$ .

Fourteen possible reactive channels and four dissociative channels were considered in this calculation:

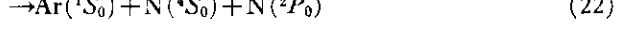
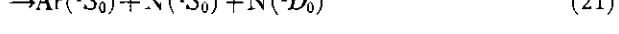
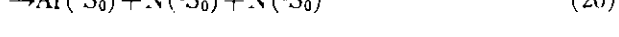
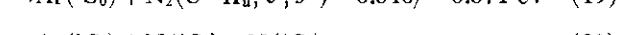
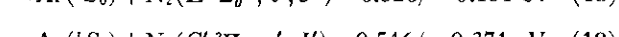
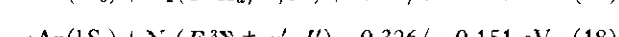
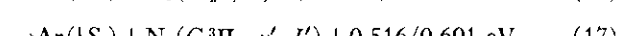
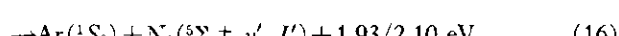
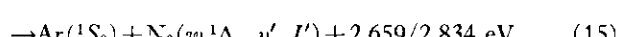
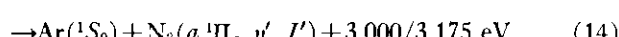
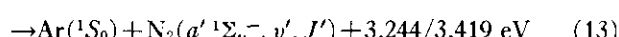
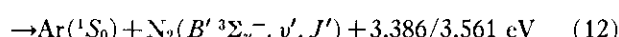
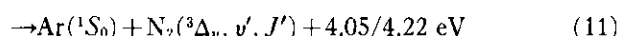
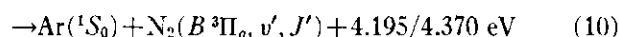
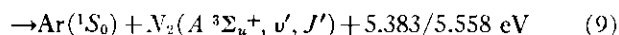
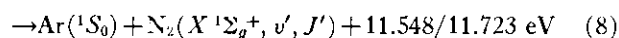
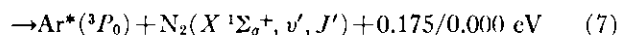
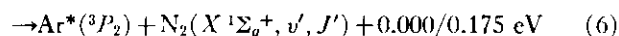
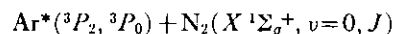


TABLE I. Spectroscopic parameters of molecular nitrogen.

State <sup>a</sup>	$\omega_e^b$ (cm <sup>-1</sup> )	$\omega_e x_e^b$ (cm <sup>-1</sup> )	$B_e^b$ (cm <sup>-1</sup> )	$\alpha_e^b$ (cm <sup>-1</sup> )	$r_e^b$ (Å)	$D_0^a$ (eV)
$X^1\Sigma_g^+$	2359.6	14.46	2.010	0.0187	1.094	9.756
$A^3\Sigma_u^+$	1460.4	13.89	1.440	0.013	1.293	3.591
$B^3\Pi_g$	1734.1	14.47	1.638	0.018	1.212	4.790
$^3\Delta_u$	1490. <sup>c</sup>	<sup>d</sup>	1.45 <sup>e</sup>	<sup>d</sup>	1.28 <sup>e</sup>	4.64 <sup>e</sup>
$B'^3\Sigma_u^-$	1517.7 <sup>a</sup>	11.0 <sup>a</sup>	1.467 <sup>a</sup>	<sup>d</sup>	1.281 <sup>a</sup>	5.170
$a'^1\Sigma_u^-$	1530.25 <sup>a</sup>	12.075 <sup>a</sup>	1.4799 <sup>a</sup>	0.01657 <sup>a</sup>	1.270 <sup>a</sup>	6.219 <sup>a</sup>
$a^1\Pi_g$	1694.20 <sup>f</sup>	13.949 <sup>f</sup>	1.6169 <sup>f</sup>	0.01793 <sup>f</sup>	1.215 <sup>f</sup>	5.975 <sup>f</sup>
$w^1\Delta_u$	1560.1	11.9	1.498 <sup>a</sup>	0.0166 <sup>a</sup>	1.263 <sup>a</sup>	5.634
$^b\Sigma_g^+$	12. <sup>c</sup>	<sup>d</sup>	0.94 <sup>a</sup>	<sup>d</sup>	1.6 <sup>e</sup>	0.14 <sup>e</sup>
$C^3\Pi_u$	2035.1	17.08	1.826	0.019	1.148	1.111
$E^3\Sigma_g^+$	2184.5	<sup>d</sup>	1.92	<sup>d</sup>	1.12 <sup>e</sup>	0.61 <sup>b</sup>
$C'^3\Pi_u$	1395. <sup>a</sup>	<sup>d</sup>	1.05	<sup>d</sup>	1.51 <sup>b</sup>	0.12 <sup>b</sup>

<sup>a</sup> A. Lofthus, "The Molecular Spectrum of Nitrogen," Spectry. Rept. 2, Dept. Phys., Univ. Oslo, Blindern, Norway, 1960.

<sup>b</sup> G. Herzberg, *Molecular Spectra and Molecular Structure I. Spectra of Diatomic Molecules* (Van Nostrand, Princeton, N. J., 1950).

<sup>c</sup> R. S. Mulliken, in *Threshold of Space, The Proceedings of the Conference on Chemical Aeronomy*, edited by M. Zelickoff (Pergamon, New York, 1957), p. 169.

<sup>d</sup> For the purpose of this calculation, the values of these parameters are assumed to be zero.

<sup>e</sup> S. G. Tilford, P. G. Wilkinson, and J. T. Vanderslice, *Astrophys. J.* **141**, 427 (1965).

<sup>f</sup> J. T. Vanderslice, S. G. Tilford, and P. G. Wilkinson, *Astrophys. J.* **141**, 395 (1965).

<sup>g</sup> Estimated from  $r_e$ .

<sup>h</sup> R. F. Gilmore, *J. Quant. Spectry. Radiative Transfer* **5**, 369 (1965).

The values of the exothermicity of each channel refer to the product molecule in its ground vibrational and rotational level, considering Ar\*(<sup>3</sup>P<sub>2</sub>) and Ar\*(<sup>3</sup>P<sub>0</sub>), in turn, as the reactant metastable specie. Vibrational and rotational energy levels of the product molecule

were compiled from the spectroscopic constants listed in Table I and used in the statistical model for the reaction channels (6)–(23).

## RESULTS AND DISCUSSION

The relative vibrational populations,  $N_{v'}$ , for the N<sub>2</sub>(C<sup>3</sup>Π<sub>u</sub>, v') state formed via channel (17) have been calculated using the statistical formalism and are presented as the solid circles in Fig. 1. As seen in this figure the computed vibrational population does not drop off with vibrational quantum number as rapidly as the experimental data of Stedman and Setser,<sup>6</sup> which are displayed as the open squares. Franck-Condon factors<sup>20</sup> for the transition N<sub>2</sub>(X<sup>1</sup>Σ<sub>g</sub><sup>+</sup>, v=0)→N<sub>2</sub>(C<sup>3</sup>Π<sub>u</sub>, v'), scaled to unity, are represented in this figure as a solid line. The coincidence for this particular reaction of the population distribution calculated from the phase-space theory and that predicted for Franck-Condon type transitions is purely fortuitous since the overlaps of vibrational wave functions for the isolated ground and excited state molecules are not considered within the framework of the statistical model.

Further examination of the applicability of the phase space treatment to energy conversion processes in the interaction of neutral atoms and molecules is presented in Fig. 2 for the same reaction channel (17). In this figure, the relative rotational populations computed for the ground vibrational level of the N<sub>2</sub>(C<sup>3</sup>Π<sub>g</sub>) state are presented as the solid circles.

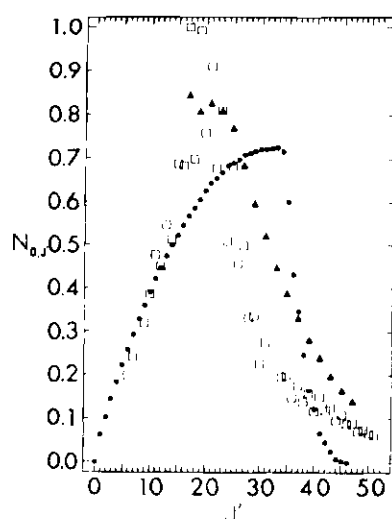


FIG. 2. Relative rotational level populations for the ground vibrational state of N<sub>2</sub>(C<sup>3</sup>Π<sub>g</sub>) formed in the reaction Ar\*(<sup>3</sup>P<sub>2,0</sub>) + N<sub>2</sub>(X<sup>1</sup>Σ<sub>g</sub><sup>+</sup>, v=0, J)→Ar(<sup>1</sup>S<sub>0</sub>) + N<sub>2</sub>(C<sup>3</sup>Π<sub>g</sub>, v'=0, J'). The open squares and closed triangles represent the experimental data of Refs. 7 and 8, respectively. The corresponding population distribution calculated for the statistical model is presented as the closed circles.

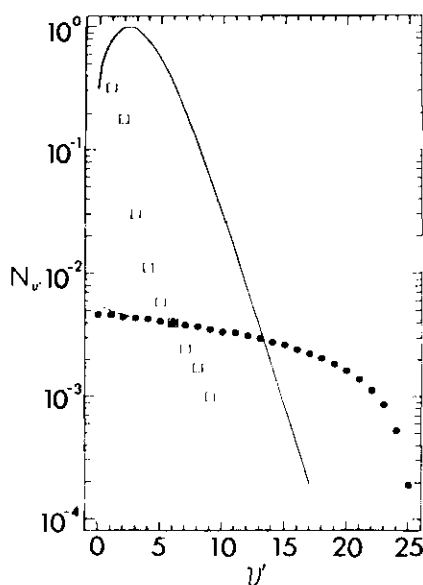


FIG. 3. Relative vibrational level populations of the  $N_2(B^3\Pi_g)$  state formed in the reaction  $Ar^*(^3P_{2,0}) + N_2(X^1\Sigma_g^+, v=0, J) \rightarrow Ar(^1S_0) + N_2(B^3\Pi_g, v')$ . The open squares represent the experimental data of Ref. 6 while the closed circles represent the calculated vibrational distribution summed over  $J'$ . Franck-Condon factors of Ref. 20 for the  $N_2(X \rightarrow B)$  transition are presented as the solid curve. The dashed line represents the change in the calculated populations when  $N_2(C^3\Pi_u) \rightarrow N_2(B^3\Pi_g)$  radiative decay is considered.

The corresponding rotational data of Ref. 7, obtained in a flowing discharge, are presented as open squares. The results of Kassal and Fishburne<sup>8</sup> for this same reaction channel are given as the triangles. Agreement between these two groups is approached in that the maximum in the rotational population distribution at  $J'=17$  of Ref. 7 is in reasonable accord with the local maximum of Ref. 8 at  $J'=21$ . These latter workers used a different type of experimental apparatus in which a high energy electron beam was used to produce the metastable  $Ar^*$  reactant. We note that whereas the distribution computed using the statistical treatment roughly approximates the experimental data, the calculated distribution is broader than these experiments indicate with a maximum near  $J'=33$ . Comparisons between the experimental data and phase space computation shown in Figs. 1 and 2 for the production of vibrationally and rotationally excited  $N_2(C^3\Pi_u)$  molecules show the model is qualitatively correct in describing the relative product internal state distributions of this slightly exothermic reaction, although quantitative agreement is lacking.

A further examination of the applicability of the statistical model to strongly exothermic reactions can be made in the case of reactions producing  $N_2(B^3\Pi_g)$  in which there is more than 4 eV to be partitioned among the various degrees of freedom in the products. The relative vibrational populations predicted by the

phase space theory for formation of this state via channel (10) are presented as solid circles in Fig. 3 while the data of Ref. 6 are represented by open squares. Franck-Condon factors<sup>20</sup> for the  $N_2(X^1\Sigma_g^+, v=0) \rightarrow N_2(B^3\Pi_g, v')$  transitions are given by the solid line. It is noted that the phase-space model predicts a larger fraction of the products to be in high vibrational states than would be expected if channel (10) were dominated by a Franck-Condon type excitation process and does not reproduce the large population densities measured for the lower  $N_2(B^3\Pi_g)$  vibrational levels. Stedman and Setser<sup>6</sup> have examined the possibility of  $N_2(C \rightarrow B)$  spontaneous radiative transitions as a dominant mechanism contributing to the overpopulation of the lower  $N_2(B^3\Pi_g)$  vibrational levels. We have considered the extent to which this mechanism might apply by weighting the calculated vibrational populations for the  $N_2(C^3\Pi_u)$  state with the Franck-Condon factors<sup>21</sup> for  $N_2(C \rightarrow B)$  transitions and adding them to the calculated vibrational populations for the  $N_2(B^3\Pi_g)$  state. The effect of including the radiative mechanism on the calculated relative vibrational populations of the  $N_2(B^3\Pi_g)$  state is represented by the dashed line in Fig. 3. Although consideration of the radiative cascade does lead to a slight enhancement of population in the lower vibrational levels, we find, as did Ref. 7, that  $N_2(C \rightarrow B)$  radiative transitions do not significantly perturb the vibrational distribution of the  $N_2(B^3\Pi_g)$  state. The statistical phase space model predicts a total cross section on the order of  $7 \text{ \AA}^2$  for thermal reactions producing the  $N_2(B^3\Pi_g)$  state while that for the corresponding reaction forming the  $N_2(C^3\Pi_u)$  state is  $0.15 \text{ \AA}^2$ . Setser *et al.*<sup>7</sup> have measured the  $C/B$  state ratio to be approximately 0.13, whereas

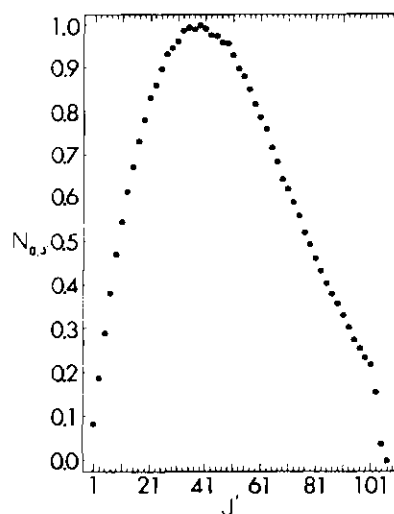


FIG. 4. Calculated relative rotational population distribution for the  $N_2(B^3\Pi_g, v'=0)$  state formed in the reaction  $Ar^*(^3P_{2,0}) + N_2(X^1\Sigma_g^+, v=0, J) \rightarrow Ar(^1S_0) + N_2(B^3\Pi_g, v'=0, J')$ . Only the odd rotational levels are shown.



the present calculations indicate a value of 0.02. The larger computed cross sections for N<sub>2</sub>(B<sup>3</sup>Π<sub>g</sub>) formation relative to that of the N<sub>2</sub>(C<sup>3</sup>Π<sub>u</sub>) state is not surprising in view of the larger exothermicity of the N<sub>2</sub>(B<sup>3</sup>Π<sub>g</sub>) reaction which tends to statistically favor this reaction channel. The inability of the statistical model to correctly predict the cross sections for forming products in energetically accessible electronic states has been documented.<sup>10f</sup> Wong<sup>9g</sup> has recently noted a failure of the phase space model in predicting the vibrational distribution of products from the reaction of Cl with H<sub>2</sub>. The rotational phase space distribution of N<sub>2</sub>(B<sup>3</sup>Π<sub>g</sub>) products from the strongly exothermic (4.195/4.370 eV) channel (10) is presented in Fig. 4 for the v'=0 level. In this reaction channel there is a lack of experimental data with which to compare the computed distribution. The lifetime of the N<sub>2</sub>(B<sup>3</sup>Π<sub>g</sub>) electronic state is sufficiently long (7×10<sup>-6</sup> sec) for rotational relaxation to occur in a flowing discharge experiment prior to spectroscopic observation of the B→A transition. Population of high rotational levels in the phase space model is consistent with the large amount of available energy in this reaction channel.

Previous comparisons of the statistical model with measured internal state distributions of products from rare gas ion-N<sub>2</sub> interactions<sup>10f,10g,22</sup> have indicated deviations between experiment and theory in the case of moderately or strongly exothermic reactions and agreement for thermoneutral or slightly exothermic interactions. The analogous Ar\*-N<sub>2</sub> case examined here exhibits a similar trend. The redistribution of energy into product internal degrees of freedom does not occur statistically for the strongly exothermic N<sub>2</sub>(B<sup>3</sup>Π<sub>g</sub>) channel, whereas product internal state distributions are in qualitative agreement with experiment for the slightly exothermic N<sub>2</sub>(C<sup>3</sup>Π<sub>u</sub>) channel of reaction.

\* Acknowledgment is made to the National Science Foundation for partial support of this research.

<sup>1</sup> (a) E. E. Muschlitz, Jr. and M. J. Weiss, in *Atomic Collisions Processes, Proceedings 3rd International Conference Physics of Electronic and Atomic Collisions*, London, 1963, edited by M. R. C. McDowell (North-Holland, Amsterdam, 1964), p. 1073. (b) E. E. Muschlitz, Jr., in *Molecular Beams*, edited by J. Ross, (Interscience, New York, 1966), p. 171. (c) E. E. Benton, E. E. Ferguson, F. A. Matsen, and W. W. Robertson, *Phys. Rev.* **128**, 206 (1962). (d) V. Čermák, *Coll. Czechoslov. Chem. Commun.*

**33**, 2739 (1968). (e) H. Hotop and A. Niehaus, *Z. Physik* **228**, 68 (1969).

<sup>2</sup> (a) W. H. Miller, *J. Chem. Phys.* **52**, 3563 (1970). (b) W. H. Miller, C. A. Slocumb, and H. F. Schaefer III, *ibid.* **56**, 1347 (1972). (c) T. Watanabe and K. Katsuura, *ibid.* **47**, 800 (1967). (d) M. Mori, *J. Phys. Soc. Japan* **26**, 773 (1969). (e) M. Matsuzawa, *J. Chem. Phys.* **55**, 2685 (1971). (f) J. S. Cohen and N. F. Lane, *Chem. Phys. Letters* **10**, 623 (1971). (g) K. Katsuura, *J. Chem. Phys.* **42**, 3771 (1965). (h) B. M. Smirnov and O. B. Firsov, *ZhETF Pis. Red.* **2**, 478 (1965) [*JETP Letters* **2**, 297 (1965)].

<sup>3</sup> (a) W. W. Robertson, *J. Chem. Phys.* **44**, 2456 (1966). (b) C. E. Brion, C. A. McDowell, and W. B. Stewart, *Chem. Phys. Letters* **13**, 79 (1972).

<sup>4</sup> W. C. Richardson, D. W. Setser, D. L. Albritton, and A. L. Schmeltekopf, *Chem. Phys. Letters* **12**, 349 (1971).

<sup>5</sup> (a) D. H. Stedman, *J. Chem. Phys.* **52**, 3966 (1970). (b) M. Cher and C. S. Hollingsworth, *J. Chem. Phys.* **50**, 4942 (1969).

<sup>6</sup> D. H. Stedman and D. W. Setser, *J. Chem. Phys.* **52**, 3957 (1970).

<sup>7</sup> D. W. Setser, D. H. Stedman, and J. A. Coxon, *J. Chem. Phys.* **53**, 1004 (1970).

<sup>8</sup> T. T. Kassal and E. S. Fishburne, *J. Chem. Phys.* **54**, 1363 (1971).

<sup>9</sup> (a) J. C. Light, *J. Chem. Phys.* **40**, 3221 (1964). (b) P. Pechukas, J. C. Light, and C. Rankin, *ibid.* **44**, 794 (1966). (c) J. Lin and J. C. Light, *ibid.* **45**, 2545 (1966). (d) R. A. White and J. C. Light, *ibid.* **55**, 379 (1971). (e) D. G. Truhlar and A. Kuppermann, *J. Phys. Chem.* **73**, 1722 (1969). (f) D. G. Truhlar, *J. Chem. Phys.* **54**, 2635 (1971). (g) W. H. Wong, *Can. J. Chem.* **50**, 633 (1972).

<sup>10</sup> (a) O. B. Firsov, *Zh. Eksp. Teor. Fiz.* **42**, 1307 (1962) [*Sov. Phys. JETP* **15**, 906 (1962)]. (b) E. E. Nikitin, *Teor. i Eksperim. Khim. Akad. Nauk. SSR*, **1**, 428 (1965). (c) J. C. Light and J. Lin, *J. Chem. Phys.* **43**, 3209 (1965). (d) F. A. Wolf, *ibid.* **44**, 1619 (1966). (e) F. A. Wolf, and J. I. Haller, *ibid.* **52**, 5910 (1970). (f) D. C. Fullerton and T. F. Moran, *ibid.* **54**, 5221 (1971). (g) T. F. Moran and D. C. Fullerton, *ibid.* **56**, 21 (1972). (h) D. G. Truhlar, *ibid.* **56**, 1481 (1972).

<sup>11</sup> K. S. Pitzer, *Advan. Chem. Phys.* **2**, 59 (1959).

<sup>12</sup> E. W. Rothe and R. B. Bernstein, *J. Chem. Phys.* **31**, 1619 (1959).

<sup>13</sup> E. Pollack, E. J. Robinson, and B. Bederson, *Phys. Rev.* **134**, A1210 (1964).

<sup>14</sup> A. Dalgarno, *Advan. Phys.* **11**, 281 (1962).

<sup>15</sup> J. O. Hirschfelder, C. F. Curtiss, and R. B. Bird, *Molecular Theory of Gases and Liquids* (Wiley, New York, 1954).

<sup>16</sup> M. A. Eliason and J. O. Hirschfelder, *J. Chem. Phys.* **30**, 1426 (1959).

<sup>17</sup> I. S. Berezin and N. P. Zhidkov, *Computing Methods* (Adison-Wesley, Reading, Mass., 1965), Vol. I, p. 234.

<sup>18</sup> C. E. Moore, *Natl. Bur. Std. (U.S.) Circ.* **467**, Vol. 1 (1949).

<sup>19</sup> It has been suggested that under certain flow conditions the fraction of <sup>3</sup>P<sub>u</sub> at the time of reaction is lower (10%) than the statistical abundance at the time of metastable atom formation (Ref. 7).

<sup>20</sup> W. Benesch, J. T. Vanderslice, S. G. Tilford, and P. G. Wilkinson, *Astrophys. J.* **143**, 236 (1966).

<sup>21</sup> R. N. Zare, E. O. Larsson, and R. A. Berg, *J. Mol. Spectry.* **15**, 117 (1965).

<sup>22</sup> G. H. Sabau and T. F. Moran, *J. Chem. Phys.* **57**, 895 (1972).

## LITERATURE CITED\*

1. M. G. Evans and M. Polanyi, *Trans. Faraday Soc.* 35, 178 (1939).
2. M. C. Moulton and D. R. Herschbach, *J. Chem. Phys.* 44, 3010 (1966).
3. T. F. Moran and L. Friedman, *J. Chem. Phys.* 39, 2491 (1963).
4. A. L. Schmeltekopf, F. C. Fehsenfeld, G. I. Gelman, and E. E. Ferguson, *Planet. Space Sci.* 15, 401 (1967).
5. V. I. Krassovski, *Space Res.* 3, 96 (1964).
6. E. W. McDaniel, V. Cermak, A. Dalgarno, E. E. Ferguson, and L. Friedman, *Ion-Molecule Reactions* (Wiley-Interscience, New York, 1970), p. 319.
7. E. E. Muschlitz, Jr., in *Molecular Beams*, edited by J. Ross (Interscience, New York, 1966), p. 171.
8. E. W. McDaniel, *Collision Phenomena in Ionized Gases* (Wiley, New York, 1964), Ch. 6.
9. R. F. Stebbings, in *Molecular Beams*, edited by J. Ross (Interscience, New York, 1966), p. 195.
10. C. F. Giese, *ibid.*, p. 247.
11. D. R. Bates and N. Lynn, *Proc. Roy. Soc.* A253, 141 (1959).
12. D. W. Setser, D. H. Stedman, and J. A. Coxon, *J. Chem. Phys.* 53, 1004 (1970).
13. A. C. Aiken and R. A. Goldberg, *J. Geophys. Res.* 78, 734 (1973).
14. R. S. Narcisi and A. D. Bailey, *J. Geophys. Res.* 70, 3587 (1965).
15. W. Roth and R. S. Narcisi, *Advan. Electron. Electron Physics* 28, 9 (1970).
16. T. M. Donahue, *Science* 159, 489 (1968).
17. D. R. Bates, *Contemp. Phys.* 2, 105 (1970).

---

\*The abbreviations used herein conform to those adopted by the IUPAC and AIP as described in the List of Periodicals, *Chem. Abstr.* 55, 1J (1961) and later supplements.

18. M. R. Flannery, P. C. Cosby and T. F. Moran, J. Chem. Phys. 59, 5494 (1973).
19. D. R. Bates and R. H. G. Reid, Proc. R. Soc. A310, 1 (1969).
20. S. Sato, J. Chem. Phys. 23, 592 (1955).
21. J. O. Hirschfelder, C. F. Curtiss and R. B. Bird, Molecular Theory of Gases and Liquids (Wiley, New York, 1954), pp. 950 and 1110.
22. Y. Yang and D. C. Conway, J. Chem. Phys. 40, 1729 (1964).
23. J. E. Jordan, S. O. Colgate, I. Amdur and E. A. Mason, J. Chem. Phys. 52, 1143 (1970).
24. D. L. Albritton, A. L. Schmeltekopf, and R. N. Zare, Diatomic Intensity Factors, (to be published); but are given in part by P. H. Krupenie, J. Phys. Chem. Ref. Data 1, 423 (1972).
25. W. McGowan and L. Kerwin, Can. J. Phys. 42, 2086 (1964).
26. T. F. Moran, F. C. Petty, and A. F. Hedrick, J. Chem. Phys. 51, 2112 (1969).
27. D. W. Turner, C. Baker, A. D. Baker and C. R. Brundle, Molecular Photoelectron Spectroscopy (Wiley, New York, 1970), p. 52.
28. O. Edquist, E. Lindholm, L. E. Selin and L. Asbrink, Physics Scripta 1, 25 (1970).
29. R. W. Carlson and D. L. Judge, J. Chem. Phys. 54, 1832 (1971).
30. A. J. Blake and J. H. Carver, J. Chem. Phys. 47, 1038 (1967).
31. G. R. Branton, D. C. Frost, T. Makita, C. A. McDowell and I. A. Stenhouse in Recent Developments in Mass Spectrometry edited by K. Ogata and T. Hayakawa (U. Tokyo Press, 1970), p. 756.
32. T. Kaneko, I. Omura, Y. Yamada, and K. Tanaka, ibid., p. 751.
33. H. Nishimura, J. Phys. Soc. Japan 24, 130 (1968).
34. W. L. Borst and E. C. Zipf, Phys. Rev. A1, 1410 (1970).
35. J. W. McConkey and J. M. Woolsey, J. Phys. B 2, 529 (1969).
36. E. H. Fink and K. H. Welge, Z. Naturforsch. 23a, 358 (1968).
37. B. R. Turner, J. A. Rutherford and D. M. J. Compton, J. Chem. Phys. 48, 1602 (1968).

38. P. C. Cosby, T. F. Moran, J. V. Hornstein, and M. R. Flannery, Chem. Phys. Letters 24, 431 (1974).
39. F. H. Dorman, J. D. Morrison and A. J. C. Nicholson, J. Chem. Phys. 32, 378 (1960).
40. J. W. McGowan, E. M. Clarke, H. P. Hanson and R. F. Stebbings, Phys. Rev. Lett. 13, 620 (1964).
41. C. E. Brion and G. E. Thomas, Int. J. Mass Spectrom. Ion Phys. 1, 25 (1968).
42. A. J. C. Nicholson, J. Chem. Phys. 39, 954 (1963)
43. J. E. Collin and P. Natalis, Int. J. Mass Spectrom. Ion Phys. 2, 231 (1969).
44. K. Tanaka and I. Tanaka, J. Chem. Phys. 59, 5042 (1973).
45. E. Lindholm, Arkiv Fysik 40, 117 (1969).
46. E. W. Thulstrup and Y. Ohrn, J. Chem. Phys. 57, 3716 (1972); H. Lefebvre-Brion and C. M. Moser, J. Chem. Phys. 44, 2951 (1966).
47. O. Edqvist, E. Lindholm, L. E. Selin, H. Sjogren, and L. Asbrink, Arkiv Fysik 40, 439 (1970).
48. D. W. Turner and D. P. May, J. Chem. Phys. 45, 471 (1966); J. A. R. Samson, Phys. Letters 28A, 391 (1968); J. E. Collin, J. Delwiche, and P. Natalis, Int. J. Mass Spectrom. Ion Phys. 7, 19 (1971).
49. J. F. M. Aarts and F. J. DeHeer, Physica 54, 609 (1971).
50. J. E. Mentall and H. D. Morgan, J. Chem. Phys. 56, 2271 (1972); E. J. Stone and E. C. Zipf, J. Chem. Phys. 56, 2870 (1972).
51. W. B. Maier and R. F. Holland, J. Chem. Phys. 54, 2693 (1971).
52. J. E. Hesser, J. Chem. Phys. 48, 2518 (1968).
53. D. Rapp, P. Englander-Golden, and D. D. Briglia, J. Chem. Phys. 42, 4081 (1965); D. Rapp and P. Englander-Golden, J. Chem. Phys. 43, 1464 (1965).
54. D. W. Vance, Phys. Rev. 169, 263 (1968).
55. R. F. Mathis, B. R. Turner, and J. A. Rutherford, J. Chem. Phys. 49, 2051 (1968).
56. P. C. Killgoar, G. E. Leroi, J. Berkowitz, and W. A. Chupka, J. Chem. Phys. 58, 803 (1973).

57. B. Cantone, V. Emma, and F. Grosso, in Advances in Mass Spectrometry, edited by E. Kendrick (The Institute of Petroleum, London, 1968) V. 4, p. 599.
58. A. J. C. Nicholson, J. Chem. Phys. 39, 954 (1963).
59. R. M. Reese and H. M. Rosenstock, J. Chem. Phys. 44, 2007 (1966).
60. R. F. Stebbings, B. R. Turner, and A. C. H. Smith, J. Chem. Phys. 38, 2277 (1963).

## VITA

The author was born in Washington, D. C. on August 9, 1945, the son of Harold and Margaret Cosby of Falls Church, Virginia. After graduation from J. E. B. Stuart High School in 1963, he entered the Virginia Military Institute, from which he received a Bachelor of Science degree in 1967.

In the fall of 1967, the author entered the Georgia Institute of Technology, receiving the degree of Master of Science in Chemistry in 1969. Following two years of military service, he returned to the School of Chemistry, Georgia Institute of Technology, to continue his Ph.D. research.

The author is a member of the Society of the Sigma Xi, the American Physical Society, and the American Association for the Advancement of Science.